Addressing urban climate hazard vulnerability in Canada through building retrofit techniques and strategies

by

Caitlyn Shum

A thesis submitted in partial fulfillment of the requirements for the degree of

Master of Science

Department of Mechanical Engineering
University of Alberta

Abstract

The rapid growth of urban centers in Canada has highlighted the need for cities to improve urban resiliency to better protect the health and comfort of its residents. A key component of urban resiliency is a city's ability to maintain occupant safety and comfort in the face of adverse climate hazards due to climate change. For many Canadian cities, the increasing prevalence of higher-than-average summer seasonal temperatures and dry conditions have led to intense wildfire seasons and the increased frequency of heatwave conditions. In response to these climate hazards, this study explored the use of building retrofit strategies to mitigate and reduce the severity of climate hazards' impacts on indoor environmental quality.

To address indoor air quality challenges associated with wildfire events, this study explored the effectiveness and feasibility of wildfire-resilient mechanical ventilation systems to maintain acceptable IAQ in single-detached residences in western Canada. Outdoor PM2.5 concentration datasets during wildfire conditions were used in conjunction with IAQ mathematical models to assess the impact of ventilation and building-related input variables on indoor PM2.5 levels. A cost-benefit analysis was conducted to compare the cost of ventilation retrofit options with regional estimates of reasonable monetary contributions per resident toward health risk mitigation. Ventilation retrofit options were recommended based on IAQ simulations, model sensitivity, and cost-benefit analysis results. It was recommended that residential ventilation systems increase the minimum filter efficiency from MERV6 to MERV11 or MERV13 during wildfire operation and implement higher recirculation ratios during peak exposure scenarios. Multi-filter mechanical ventilation system configurations were recommended for residential dwellings located in regions prone to severe PM2.5 exposure. This study provides insight into the integration of wildfire

resiliency in existing residential mechanical ventilation systems for IAQ improvement. This study sets the foundation for future experimental verification of the performance of ventilation strategies to improve urban safety, health and wellness during the wildfire season.

To mitigate the impact of heatwave conditions on the indoor space and maintain indoor thermal comfort, this study focused on the optimization of automated shading systems to maintain indoor thermal conditions during both the heating and cooling seasons. Preliminary building energy modelling was used to develop a cold-climate optimized sensorless control strategy for automated roller shades. A mathematical model was developed to estimate shading system energy performance based on user-defined building specifications and weather-related variables. The effectiveness of the automated roller shading system as a green retrofit technology was explored by comparing season-specific energy savings and payback periods for various cold climate zones. A field study quantified the impact of roller shade operation on indoor thermal conditions. The technology exhibited a payback period range of approximately 5 – 15 years, depending on factors such as glazing type, orientation, solar exposure, and local climate conditions. Findings from both the simulation and prototype field study support the use of cold climate-optimized automated shading systems as a year-round green retrofit strategy for buildings. This study serves as a pioneering effort and justification for cold climate zone buildings to implement retrofit technologies for improved indoor thermal control during heatwave conditions while ensuring year-round technology functionality.

Overall, wildfire-resilient mechanical ventilation and cold climate-optimized automated shading are effective strategies for maintaining IAQ and indoor thermal comfort within the built environment. The implementation of these technologies can improve climate change resiliency within the built environment while ensuring comfortable indoor conditions for all occupants.

Preface

The contents within Section 1.3.2 Heat Flux and Solar Gain were published as a part of Shum, Caitlyn and Zhong, Lexuan. 2023. "A review of smart solar shading systems and their applications: Opportunities in cold climate zones", Journal of Building Engineering, Vol. 64 (105583).

The contents of Chapter 2 were published as Shum, Caitlyn and Zhong, Lexuan. 2022. "Wildfire-resilient mechanical ventilation systems for single-detached homes in cities of Western Canada" Sustainable Cities and Society, Vol. 79 (103668). The data used in Chapter 2 was publicly available online through Canadian government databases.

The contents of Chapter 3 were submitted for publishing as Shum, Caitlyn and Zhong, Lexuan. 2023. "Optimizing automated shading systems for enhanced energy performance in cold climate zones: strategies, savings, and comfort." in Energy and Buildings.

I was responsible for the investigation, data collection, data analysis, and manuscript composition in all works mentioned. Dr. Lexuan Zhong was the supervisory author and was responsible for project conceptualization, project administration, funding acquisition, and the reviewing and editing of the manuscripts.

Acknowledgements

The last two years in this master's degree have been a remarkable journey and a true test of grit. In addition to the technical knowledge that I have gained, research has also taught me the importance of patience, resilience, and endurance. This journey was not a solo adventure, so I would like to acknowledge all of those who have helped me along the way.

First, I would like to thank my supervisor, Dr. Lexuan Zhong, for her unwavering support and mentorship. Her guidance and encouragement allowed me to develop as a researcher and discover my passion for building science research. I will always think back fondly on the weekly meetings, lab group presentations, conferences, and the occasional 2 am panic email.

For the wildfire-resilient ventilation system project, I would like to recognize the financial support from BC Housing through the Building Excellence Research & Education Grant. For the automated shading project, I would like to recognize the financial support from MITACS (IT33500). In addition, I would like to express my gratitude to Zack Zhang and the AI Shading team. Zack, you and your team provided valuable contributions and industrial insights into automated shading systems that greatly enhanced my project.

Finally, I am grateful for family. To the lab, I will always cherish the comradery and lasting friendships that were forged in the last two years. To my family, I would like to thank my parents and my sister for their unconditional love and support. I dedicate this thesis to my mom and dad; thank you for nurturing creativity, curiosity, and a good work ethic throughout my life.

Table of Contents

List of Tables

List of Figures

Nomenclature

A	window area [m^2]
C_{bz}	beathing zone PM2.5 concentration [$\mu g/m^3$]
$C_{incentive}$	technology incentive rate [$/kWh, $/GJ]
C_o	outdoor PM2.5 concentration [$\mu g/m^3$]
$C_{utility}$	utility rate [$/kWh, $/GJ]
CS	control strategy
$E_{f(A,B,C)}$	filter efficiency at location A, B, or C [%eff]
E_z	zone air distribution effectiveness
DNI, I_{direct}	direct normal irradiance [W/m^2]
GHI	global horizontal irradiance [W/m^2]
$DHI, I_{diffuse}$	diffuse horizontal irradiance [W/m^2]
F_r	flow reduction factor
IAC	indoor attenuation coefficient
$\dot{N}$	indoor PM2.5 generation rate [$\mu g/m^3$]
$Q_{cond,conv}$	conductive heat flux [kJ]
Q_{rad}	solar radiative heat flux [Wh]
$Q_{savings}$	heating/cooling load reduction [kWh, GJ]
$Q_{total,baseline}$	baseline total heat flux [Wh, kJ]
$Q_{total,dynamic}$	dynamic mode total heat flux [Wh, kJ]
R	recirculation ratio
R_{eq}	wall thermal resistance [m^2K/W]
$RMSD$	root mean square distance
S_{annual}	annual monetary savings [$]
$SHGC_{diffuse}$	diffuse solar heat gain coefficient
$SHGC_{direct}$	direct solar heat gain coefficient
ΔT	indoor/outdoor temperature difference [°C]
T_{out}	outdoor temperature [°C]
$\dot{V}_{inf}$	building infiltration rate [ACH]
$\dot{V}_{ez}$	outdoor air flowrate [ACH]
$\dot{V}_r$	recirculated air flowrate [ACH]
β	solar altitude angle
η_{eq}	heating/cooling equipment efficiency
$theta, \theta$	incident angle
θ_z	solar zenith angle
Σ	surface angle
Υ	surface-solar azimuth angle
Φ	solar azimuth angle
Ψ	surface azimuth angle

1. Introduction

1.1 Climate hazards and Indoor Environmental Quality (IEQ)

Climate change poses a significant threat to the stability of existing climate systems around the world [1, 2]. Rising sea levels, increasing ocean temperatures, and abnormal weather patterns are most often attributed as indicators of climate change and global warming [3, 4]. Rapid urbanization has emphasized the need to address and mitigate these climate hazards within the urban setting. In their 2022 report, the Intergovernmental Panel on Climate Change (IPCC) provided recommendations to address existing vulnerabilities and climate hazards resulting from climate change [2]. Regarding cities and infrastructure, both climate risk reduction and sustainability must be considered in climate change-resilient urban development [2]. These include the development of green cities and prioritizing a focus on human well-being and comfort [2].

Urban residents spend the majority of their time indoors and day-to-day activities typically occur within a built environment. A study by Matz et al. regarding Canadian human time-activity patterns found that Canadians spend up to 88.9% of their day indoors [5]. As a result, the built environment must be able to mitigate the impact of outdoor climate hazards on indoor environmental quality (IEQ). IEQ is an umbrella term that encompasses the assessment of the air quality, thermal, acoustic, and visual conditions within an indoor space. From the perspective of building systems design and retrofit, climate hazard-specific engineering controls are crucial to improve the climate change-resiliency of built environments and to maintain acceptable IEQ for its occupants.

Within Canada and the United States, climate change has been linked to the increased frequency of extreme weather events such as heatwaves and droughts [6-8]. Exposure to both heatwave and drought conditions has negative impacts on human health including heat-related illnesses [9],

respiratory illnesses [10] and poor mental health outcomes [11]. In addition to the direct impact of their outdoor exposure on human health, heatwaves and drought conditions have created novel challenges in IEQ management. These challenges relate to maintaining acceptable indoor air quality (IAQ) and indoor thermal conditions amid extreme weather conditions such as wildfires and heatwaves.

1.1.1 Wildfires

Abnormal climate patterns resulting from climate change have caused an increase in heatwaves and dry, drought-like conditions. These have, in turn, fueled an increase in the frequency and severity of wildfires across Canada. Most notably, the severity of wildfires within Western Canada has experienced numerous record-breaking fire seasons within the past two decades [12-14]. During active wildfire events, large amounts of smoke are released into the air. Wildfire smoke contains high amounts of particulate matter (PM), carbon monoxide, polycyclic aromatic hydrocarbons, and volatile organic compounds (VOCs) [15, 16]. Exposure to high levels of these compounds has been shown to have both acute and long-term health effects on humans [16, 17]. The degradation of outdoor air quality from active wildfire events often leads to subsequent degradation of IAQ. This phenomenon is a result of both insufficient air filtration within the building's mechanical ventilation system and excessive infiltration due to poor air tightness within the building envelope [18, 19]. Different regions will experience varying degrees of outdoor air quality degradation due to wildfires depending on their proximity to active wildfire events and local weather conditions [20]. Cities located within or near wildland-urban interfaces (WUIs) are prone to severe air quality degradation due to their proximity to active wildfire events [20, 21]. Thus, wildfire resiliency must be addressed as a part of climate hazard mitigation in the built environment.

1.1.2 Heatwaves and Climate Zone Shift

Heatwaves or prolonged hot weather events are becoming increasingly prevalent during summer seasons around the world. Within the past two decades, warm climate zone regions have experienced prolonged heatwaves with peak daytime conditions reaching temperatures above 45°C [22-24]. Cold climate zone regions, like Canada, have also experienced worsening heatwaves with peak outdoor temperatures well above 40°C and numerous locations breaking maximum temperature records by over 5°C [25]. Daytime heatwaves are caused by warm advection from anticyclonic circulation within the troposphere [22, 26]. The high air pressures associated with warming also prevent cloud formation, thereby increasing direct solar irradiance exposure and heatwave intensity [27]. Within urban zones, the effects of heatwaves are often compounded by the Urban Heat Island (UHI) effect [28]. UHI is a phenomenon that occurs when heat is absorbed and stored by building materials, asphalt, and concrete causing localized temperature increases within urban zones [28, 29]. High outdoor temperatures from both heatwaves and UHI increases the risk of urban heat-related illness and mortality for urban zone occupants [30]. In colder climate zones, existing summer design conditions do not account for heatwave-induced outdoor design temperatures [31]. As a result, many existing constructions may not be designed nor equipped to maintain adequate indoor thermal conditions in heatwave conditions [32, 33]. This highlights the need for the proactive implementation of engineering controls to better regulate indoor thermal conditions in the summer season.

1.2 Building Envelope

The building envelope serves as a barrier between outdoor conditions and the indoor environment. Thus, building envelope quality greatly impacts a building's ability to maintain adequate IEQ amid variable outdoor conditions. Achieving heatwave-related hazard resiliency in buildings requires

the identification of key building envelope components that impact both indoor air quality and indoor thermal control. Building air tightness describes the amount of infiltration or uncontrolled airflow that occurs across the building envelope through gaps, cracks, and transition points between envelope components [34]. Limiting infiltration in buildings is crucial to maintaining desired building pressurization and minimizing non-conditioned airflow sources into the indoor space [35, 36]. In the case of wildfire-related hazards, building air tightness ensures that airflow into the indoor space is limited to the supply air that has been filtered and conditioned through a dedicated mechanical ventilation system.

Effective control of indoor thermal conditions requires managing heat flux across the building envelope. Heat flux, in the form of conduction, convection, and radiation, occurs across various components of a building envelope. Studies on building energy efficiency have identified windows as the weakest link among building envelope components with their associated inefficiencies contributing up to 10% of a building's energy use [37, 38]. Energy inefficiencies associated with glazing are further amplified in new building constructions that favor glazing-dominant exterior facades [39]. In addition to the thermal resistivity limitations of glazing units, they also result in indoor heat gain due to solar irradiance. High Window-to-Wall ratio (WWR) indoor spaces will face challenges in maintaining comfortable indoor thermal conditions during heatwaves resulting from excess heat gain from both direct solar irradiance exposure and high outdoor temperatures. Thus, implementing technologies and strategies that improve the glazing thermal properties and optimize indoor solar gain is crucial in maintaining indoor thermal conditions.

1.3 Climate Hazard Mitigation Techniques and Strategies

1.3.1 Wildfire Smoke

Wildfire smoke-related hazard mitigation techniques generally involve minimizing indoor exposure to particulate matter. However, there is currently no standard that outlines best practices in wildfire-resilient building systems design. In response, the American Society of Heating, Refrigerating and Air-Conditioning Engineers (ASHRAE) released a planning framework that outlined wildfire-optimized or "Smoke Ready Mode" operation of commercial heating, ventilation, and air conditioning (HVAC) systems [40]. This document highlighted the importance of limiting points of infiltration within the building envelope and mechanical ventilation system upgrades to prevent particulate matter from being introduced into the indoor space. Topics related to the impact of air filter development [41-43], particle removal mechanisms [42-44], and mechanical ventilation system parameters [45, 46] have been previously studied within building science research. However, research on the interactions between all these variables and their overall impact on indoor air quality has not been studied. Thus, the first part of this thesis focuses on the development of wildfire-resilient mechanical ventilation systems as a mitigation strategy for wildfire smoke exposure. Both mechanical ventilation system-related variables and geographical location-related variables – such as intensity of wildfire smoke exposure and building design specifications – were considered to ensure the resultant system recommendation was tailored to the needs of the location of interest.

1.3.2 Heat Flux and Solar Gain

To improve building energy performance, researchers have focused on the development of technologies and strategies to improve the energy efficiency of fenestration systems. These technologies and strategies (treatments) differ based on where they are implemented within the fenestration system and the mechanism behind the technology's obtained energy savings. Some treatment interacts directly with the surface of the window or frame, such as in the case of window

films [47-49], insulation panels [50, 51], and window frame thermal bridging reduction [52, 53]. Other treatments act at a distance away from the surface of the fenestration system, such as in the case of window coverings [54-56]. Fenestration-related technologies are effective for improving building energy performance – given their mechanism for energy-saving is strategically relevant for the building of interest. Due to the effectiveness of automated shading systems for cooling load reduction by regulating solar radiative gain, this thesis focused on further developing this technology for use in Canadian climates. The warm climate zone implementation of automated shading systems and its impact on building energy performance has been studied in detail within building science research. However, it is unknown whether the technology has the same impact on thermal comfort regulation and building energy performance for buildings located in cold climate zones. Thus, the second part of this thesis focuses on the development of a cold climate-optimized automated shading system as a mitigation strategy for indoor thermal discomfort due to heatwave conditions.

1.4 Mathematical Modelling

System-specific mathematical models were developed to gain a detailed understanding of the governing variables that impact technology effectiveness. For wildfire-resilient ventilation systems, single-zone IAQ models from Table E-1 within Appendix E of ANSI/ASHRAE Standard 62.2-2019 were used as the basis where which all other mechanical ventilation system configurations were derived. The fundamental model was a particulate matter mass balance model for a single-zone mechanical ventilation system that considered building envelope infiltration and particle depositional losses. In practice, both variable air volume (VAV) and constant air volume (CAV) systems are used in buildings for mechanical ventilation. As a result, the mathematical models developed differentiated between the two systems to assess their respective performances

in wildfire-induced outdoor air quality conditions. Mathematical modelling was also used to understand the impact of automated shading systems on the heat flux across glazing units. The governing equations for complex fenestration outlined by the ASHRAE Fundamentals handbook were used to model the shading system and its interactions with the window [34]. Variables specific to the automated shading system including shade material opacity and reflectivity was provided by AI Shading, the manufacturer of the automated shading prototype.

The benefit of mathematical modelling over the conventional industry practice of building energy modelling is the ability to analyze the impact of a particular variable and its effect on the rest of the system. In this thesis, a variance-based global sensitivity analysis methodology (also known as the Sobol' method) was applied to assess the effect of various building, and climate zone-based variables on the overall effectiveness of a retrofit technology [57]. Variance-based sensitivity analyses represent uncertainties in input and output variables in the form of probability distributions. In comparison to regression analysis – which utilizes linear regression and calculated regression coefficients to assess the impact of variation in input variables, the Sobol' method represents the variance of input and output variables in the form of probability distributions. This approach allows for input variable interactions and non-linear model behaviors to be captured within the analysis. The relative impact of individual variables is represented through their first-order and total-order sensitivity indices. The first-order index relates to the direct impact variation in a particular input variable on the modelled output. The total-order index considers the total impact of variability in a particular input variable - including its covariance and interaction effects with other input variables – on the modelled output. Note that a total order index much larger than its corresponding first order index of an input variable indicates that there are strong interaction effects present between the input variable and other model inputs. The indices range from 0 to 1

with larger values representative of variables where variation or uncertainty results in large variations of the modelled result. SALib, an open-source Python library was used to execute the sensitivity analyses within this thesis [57].

1.5 Analysis of Technology Feasibility

Assessing the feasibility of building retrofit strategies is critical in justifying their real-world implementation in buildings. The methodology used to assess technology feasibility is dependent upon the value that it adds to the building or the building needs that it addresses. In this thesis, feasibility has been assessed through a cost-benefit analysis. In a cost-benefit analysis, the overall cost of the technology is compared with a monetary estimate of the benefit achieved through technology implementation. The definition of technology benefit is dependent upon the function of the technology. For wildfire-resilient ventilation systems, the benefit attributed to the technology is the mitigation of acute and long-term health effects from indoor exposure to wildfire-sourced particulate matter. Chestnut et al. developed a set of Canadian policy-specific economic valuations regarding mortality risk reduction [58]. Based on an aggregate willingness to pay (WTP) for mortality risk reduction, the study proposed a range of acceptable value of statistical life (VSL) estimates [58]. VSL is often used in cost-benefit analyses to quantify the benefits associated with programs and technologies that reduce the risk of premature mortality. It should be clarified that although VSL is a representative value that relates to risk reduction and human mortality, it is not an estimate of the value of a person's life [58]. A mid-range VSL of CAD 6.5M was used in conjunction with region-specific risk for premature mortality due to wildfire smoke exposure to determine financially feasible mechanical ventilation system upgrade configurations for a particular test city of interest. For automated shading systems, the benefit attributed to the technology are the energy savings achieved through optimizing solar irradiance and heat transfer

at the window. Heating and cooling energy savings were presented as a monetary amount representative of annual energy savings based on regional heat and electricity utility costs. The annual monetary savings from automated shading implementation was used in conjunction with the cost of shading system manufacturing and installation to generate a technology payback period. These were compared with similar building envelope measures that also improve building energy performance.

1.6 Objectives

This thesis provides insights into urban climate change resiliency by addressing various climate hazards related to heatwaves in Canada. In this thesis, two climate hazard mitigation strategies are developed for Canadian climate zones to improve the climate change adaptability of the built environment in response to wildfire conditions and prolonged hot weather events.

To maintain adequate IAQ, particularly during the wildfire season, wildfire mitigation strategies were explored through the following research objectives:

- Development of mathematical models representative of advanced mechanical ventilation system configurations.
- Assessment of mechanical ventilation system configuration effectiveness in a range of wildfire conditions.
- Cost-benefit analysis of the proposed wildfire-resilient mechanical ventilation system configuration to justify the feasibility of its implementation in select test cities in Western Canada.

To maintain indoor thermal comfort during heatwave conditions, heatwave adaptability using automated shading systems was explored through the following research objectives:

- Development of a cold climate-optimized sensorless control strategy for automated roller shades.
- Assessment of automated shading system energy performance through building energy simulations and mathematical modelling.
- Quantification of the impact of automated shading system implementation on year-round building energy performance through a technology payback period.
- Verification of the cold climate-optimized automated control strategy effectiveness through executing a prototype field study to monitor indoor thermal conditions fluctuation in response to roller shade operation.

1.7 Thesis Outline

Chapter 1 provides background information on the effects of climate change and the various climate hazards relevant to Canadian climate zones. Fundamental knowledge is provided regarding the impact of climate hazards on indoor environmental quality, relevant building envelope components, and relevant climate hazard mitigation strategies. Building energy simulations, mathematical modelling, and feasibility analysis techniques are also described. Chapter 2 discusses the development and analysis of wildfire-resilient mechanical ventilation systems for use in single-detached residences located in various cities across Western Canada. The feasibility of the proposed mechanical ventilation system configuration was assessed through a cost-benefit analysis. Chapter 3 discusses the development and analysis of a cold climate-optimized automated shading system. Research findings from building energy simulations, mathematical modelling and prototype field study were used to quantify the effectiveness of automated shading systems to improve indoor thermal comfort and building energy performance. Finally, Chapter 4 provides a summary of the key research methods and findings of this work. The section concludes with a discussion regarding the limitations of this work and future research directions.

2. Wildfire-resilient mechanical ventilation systems for single-detached homes in cities of Western Canada

2.1.Introduction

In the past decade, higher-than-average seasonal temperatures have fueled an increase in wildfire frequency and intensity in Canada [12, 59, 60] and worldwide [17, 61, 62]. Studies regarding the impact of climate change on wildfires have noted that rising peak temperatures and drought conditions from precipitation anomalies are projected to result in an increase in the duration and frequency of wildfires on a global scale [17, 63]. Rapid urban development and its associated energy demands have been correlated with increases in human-induced carbon emissions [64]. In response, significant research efforts have been focused on technological developments to reduce greenhouse gas emissions from human activities [65, 66] and to stabilize the increasing global temperature trends [67]. There remains a need to equip communities and their respective inhabitants with strategies and technological innovations to cope with the localized effects of climate change [68, 69]. The goal of these strategies and innovations is to improve urban resiliency to increasingly variable outdoor conditions. Through resilient city planning, communities will benefit from enhanced liveability and functionality amid adverse climate-induced conditions. During the annual wildfire season, cities in close proximity to wooded areas experience a deterioration of outdoor air quality – and in turn, deterioration of IAQ – due to the release of smoke and particulate matter from active wildfire events. According to the results from the National Human Activity Pattern Survey (NHAPS), it was found that Americans spend up to 93% of their lives indoors [70]. Thus, wildfire resiliency must be considered in indoor environmental design to improve urban resiliency in cities prone to wildfire-related air quality concerns. This research aims to assess the ability of advanced mechanical ventilation strategies to minimize the introduction of wildfire smoke into indoor spaces.

Wildfire events release large volumes of gases and particulates – such as carbon monoxide (CO), ozone (O_3), VOCs, and PM – into the air. Of these contaminants, the PM2.5 concentration is often used as a primary measure of outdoor air quality due to the health risks associated with prolonged exposure to the contaminant [71, 72]. PM2.5 refers to particulate matter that is between 1 - 2.5 μm in size [72]. Due to their size, PM2.5 can infiltrate deep into lung tissue to impede normal respiratory function [72].

PM2.5 exposure at high concentrations within the indoor environment can lead to short-term and long-term adverse health effects in building occupants; these include acute respiratory symptoms, pulmonary inflammation, decreased lung function, aggravation of existing chronic respiratory conditions, and premature mortality [15, 73, 74]. Studies regarding the financial impact of wildfire events have quantified the cost of healthcare and pre-emptive symptom mitigation related to wildfire PM2.5 exposure [75, 76]. Richardson et al. detailed two approaches for quantifying the cost of wildfire health impacts: the illness method and the defensive behavior method [75]. Using the formula from Alberini et al. [77], the cost of illness method calculated the cost of each symptomatic day during the wildfire season [75]. The defensive behavior method was based on the average cost of averting and mitigating actions taken to minimize exposure to wildfire pollutants [75]. This is the preferred approach for quantifying health costs due to the ability to holistically represent health-related costs and includes factors that are not directly related to the cost of illness - including mitigation and aversion strategies employed by community members during active wildfire events [75]. A study by Pimpin et al. created a financial model to estimate the total health and social care cost associated with air pollutant exposure [76]. The study modeled the long-term effects of air pollutant exposure using mortality statistics obtained from national public health databases and data regarding various chronic terminal illnesses [76]. The Canadian

Ambient Air Quality Standard (CAAQS) recommends that daily PM2.5 exposure be limited to below 27 $\mu g/m^3$ [78]. However, depending on a city's proximity to an active wildfire event, the outdoor PM2.5 level can vary from 30 $\mu g/m^3$ to over 500 $\mu g/m^3$ [74, 79, 80].

To reduce direct exposure to PM2.5, public health recommendations often include remaining indoors and closing all doors and windows on smoky days [71, 72]. This emphasizes a need for ventilation-related control measures and continuous monitoring of IAQ to minimize human exposure to wildfire contaminants in indoor spaces. ASHRAE recently published a planning framework regarding an operations guideline for HVAC systems during wildfire events [40]. This planning framework discusses ways in which standard commercial HVAC systems can be configured for wildfire-optimized operation ("Smoke Ready Mode") to minimize occupant exposure to pollutants – such as PM2.5 – during active wildfire and prescribed burn events [40]. The guide details pre-wildfire HVAC maintenance, matching filter selection with the airflow capacity of the existing HVAC system, portable air cleaner usage, and the development and implementation of a "smoke readiness plan". Specific to the contaminants generated during wildfire events, the ASHRAE planning framework recommended that at minimum, MERV 11 or MERV 13 rated filters should be used in wildfire indoor ventilation systems. MERV 11 and MERV 13 filters showed effective at filtering out smaller particulates such as PM2.5 [41, 42]. In addition, the ASHRAE planning framework highlights the importance of IAQ monitoring to ensure the concentration of fine particulate matter and other contaminants are below the exposure limit [40].

Air filtration is commonly used in residential and commercial buildings to maintain acceptable IAQ. This process involves routing unfiltered air through filter media before introducing the air to the indoor space. Filter media captures debris and contaminants while allowing the cleaned air to pass through the filter. Several studies found that high-efficiency mechanical filters are effective

in reducing indoor PM2.5 concentration [41, 43, 74, 81, 82]. It has also been found that higher MERV ratings on filters were positively correlated to the filter's contaminant removal efficiency [41, 82]. Employing multiple filters at various locations within the air filtration system has also shown to be effective in maintaining acceptable IAQ [83]. Though air filtration is effective at reducing indoor pollutant exposure, filters introduce unwanted pressure drops and backpressure into the ventilation system [82, 84, 85]. Zhang et al. developed an electret filter coated with porous metal-organic particles capable of removing both VOCs and PM2.5 [20] to reduce filter-induced pressure losses. The novel filter had a higher initial filtration efficiency while inducing a significantly lower pressure drop than conventional mechanical filters [43]. Research regarding adaptive ventilation systems has demonstrated the technologies potential to optimize system energy usage while maintaining its filtration capacity [84, 86]. A study by Cao et al. proposed an adaptive ventilation system that adjusted the ventilation strategy in response to the outdoor air quality [84]. The type of filter used for air filtration varied for each ventilation configuration to obtain acceptable IAQ while minimizing the total energy consumption; a medium-efficiency filter was used for slightly polluted outdoor conditions, while a high efficiency particulate air (HEPA) filter was used for the mid to heavily polluted outdoor conditions [84]. Several studies have demonstrated the effectiveness of portable air cleaners (PAC) to provide additional localized air filtration in indoor spaces [44, 87-90]. It was found that PAC effectiveness was the highest when the device was run on an automatic setting rather than a user-controlled setting [44, 88]. Stauffer et al. conducted a field study investigating PAC effectiveness to remove wildfire-related PM2.5 from an indoor office environment [87]. The field study found that the PACs were able to reduce the PM2.5 concentration within an office space by 73% and 92% during occupied and non-occupied hours, respectively [87]. Barn et al. conducted a field study in British Columbia, Canada,

to investigate the impact of PAC usage on reducing the indoor concentration of PM2.5 from both wildfire smoke infiltration and residential wood-burning [89]. It was found that PAC usage reduced the indoor PM2.5 concentration by approximately 55% and 65% for residential wood-burning and wildfire smoke, respectively [89]. It should be mentioned that PAC effectiveness is limited by the clean air delivery rate (CADR) [91]. Thus, PACs must be appropriately sized for the floor area of the indoor space to provide the expected air cleaning efficiency.

IAQ relating to PM2.5 concentration is also affected by various factors unrelated to the air filtration setup. Such factors include occupant activities [92, 93], building infiltration rate [88], building envelope quality [94], air recirculation rate [46, 83], and building type-dependent air change rate [95, 96]. Factors that affect IAQ have been individually studied in great detail. However, there is limited research regarding the combined effect of these factors with various ventilation system configurations on IAQ. Also, the economic and health benefits of the implementation of smoke-mode ventilation strategies are unclear. This section aims to model the combined effect of ventilation system configurations and variables to determine viable ventilation strategies for improving IAQ in wildfire conditions. IAQ data is used in conjunction with cost estimate variables – ventilation system hardware costs, cost of installation and maintenance, and health costs related to PM2.5 exposure – within a cost-benefit financial analysis to assess the economic feasibility of the proposed ventilation configurations for application in single-detached homes.

2.2. Methodology

2.2.1. City Selection and Compilation of Wildfire Data

Four major cities in Western Canada were selected for the simulation study: Prince George, Vancouver, Victoria, and Edmonton. These cities varied in their proximity to typical wildfire event hotspots and therefore differed in their level of exposure to PM2.5. For example, Prince George is considered a city within the Wildland-Urban Interface (WUI) and typically experiences the highest

exposure to wildfire-related pollutants [97]. In comparison, Victoria, Vancouver, and Edmonton are located further away from wildland zones and therefore experience less severe levels of pollutant exposure during active wildfire events. For cities within British Columbia (BC), air quality data between May and September of 2018 were selected due to the severity and intensity of the 2018 wildfire season [14]. Similar criteria were used to select the wildfire dataset most representative of worst-case wildfire pollution levels for Edmonton, Alberta. It was found that the 2018 BC wildfires had a comparatively mild effect on the outdoor air quality in Edmonton. As a result, the Edmonton air quality data from the 2019 wildfire season between May and September was selected for the simulation study.

The hourly outdoor PM2.5 level from May to the end of September 2018 was obtained from the British Columbia Ministry of Environment air data archive for Prince George, Vancouver, and Victoria [80]. For Edmonton, the hourly outdoor PM2.5 level from May to the end of September 2019 was obtained from Alberta Environment and Parks and Airshed [79]. The PM2.5 level per day was found by taking a simple average of the PM2.5 measurements over 24 hours. This was carried out on each outdoor air quality dataset to determine peak pollutant exposure days and allow for further analysis based on the requirements stated in the CAAQS [78]. A 10-day span in August 2018 was selected as the outdoor PM2.5 dataset for Prince George, Vancouver, and Victoria, while a 10-day span from May – June 2019 was selected for Edmonton, representing worst-case outdoor PM2.5 exposure conditions. The outdoor PM2.5 ranges for the selected 10-day datasets were as follows: Prince George (19 – 788 $\mu g/m^3$), Vancouver (0 – 165 $\mu g/m^3$), Victoria (0 – 298 $\mu g/m^3$), Edmonton (2 – 1479 $\mu g/m^3$).

2.2.2. IAQ Models

IAQ models were developed to determine the effect of filter efficiency, outdoor airflow rate, and various ventilation flow setups on the steady-state indoor PM2.5 concentration. Figure 1 shows a general schematic of the single-zone ventilation system referenced in developing 17 single-zone IAQ models used in the study. The first six IAQ models were taken from Appendix Table E-1 of ANSI/ASHRAE Standard 62.1-2019 [95] and modified to include two additional variables: building envelope infiltration and PM2.5 depositional losses. The remaining 11 models were derived based on the mass balance principle and included both the infiltration and depositional loss terms. Each IAQ model considers the effect of outdoor PM2.5 concentration, building infiltration, and ventilation system-dependent factors – such as air distribution effectiveness, flow reduction, and air recirculation – on the steady-state PM2.5 levels.

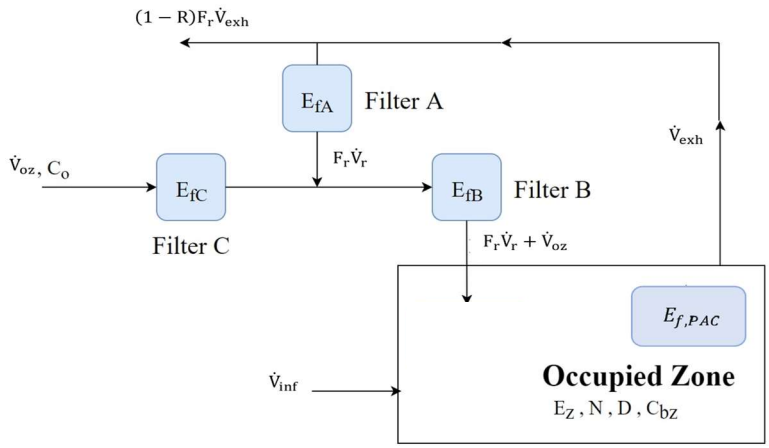

Figure 1. General schematic of the single-zone ventilation system used for IAQ model development.

The IAQ models developed for this study were governed by the conservation of mass for open systems.

$$\sum \dot{V}_{in} - \sum \dot{V}_{out} = \frac{dV_{CV}}{dt}$$

Since the models represented the mechanical ventilation system at steady-state operating conditions, the time differential of air volume within the control volume would approach zero as $t \to \infty$.

$$\sum \dot{V}_{in} - \sum \dot{V}_{out} = 0$$

Therefore,

$$\sum \dot{V}_{in} = \sum \dot{V}_{out} \tag{1}$$

It is assumed that air volume in the indoor space (CV) is constant when system equilibrium is reached. Thus, as $t \to \infty$ the time differential of air volume in the CV, $\frac{dV_{CV}}{dt} = 0$.

$$\sum \dot{V}_{in} - \sum \dot{V}_{out} = 0 \tag{2}$$

Equation (3) is the rearranged form of Equation (2) - the original mass balance that equates the inlet and outlet air volume flow rate.

$$\sum \dot{V}_{in} = \sum \dot{V}_{out} \tag{3}$$

Equation (4) shows the application of Equation (3) to the context of the study's IAQ model. The air mass balance of the ventilation system is of the following form where $\dot{V}_{oz}$ is the volumetric flowrate of outdoor air, $\dot{V}_r$ is the volumetric flow rate of recirculated air, $\dot{V}_{inf}$ is the infiltration rate,

and $\dot{V}_{ex}$ is the volumetric flow rate of exhaust air. Note that the volumetric flow rate of PM2.5 is directly related to the volumetric flow rate of the air into and out of the indoor space.

$$(1 - R)\dot{V}_{oz} + \dot{V}_r + \dot{V}_{inf} = \dot{V}_{exh} \tag{4}$$

In the context of a ventilation system, the recirculated air volumetric flow rate ($\dot{V}_r$) is related to the outdoor air volumetric flow rate ($\dot{V}_{oz}$), infiltration rate ($\dot{V}_{inf}$), and exhaust air volumetric flow rate ($\dot{V}_{exh}$) through the recirculation factor (R) as follows:

$$\dot{V}_r = R\dot{V}_{ex} \tag{5}$$

Using Equation (5), Equation (4) can be re-written as follows:

$$\dot{V}_{oz} + \dot{V}_{inf} + R\dot{V}_{exh} = \dot{V}_{ex} \tag{6.1}$$

Rearranging for $\dot{V}_{exh}$:

$$\dot{V}_{exh} = \frac{\dot{V}_{oz} + \dot{V}_{inf}}{1 - R} \tag{6.2}$$

Combining equations (5) and (6.2), $\dot{V}_r$ can be re-defined in terms of $\dot{V}_{oz}$ and $\dot{V}_{inf}$.

$$\dot{V}_r = R\left(\frac{\dot{V}_{oz} + \dot{V}_{inf}}{1 - R}\right) \tag{7}$$

Model 1 represents a rudimentary VAV mechanical ventilation system with no filters and no recirculation (100% outdoor air). The derivation of the model 1 is as follows.

Mass Balance:

$$C_o E_Z \dot{V}_{oz} + \dot{N} + C_o E_z \dot{V}_{inf} = \dot{D} + C_{bz} E_z \dot{V}_{exh} + C_{bz} E_z \dot{V}_{inf}$$

Substituting $\dot{V}_{exh}$ with the mass balance relation as shown in Eq. 6.2. Note that there is no recirculation in this model, therefore $\dot{V}_r = 0$:

$$C_o E_Z \dot{V}_{oz} + \dot{N} + C_o E_z \dot{V}_{inf} = \dot{D} + C_{bz} E_z \left(F_r \dot{V}_{oz} + \dot{V}_{inf}\right) + C_{bz} E_z \dot{V}_{inf}$$

Isolating for C_{bz}:

$$C_{bz} = \frac{\dot{N} - \dot{D}}{E_z \left(F_r \dot{V}_{oz} + \dot{V}_{inf}\right)} + C_o$$

Isolating for $\dot{V}_{oz}$:

$$\dot{V}_{oz} = \frac{N - D}{E_Z F_r (C_{bz} - C_o)} - \frac{\dot{V}_{inf}}{F_r}$$

Model 2 represents a CAV mechanical ventilation system with a filter located at location A and constant outdoor air. The derivation of Model 2 is as follows.

Mass Balance:

$$C_o E_Z \dot{V}_{oz} + C_{bz} E_z \left(1 - E_{fA}\right) \dot{V}_r + \dot{N} + C_o E_z \dot{V}_{inf} = \dot{D} + C_{bz} E_z \dot{V}_{exh}$$

Substituting $\dot{V}_{exh}$ with the mass balance relation as shown in Eq. 6.2:

$$C_o E_Z \dot{V}_{oz} + C_{bz} E_z \left(1 - E_{fA}\right) \dot{V}_r + \dot{N} + C_o E_z \dot{V}_{inf} = \dot{D} + C_{bz} E_z \left(\dot{V}_{oz} + \dot{V}_r + \dot{V}_{inf}\right)$$

Isolating for C_{bz}:

$$C_{bz} = \frac{\dot{N} - \dot{D} + C_o E_z(\dot{V}_{inf} + \dot{V}_{oz})}{E_z(\dot{V}_{oz} + E_{fA}\dot{V}_r + \dot{V}_{inf})}$$

Isolating for V_{oz}:

$$\dot{V}_{oz} = \frac{N - D - E_Z C_{bz}(E_{f_A}\dot{V}_r + \dot{V}_{inf}) + C_o E_Z \dot{V}_{inf}}{E_Z(C_{bz} - C_o)}$$

Model 3 represents a VAV mechanical ventilation system with a filter located at location A and constant outdoor air. The derivation of Model 3 is as follows.

Mass Balance:

$$C_o E_Z \dot{V}_{oz} + C_{bz} E_z F_r(1 - E_{fA})\dot{V}_r + \dot{N} + C_o E_z \dot{V}_{inf} = \dot{D} + C_{bz} E_z \dot{V}_{exh}$$

Substituting $\dot{V}_{exh}$ with the mass balance relation as shown in Eq. 6.2:

$$C_o E_Z \dot{V}_{oz} + C_{bz} E_z F_r(1 - E_{fA})\dot{V}_r + \dot{N} + C_o E_z \dot{V}_{inf} = \dot{D} + C_{bz} E_z(\dot{V}_{oz} + F_r\dot{V}_r + \dot{V}_{inf})$$

Isolating for C_{bz}:

$$C_{bz} = \frac{\dot{N} - \dot{D} + C_o E_z(\dot{V}_{inf} + \dot{V}_{oz})}{E_z(\dot{V}_{oz} + F_r E_{fA}\dot{V}_r + \dot{V}_{inf})}$$

Isolating for V_{oz}:

$$\dot{V}_{oz} = \frac{N - D - E_Z C_{bz}(F_r E_{f_A}\dot{V}_r + \dot{V}_{inf}) + C_o E_Z \dot{V}_{inf}}{E_Z(C_{bz} - C_o)}$$

Model 4 represents a CAV mechanical ventilation system with a filter located at location B and constant outdoor air. The derivation of Model 4 is as follows.

Mass Balance:

$$C_o E_Z \dot{V}_{oz}(1 - E_{fB}) + C_{bz} E_z \left(1 - E_{fB}\right)\dot{V}_r + \dot{N} + C_o E_z \dot{V}_{inf} = \dot{D} + C_{bz} E_z \dot{V}_{exh}$$

Substituting $\dot{V}_{exh}$ with the mass balance relation as shown in Eq. 6.2:

$$C_o E_Z \dot{V}_{oz}(1 - E_{fB}) + C_{bz} E_z \left(1 - E_{fB}\right)\dot{V}_r + \dot{N} + C_o E_z \dot{V}_{inf} = \dot{D} + C_{bz} E_z \left(\dot{V}_{oz} + \dot{V}_r + \dot{V}_{inf}\right)$$

Isolating for C_{bz}:

$$C_{bz} = \frac{\dot{N} - \dot{D} + C_o E_Z \left(\dot{V}_{oz}\left(1 - E_{fB}\right) + \dot{V}_{inf}\right)}{E_z \left(\dot{V}_{oz} + E_{fB}\dot{V}_r + \dot{V}_{inf}\right)}$$

Isolating for V_{oz}:

$$\dot{V}_{oz} = \frac{\dot{N} - \dot{D} - E_z \left(C_o \dot{V}_{inf} - C_{bz}\left(E_{fB}\dot{V}_r + \dot{V}_{inf}\right)\right)}{E_Z \left(C_{bz} - C_o\left(1 - E_{fB}\right)\right)}$$

Model 5 represents a VAV mechanical ventilation system with a filter located at location B and no recirculation (100% outdoor air). The derivation of Model 5 is as follows.

Mass Balance:

$$C_o E_Z \dot{V}_{oz}(1 - E_{fB}) + \dot{N} + C_o E_z \dot{V}_{inf} = \dot{D} + C_{bz} E_z \dot{V}_{ex}$$

Substituting $\dot{V}_{ex}$ with the mass balance relation as shown in Eq. 6.2. Note that there is no recirculation in this model, therefore $\dot{V}_r = 0$:

$$C_o E_Z \dot{V}_{oz}(1 - E_{fB}) + \dot{N} + C_o E_z \dot{V}_{inf} = \dot{D} + C_{bz} E_z \left(F_r \dot{V}_{oz} + \dot{V}_{inf}\right)$$

Isolating for C_{bz}:

$$C_{bz} = \frac{\dot{N} - \dot{D} + C_o E_Z\left(\dot{V}_{oz}\left(1 - E_{fB}\right) + \dot{V}_{inf}\right)}{E_z\left(F_r \dot{V}_{oz} + \dot{V}_{inf}\right)}$$

Isolating for V_{oz}:

$$\dot{V}_{oz} = \frac{\dot{N} - \dot{D} - E_z \dot{V}_{inf}(C_o - C_{bz})}{E_Z\left(F_r C_{bz} - C_o\left(1 - E_{fB}\right)\right)}$$

Model 6 represents a VAV mechanical ventilation system with a filter located at location B and constant outdoor air. The derivation for Model 6 is as follows.

Mass Balance:

$$C_o E_Z \dot{V}_{oz}(1 - E_{fB}) + C_{bz} F_r E_z\left(1 - E_{fB}\right)\dot{V}_r + \dot{N} + C_o E_z \dot{V}_{inf} = \dot{D} + C_{bz} F_r E_z \dot{V}_{exh}$$

Substituting $\dot{V}_{exh}$ with the mass balance relation as shown in Eq. 6.2:

$$C_o E_Z \dot{V}_{oz}(1 - E_{fB}) + C_{bz} F_r E_z\left(1 - E_{fB}\right)\dot{V}_r + \dot{N} + C_o E_z \dot{V}_{inf} = \dot{D} + C_{bz} E_z\left(\dot{V}_{oz} + F_r \dot{V}_r + \dot{V}_{inf}\right)$$

Isolating for C_{bz}:

$$C_{bz} = \frac{\dot{N} - \dot{D} + C_o E_Z\left(\dot{V}_{oz}\left(1 - E_{fB}\right) + \dot{V}_{inf}\right)}{E_z\left(\dot{V}_{oz} + F_r E_{fB} \dot{V}_r + \dot{V}_{inf}\right)}$$

Isolating for $\dot{V}_{oz}$:

$$\dot{V}_{oz} = \frac{\dot{N} - \dot{D} + E_z\left(C_o \dot{V}_{inf} - C_{bz}\left(F_r E_{fB} \dot{V}_r + \dot{V}_{inf}\right)\right)}{E_Z\left(C_{bz} - C_o\left(1 - E_{fB}\right)\right)}$$

Model 7a represents a CAV mechanical ventilation system with a filter located at location C and constant outdoor air. The derivation for Model 7a is as follows.

Mass Balance:

$$C_o E_Z \dot{V}_{oz}(1 - E_{fC}) + C_{bz} E_z \dot{V}_r + \dot{N} + C_o E_z \dot{V}_{inf} = \dot{D} + C_{bz} E_z \dot{V}_{exh}$$

Substituting $\dot{V}_{exh}$ with the mass balance relation as shown in Eq. 6.2:

$$C_o E_Z \dot{V}_{oz}(1 - E_{fC}) + C_{bz} E_z \dot{V}_r + \dot{N} + C_o E_z \dot{V}_{inf} = \dot{D} + C_{bz} E_z \left(\dot{V}_{oz} + \dot{V}_r + \dot{V}_{inf}\right)$$

Isolating for C_{bz}:

$$C_{bz} = \frac{\dot{N} - \dot{D} + C_o E_Z \left(\dot{V}_{oz}\left(1 - E_{fC}\right) + \dot{V}_{inf}\right)}{E_z \left(\dot{V}_{oz} + \dot{V}_{inf}\right)}$$

Isolating for $\dot{V}_{oz}$:

$$\dot{V}_{oz} = \frac{\dot{N} - \dot{D} + E_z \dot{V}_{inf}(C_o - C_{bz})}{E_Z \left(C_{bz} - C_o\left(1 - E_{fC}\right)\right)}$$

Model 7b represents a VAV mechanical ventilation system with a filter located at location C and constant outdoor air. The derivation for Model 7b is as follows.

Mass Balance:

$$C_o E_Z \dot{V}_{oz}(1 - E_{fC}) + C_{bz} E_z F_r \dot{V}_r + \dot{N} + C_o E_z \dot{V}_{inf} = \dot{D} + C_{bz} E_z \dot{V}_{exh}$$

Substituting $\dot{V}_{exh}$ with the mass balance relation as shown in Eq. 6.2:

$$C_o E_Z \dot{V}_{oz}(1 - E_{fC}) + C_{bz} E_z F_r \dot{V}_r + \dot{N} + C_o E_z \dot{V}_{inf} = \dot{D} + C_{bz} E_z \left(\dot{V}_{oz} + F_r \dot{V}_r + \dot{V}_{inf}\right) + C_{bz} E_z \dot{V}_{inf}$$

Isolating for C_{bz}:

$$C_{bz} = \frac{\dot{N} - \dot{D} + C_o E_Z\left(\dot{V}_{oz}\left(1 - E_{fC}\right) + \dot{V}_{inf}\right)}{E_z\left(\dot{V}_{oz} + \dot{V}_{inf}\right)}$$

Isolating for $\dot{V}_{oz}$:

$$\dot{V}_{oz} = \frac{\dot{N} - \dot{D} + E_z \dot{V}_{inf}(C_o - C_{bz})}{E_Z\left(C_{bz} - C_o\left(1 - E_{fC}\right)\right)}$$

Model 8 represents a VAV mechanical ventilation system with a filter located at C and no recirculation (100% outdoor air). The derivation for Model 8 is as follows.

Mass Balance:

$$C_o E_Z F_r \dot{V}_{oz}(1 - E_{fC}) + C_{bz} E_z F_r \dot{V}_r + \dot{N} + C_o E_z \dot{V}_{inf} = \dot{D} + C_{bz} F_r E_z \dot{V}_{exh}$$

Substituting $\dot{V}_{exh}$ with the mass balance relation as shown in Eq. 6.2. Note that there is no recirculation in this model, therefore $\dot{V}_r = 0$:

$$C_o E_Z F_r \dot{V}_{oz}(1 - E_{fC}) + \dot{N} + C_o E_z \dot{V}_{inf} = \dot{D} + C_{bz} E_z\left(F_r \dot{V}_{oz} + \dot{V}_{inf}\right)$$

Isolating for C_{bz}:

$$C_{bz} = \frac{\dot{N} - \dot{D} + C_o E_Z\left(F_r \dot{V}_{oz}\left(1 - E_{fC}\right) + \dot{V}_{inf}\right)}{E_z\left(F_r \dot{V}_{oz} + \dot{V}_{inf}\right)}$$

Isolating for $\dot{V}_{oz}$:

$$\dot{V}_{oz} = \frac{\dot{N} - \dot{D} + E_z \dot{V}_{inf}(C_o - C_{bz})}{E_Z F_r\left(C_{bz} - C_o\left(1 - E_{fC}\right)\right)}$$

Model 9 represents a double filter, CAV mechanical ventilation system with filters located at locations A and B and constant outdoor air. The derivation for Model 9 is as follows.

Mass Balance:

$$C_o E_Z \dot{V}_{oz}(1 - E_{fB}) + C_{bz} E_z \big(1 - E_{fA}\big)\big(1 - E_{fB}\big)\dot{V}_r + \dot{N} + C_o E_z \dot{V}_{inf} = \dot{D} + C_{bz} E_z \dot{V}_{exh}$$

Substituting $\dot{V}_{exh}$ with the mass balance relation as shown in Eq. 6.2:

$$C_o E_Z \dot{V}_{oz}(1 - E_{fB}) + C_{bz} E_z \big(1 - E_{fA}\big)\big(1 - E_{fB}\big)\dot{V}_r + \dot{N} + C_o E_z \dot{V}_{inf}$$

$$= \dot{D} + C_{bz} E_z \big(\dot{V}_{oz} + \dot{V}_r + \dot{V}_{inf}\big)$$

Isolating for C_{bz}:

$$C_{bz} = \frac{\dot{N} - \dot{D} + C_o E_Z \big(\dot{V}_{oz}\big(1 - E_{fB}\big) + \dot{V}_{inf}\big)}{E_z \big(\dot{V}_{oz} + \dot{V}_{inf} + \big(E_{fA} + E_{fB} - E_{fA} E_{fB}\big)\dot{V}_r\big)}$$

Isolating for V_{oz}:

$$\dot{V}_{oz} = \frac{\dot{N} - \dot{D} + E_z \left(C_o \dot{V}_{inf} - C_{bz}\big(\dot{V}_{inf} + \big(E_{fA} + E_{fB} - E_{fA} E_{fB}\big)\dot{V}_r\big)\right)}{E_Z \left(C_{bz} - C_o\big(1 - E_{fB}\big)\right)}$$

Model 10 represents a double filter, VAV mechanical ventilation system with filters located at locations A and B and constant outdoor air. The derivation for Model 10 is as follows.

Mass Balance:

$$C_o E_Z \dot{V}_{oz}(1 - E_{fB}) + C_{bz} E_z F_r \big(1 - E_{fA}\big)\big(1 - E_{fB}\big)\dot{V}_r + \dot{N} + C_o E_z \dot{V}_{inf} = \dot{D} + C_{bz} E_z \dot{V}_{exh}$$

Substituting $\dot{V}_{exh}$ with the mass balance relation as shown in Eq. 6.2:

$$C_o E_Z \dot{V}_{oz}(1 - E_{fB}) + C_{bz} F_r E_z \big(1 - E_{fA}\big)\big(1 - E_{fB}\big)\dot{V}_r + \dot{N} + C_o E_z \dot{V}_{inf}$$

$$= \dot{D} + C_{bz} E_z \big(\dot{V}_{oz} + F_r \dot{V}_r + \dot{V}_{inf}\big)$$

Isolating for C_{bz}:

$$C_{bz} = \frac{\dot{N} - \dot{D} + C_o E_Z \big(F_r \dot{V}_{oz}\big(1 - E_{fB}\big) + \dot{V}_{inf}\big)}{E_z \big(\dot{V}_{oz} + \dot{V}_{inf} + F_r \big(E_{fA} + E_{fB} - E_{fA} E_{fB}\big)\dot{V}_r\big)}$$

Isolating for V_{oz}:

$$\dot{V}_{oz} = \frac{\dot{N} - \dot{D} + E_z \left(C_o \dot{V}_{inf} - C_{bz}\big(\dot{V}_{inf} + F_r \big(E_{fA} + E_{fB} - E_{fA} E_{fB}\big)\dot{V}_r\big)\right)}{E_Z \left(C_{bz} - C_o \big(1 - E_{fB}\big)\right)}$$

Model 11 represents a double filter, CAV mechanical ventilation system with filters located at locations B and C and constant outdoor air. The derivation for Model 11 is as follows.

Mass Balance:

$$C_o E_Z \dot{V}_{oz}\big(1 - E_{fB}\big)\big(1 - E_{fC}\big) + C_{bz} E_z \big(1 - E_{fB}\big)\dot{V}_r + \dot{N} + C_o E_z \dot{V}_{inf} = \dot{D} + C_{bz} E_z \dot{V}_{exh}$$

Substituting $\dot{V}_{ex}$ with the mass balance relation as shown in Eq. 6.2:

$$C_o E_Z \dot{V}_{oz}(1 - E_{fB})\big(1 - E_{fC}\big) + C_{bz} E_z \big(1 - E_{fB}\big)\dot{V}_r + \dot{N} + C_o E_z \dot{V}_{inf}$$

$$= \dot{D} + C_{bz} E_z \big(\dot{V}_{oz} + \dot{V}_r + \dot{V}_{inf}\big)$$

Isolating for C_{bz}:

$$C_{bz} = \frac{\dot{N} - \dot{D} + C_o E_Z \big(\dot{V}_{oz}\big(1 - E_{fB}\big)\big(1 - E_{fC}\big) + \dot{V}_{inf}\big)}{E_z \big(\dot{V}_{oz} + E_{fB} \dot{V}_r + \dot{V}_{inf}\big)}$$

Isolating for V_{oz}:

$$V_{oz} = \frac{\dot{N} - \dot{D} + E_z\left(C_o\dot{V}_{inf} - C_{bz}\left(E_{fB}\dot{V}_r + \dot{V}_{inf}\right)\right)}{E_Z\left(C_{bz} - C_o\left(1 - E_{fB}\right)\left(1 - E_{fC}\right)\right)}$$

Model 12 represents a double filter, VAV mechanical ventilation system with filters located at locations B and C and no recirculation (100% outdoor air). The derivation for Model 12 is as follows.

Mass Balance:

$$C_o E_Z F_r \dot{V}_{oz}\left(1 - E_{fB}\right)\left(1 - E_{fC}\right) + C_{bz} E_z F_r\left(1 - E_{fB}\right)\dot{V}_r + \dot{N} + C_o E_z \dot{V}_{inf} = \dot{D} + C_{bz} E_z \dot{V}_{ex}$$

Substituting $\dot{V}_{exh}$ with the mass balance relation as shown in Eq. 6.2. Note that there is no recirculation in this model, therefore $\dot{V}_r = 0$:

$$C_o E_Z F_r \dot{V}_{oz}(1 - E_{fB})\left(1 - E_{fC}\right) + \dot{N} + C_o E_z \dot{V}_{inf} = \dot{D} + C_{bz} E_z\left(F_r \dot{V}_{oz} + \dot{V}_{inf}\right)$$

Isolating for C_{bz}:

$$C_{bz} = \frac{\dot{N} - \dot{D} + C_o E_Z\left(F_r \dot{V}_{oz}\left(1 - E_{fB}\right)\left(1 - E_{fC}\right) + \dot{V}_{inf}\right)}{E_z\left(F_r \dot{V}_{oz} + \dot{V}_{inf}\right)}$$

Isolating for V_{oz}:

$$\dot{V}_{oz} = \frac{\dot{N} - \dot{D} + E_z \dot{V}_{inf}(C_o - C_{bz})}{E_Z F_r\left(C_{bz} - C_o\left(1 - E_{fB}\right)\left(1 - E_{fC}\right)\right)}$$

Model 13 represents a double filter, VAV mechanical ventilation system with filters located at locations B and C and constant outdoor air. The derivation for Model 13 is as follows.

Mass Balance:

$$C_o E_Z F_r \dot{V}_{oz}(1 - E_{fB})(1 - E_{fC}) + C_{bz} E_z F_r (1 - E_{fB}) \dot{V}_r + \dot{N} + C_o E_z \dot{V}_{inf} = \dot{D} + C_{bz} F_r E_z \dot{V}_{exh}$$

Substituting $\dot{V}_{exh}$ with the mass balance relation as shown in Eq. 6.2:

$$C_o E_Z F_r \dot{V}_{oz}(1 - E_{fB})(1 - E_{fC}) + C_{bz} E_z F_r (1 - E_{fB}) \dot{V}_r + \dot{N} + C_o E_z \dot{V}_{inf}$$

$$= \dot{D} + C_{bz} E_z (\dot{V}_{oz} + F_r \dot{V}_r + \dot{V}_{inf})$$

Isolating for C_{bz}:

$$C_{bz} = \frac{\dot{N} - \dot{D} + C_o E_Z (\dot{V}_{oz}(1 - E_{fB})(1 - E_{fC}) + \dot{V}_{inf})}{E_z (\dot{V}_{oz} + F_r E_{fB} \dot{V}_r + \dot{V}_{inf})}$$

Isolating for V_{oz}:

$$\dot{V}_{oz} = \frac{\dot{N} - \dot{D} + E_z \left(C_o \dot{V}_{inf} - C_{bz} (F_r E_{fB} \dot{V}_r + \dot{V}_{inf}) \right)}{E_Z \left(C_{bz} - C_o (1 - E_{fB})(1 - E_{fC}) \right)}$$

Model 14 represents a double filter, CAV mechanical ventilation system with filters located at locations A and C and constant outdoor air. The derivation for Model 14 is as follows.

Mass Balance:

$$C_o E_Z \dot{V}_{oz}(1 - E_{fC}) + C_{bz} E_z (1 - E_{fA}) \dot{V}_r + \dot{N} + C_o E_z \dot{V}_{inf} = \dot{D} + C_{bz} E_z \dot{V}_{exh}$$

Substituting $\dot{V}_{exh}$ with the mass balance relation as shown in Eq. 6.2:

$$C_o E_Z \dot{V}_{oz}(1 - E_{fC}) + C_{bz} E_z (1 - E_{fA}) \dot{V}_r + \dot{N} + C_o E_z \dot{V}_{inf} = \dot{D} + C_{bz} E_z (\dot{V}_{oz} + \dot{V}_r + \dot{V}_{inf})$$

Isolating for C_{bz}:

$$C_{bz} = \frac{\dot{N} - \dot{D} + C_o E_Z\left(\dot{V}_{oz}\left(1 - E_{fC}\right) + \dot{V}_{inf}\right)}{E_z\left(\dot{V}_{oz} + E_{fA}\dot{V}_r + \dot{V}_{inf}\right)}$$

Isolating for V_{oz}:

$$\dot{V}_{oz} = \frac{\dot{N} - \dot{D} + E_z\left(C_o\dot{V}_{inf} - C_{bz}\left(E_{fA}\dot{V}_r + \dot{V}_{inf}\right)\right)}{E_Z\left(C_{bz} - C_o\left(1 - E_{fC}\right)\right)}$$

Model 15 represents a double filter, VAV mechanical ventilation system with filters located at locations A and C and constant outdoor air. The derivation for Model 15 is as follows.

Mass Balance:

$$C_o E_Z\dot{V}_{oz}(1 - E_{fC}) + C_{bz}E_z F_r\left(1 - E_{fA}\right)\dot{V}_r + \dot{N} + C_o E_z\dot{V}_{inf} = \dot{D} + C_{bz}F_r E_z\dot{V}_{ex}$$

Substituting $\dot{V}_{exh}$ with the mass balance relation as shown in Eq. 6.2:

$$C_o E_Z\dot{V}_{oz}(1 - E_{fC}) + C_{bz}E_z F_r\left(1 - E_{fA}\right)\dot{V}_r + \dot{N} + C_o E_z\dot{V}_{inf} = \dot{D} + C_{bz}E_z\left(\dot{V}_{oz} + F_r\dot{V}_r + \dot{V}_{inf}\right)$$

Isolating for C_{bz}:

$$C_{bz} = \frac{\dot{N} - \dot{D} + C_o E_Z\left(F_r\dot{V}_{oz}\left(1 - E_{fC}\right) + \dot{V}_{inf}\right)}{E_z\left(\dot{V}_{oz} + F_r E_{fA}\dot{V}_r + \dot{V}_{inf}\right)}$$

Isolating for V_{oz}:

$$\dot{V}_{oz} = \frac{\dot{N} - \dot{D} + E_z\left(C_o\dot{V}_{inf} - C_{bz}\left(F_r E_{fA}\dot{V}_r + \dot{V}_{inf}\right)\right)}{E_Z F_r\left(C_{bz} - C_o\left(1 - E_{fC}\right)\right)}$$

Model 16 represents a triple filter, CAV mechanical ventilation system with constant outdoor air. The derivation for Model 16 is as follows.

Mass Balance:

$$C_o E_Z \dot{V}_{oz}(1-E_{fC})(1-E_{fB}) + C_{bz}E_z\left(1-E_{fA}\right)(1-E_{fB})\dot{V}_r + \dot{N} + C_o E_z \dot{V}_{inf} = \dot{D} + C_{bz}E_z\dot{V}_{exh}$$

Substituting $\dot{V}_{ex}$ with the mass balance relation as shown in Eq. 6.2:

$$C_o E_Z \dot{V}_{oz}(1-E_{fC})(1-E_{fB}) + C_{bz}E_z\left(1-E_{fA}\right)(1-E_{fB})\dot{V}_r + \dot{N} + C_o E_z \dot{V}_{inf}$$
$$= \dot{D} + C_{bz}E_z\left(\dot{V}_{oz} + \dot{V}_r + \dot{V}_{inf}\right)$$

Isolating for C_{bz}:

$$C_{bz} = \frac{\dot{N} - \dot{D} + C_o E_Z\left(\dot{V}_{oz}\left(1-E_{fC}\right)(1-E_{fB}) + \dot{V}_{inf}\right)}{E_z\left(\dot{V}_{oz} + \dot{V}_{inf} + \left(E_{f_A} + E_{f_B} - E_{f_A}E_{f_B}\right)\dot{V}_r\right)}$$

Isolating for V_{oz}:

$$\dot{V}_{oz} = \frac{\dot{N} - \dot{D} + E_z(C_o\dot{V}_{inf} - C_{bz}\left(\dot{V}_{inf} + \left(E_{f_A} + E_{f_B} - E_{f_A}E_{f_B}\right)\dot{V}_r\right)}{E_Z\left(C_{bz} - C_o\left(1-E_{fC}\right)(1-E_{fB})\right)}$$

Model 17 represents a triple filter, VAV mechanical ventilation system with constant outdoor air. The derivation for Model 17 is as follows.

Mass Balance:

$$C_o E_Z \dot{V}_{oz}(1-E_{fC})(1-E_{fB}) + C_{bz}E_z F_r\left(1-E_{fA}\right)(1-E_{fB})\dot{V}_r + \dot{N} + C_o E_z \dot{V}_{inf}$$
$$= \dot{D} + C_{bz}F_r E_z\dot{V}_{ex}$$

Substituting $\dot{V}_{ex}$ with the mass balance relation as shown in Eq. 6.2:

$$C_o E_Z \dot{V}_{oz}(1-E_{fC})(1-E_{fB}) + C_{bz} E_z F_r \left(1-E_{fA}\right)(1-E_{fB})\dot{V}_r + \dot{N} + C_o E_z \dot{V}_{inf}$$

$$= \dot{D} + C_{bz} E_z \left(\dot{V}_{oz} + F_r \dot{V}_r + \dot{V}_{inf}\right)$$

Isolating for C_{bz}:

$$C_{bz} = \frac{\dot{N} - \dot{D} + C_o E_Z \left(\dot{V}_{oz}\left(1-E_{fC}\right)(1-E_{fB}) + \dot{V}_{inf}\right)}{E_z \left(\dot{V}_{oz} + F_r \left(E_{f_A} + E_{f_B} - E_{f_A} E_{f_B}\right)\dot{V}_r + \dot{V}_{inf}\right)}$$

Isolating for V_{oz}:

$$\dot{V}_{oz} = \frac{\dot{N} - \dot{D} + E_z (C_o \dot{V}_{inf} - C_{bz}\left(F_r \left(E_{f_A} + E_{f_B} - E_{f_A} E_{f_B}\right)\dot{V}_r + \dot{V}_{inf}\right)}{E_Z F_r \left(C_{bz} - C_o \left(1-E_{fC}\right)(1-E_{fB})\right)}$$

Table 1 contains a summary of IAQ models and their associated equations. Note that the difference between the Variable Air Volume (VAV) system and constant airflow (CAV) system is reflected in the flow reduction factor (F_r). In the case that $F_r = 1$ in a VAV system, the system is equivalent to that of a constant flow system. When $R = 0$ in a recirculation ventilation system, the system is equivalent to that of a pure outdoor air ventilation system.

Table 1. Summary of IAQ models for the determination of breathing zone PM2.5 concentration.

Model Number	Required Recirculation Rate			Space Breathing Zone Contaminant Concentration (C_{bz})
	Filter Location	Flow	Outdoor Airflow	
1	None	VAV	100%	$C_o + \frac{N-D}{E_Z(F_r V_{oz} + V_{inf})}$
2	A	Const.	Const.	$\frac{N - D + E_Z C_o (V_{oz} + V_{inf})}{E_Z (V_{oz} + R V_r E_{f_A} + V_{inf})}$
3	A	VAV	Const.	$\frac{N - D + E_Z C_o (V_{oz} + V_{inf})}{E_Z (V_{oz} + F_r R V_r E_{f_A} + V_{inf})}$
4	B	Const.	Const.	$\frac{N - D + E_Z C_o [V_{oz}\left(1 - E_{f_B}\right) + V_{inf}]}{E_Z (V_{oz} + R V_r E_{f_B} + V_{inf})}$

5	B	VAV	100%	$\frac{N - D + E_Z C_o [F_r V_{oz}(1 - E_{f_B}) + V_{inf}]}{E_Z(F_r V_{oz} + V_{inf})}$
6	B	VAV	Const.	$\frac{N - D + E_Z C_o [V_{oz}(1 - E_{f_B}) + V_{inf}]}{E_Z(V_{oz} + F_r R V_r E_{f_B} + V_{inf})}$
7	C	Const.	Const.	$\frac{N - D + E_Z C_o [V_{oz}(1 - E_{f_C}) + V_{inf}]}{E_Z(V_{oz} + V_{inf})}$
	C	VAV	Const.	$\frac{N - D + E_Z C_o [V_{oz}(1 - E_{f_C}) + V_{inf}]}{E_Z(V_{oz} + V_{inf})}$
8	C	VAV	100%	$\frac{N - D + E_Z C_o [F_r V_{oz}(1 - E_{f_C}) + V_{inf}]}{E_Z(F_r V_{oz} + V_{inf})}$
9	A, B	Const.	Const.	$\frac{N - D + E_Z C_o [V_{oz}(1 - E_{f_B}) + V_{inf}]}{E_Z[V_{oz} + R V_r(E_{f_A} + E_{f_B} - E_{f_A} E_{f_B}) + V_{inf}]}$
10	A, B	VAV	Const.	$\frac{N - D + E_Z C_o [V_{oz}(1 - E_{f_B}) + V_{inf}]}{E_Z[V_{oz} + R V_r F_r(E_{f_A} + E_{f_B} - E_{f_A} E_{f_B}) + V_{inf}]}$
11	B, C	Const.	Const.	$\frac{N - D + E_Z C_o [V_{oz}(1 - E_{f_B})(1 - E_{f_C}) + V_{inf}]}{E_Z[V_{oz} + R V_r E_{f_B} + V_{inf}]}$
12	B, C	VAV	100%	$\frac{N - D + E_Z C_o [F_r V_{oz}(1 - E_{f_B})(1 - E_{f_C}) + V_{inf}]}{E_Z[V_{oz} F_r + V_{inf}]}$
13	B, C	VAV	Const.	$\frac{N - D + E_Z C_o [V_{oz}(1 - E_{f_B})(1 - E_{f_C}) + V_{inf}]}{E_Z[V_{oz} + R V_r F_r E_{f_B} + V_{inf}]}$
14	A, C	Const.	Const.	$\frac{N - D + E_Z C_o [V_{oz}(1 - E_{f_C}) + V_{inf}]}{E_Z[V_{oz} + R V_r E_{f_A} + V_{inf}]}$
15	A, C	VAV	Const.	$\frac{N - D + E_Z C_o [V_{oz}(1 - E_{f_C}) + V_{inf}]}{E_Z[V_{oz} + R V_r F_r E_{f_A} + V_{inf}]}$
16	A, B, C	Const.	Const.	$\frac{N - D + E_Z C_o [V_{oz}(1 - E_{f_B})(1 - E_{f_C}) + V_{inf}]}{E_Z[V_{oz} + R V_r(E_{f_A} + E_{f_B} - E_{f_A} E_{f_B}) + V_{inf}]}$
17	A, B, C	VAV	Const.	$\frac{N - D + E_Z C_o [V_{oz}(1 - E_{f_B})(1 - E_{f_C}) + V_{inf}]}{E_Z[V_{oz} + R V_r F_r(E_{f_A} + E_{f_B} - E_{f_A} E_{f_B}) + V_{inf}]}$

2.2.3. IAQ Simulations

2.2.3.1. Selection of Simulated Indoor Environments

A 186 m^2 (2000 ft^2) single-detached house was selected as the residential test space for the study. The ventilation system specifications were selected in adherence to the existing building and ventilation-specific codes and standards [95, 96, 98, 99]. The zone air distribution effectiveness options for the indoor space were obtained from ANSI/ASHRAE 62.1-2019 and ANSI/ASHRAE 62.2-2019 [95, 96]. The floor area of the residence was representative of an average detached single-family dwelling typically found in larger Canadian provinces [100]. The BC building code requires that the minimum ceiling height for residential buildings be no less than 2.1m (6.9ft) [98]. Similarly, the Alberta building code requires that the minimum ceiling height for residential buildings be no less than 2.13m (7ft) [99]. Thus, a floor-to-ceiling height of 2.13m (7ft) was selected for the single-detached house simulations under BC and Alberta building codes. According to ANSI/ASHRAE 62.2, the minimum outdoor ventilation rate for residential buildings is calculated based on the total floor area and number of bedrooms within the dwelling. It was assumed that the simulated detached residence had 3 bedrooms with an average occupancy of 2 – 4 occupants. Therefore, the minimum outdoor ventilation rate was determined to be 90 cfm or 0.39 ACH calculated based on Equation 4-1a of ANSI/ASHRAE 62.2 and the assumed floor-to-ceiling height [96].

2.2.3.2. Filter Selection

The effect of filter efficiencies and filter configurations within a single-zone ventilation system was investigated in the IAQ simulations. The capacity of various MERV ratings and HEPA filters to reduce the indoor PM2.5 concentration was assessed. Filters were represented in the model by the filter effectiveness associated with its MERV rating. Table 2 summarizes the filter efficiencies of various air filters assessed in the simulation. Filter efficiencies were obtained from a study by Fazli et al. regarding removing ultrafine particles using residential HVAC systems [42]. MERV 6 filters are the minimum required MERV-rated filter for single detached residential dwellings as per ASHRAE 62.2-2019 [96]. To understand the impact of higher efficiency filters for improving IAQ during wildfire season, MERV 8, MERV 11, MERV 16, and HEPA filters were also considered within the residential IAQ simulations.

Table 2. Summary of various types of air filters with their respective filter efficiency values.

Filter Type	**PM 2.5 removal efficiency, E_f [%]**
MERV 6	7.2
MERV 8	27.1
MERV 11	50
MERV 13	70
MERV 16	96.3
HEPA	99.7

A preliminary IAQ simulation was conducted to find the optimal one-filter, two-filter, and three-filter ventilation configurations to run the remainder of the simulations. The simulation results for Vancouver and Prince George are presented in Table 3, and Figures 2 and 3. It was found that models 4, 11, and 16 were the best in their class (1-filter, 2-filter, and 3-filter configurations, respectively) in their ability to reduce the concentration of PM2.5 introduced into the indoor space.

Thus, models 4, 11, and 16 were employed in subsequent simulations to assess the impact of various building and ventilation-related factors on the indoor PM2.5 level.

Table 3. Summary of simulation results using various mechanical ventilation configurations.

City	Model Type	24-hour average indoor PM2.5 level [μg/m^3]	
		Peak Exposure Day 1	Peak Exposure Day 2
Vancouver	***Outdoor PM2.5***	44.68	121.81
	Model 1	40.23	117.36
	Model 2/3	32.08	93.58
	Model 4/6/14/15	13.42	42.72
	Model 5/7/8	16.83	53.59
	Model 11/13	7.83	27.47
	Model 12	9.82	34.46
	Model 16/17	7.38	25.90
Prince George	***Outdoor PM2.5***	349.87	268.33
	Model 1	345.42	263.88
	Model 2/3	275.43	210.41
	Model 4/6/14/15	129.37	98.40
	Model 5/7/8	162.25	123.40
	Model 11/13	85.56	64.79
	Model 12	107.30	81.25
	Model 16/17	80.66	61.08

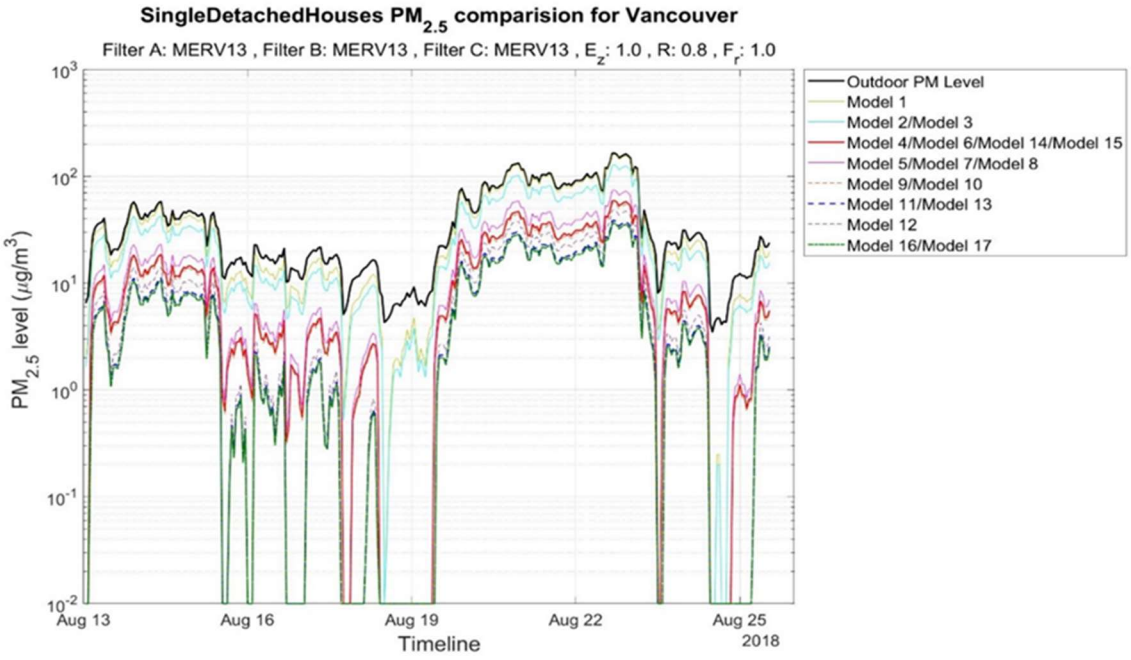

Figure 2. Indoor PM2.5 concentration comparison in Vancouver with various ventilation configurations. Default selection for filter efficiency, recirculation, zone air distribution effectiveness, and design flow reduction (E_f=0.7 (MERV13), R = 0.5, E_z = 1, F_r = 1).

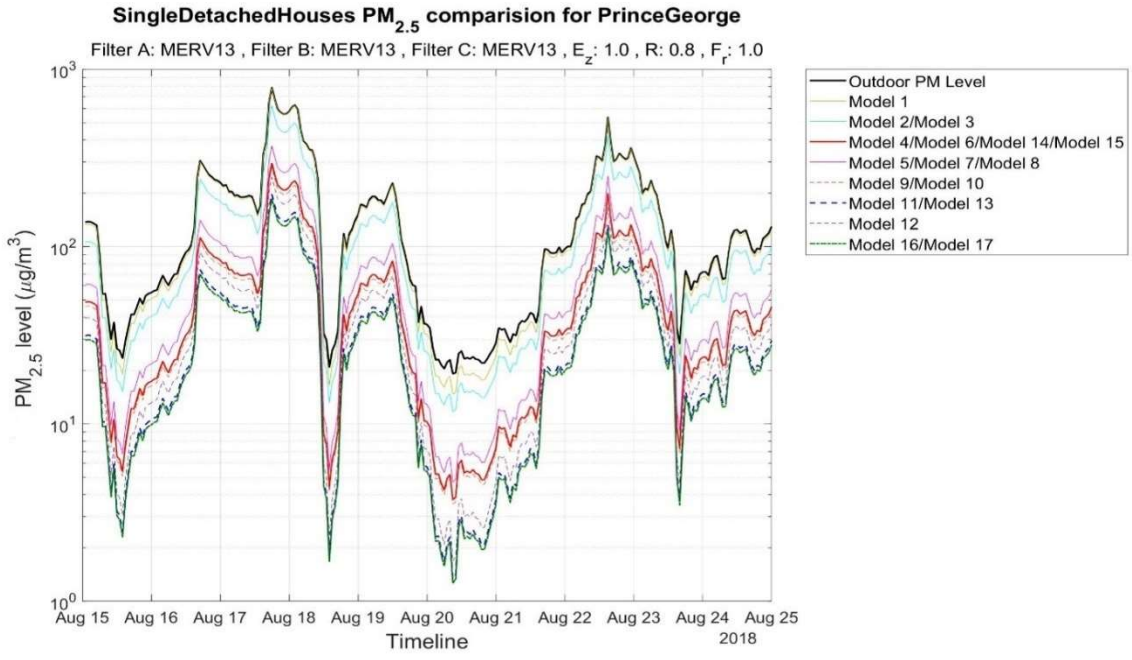

Figure 3. Indoor PM2.5 concentration comparison in Prince George with various ventilation configurations. Default selection for filter efficiency, recirculation, zone air distribution effectiveness, and design flow reduction (E_f=0.7 (MERV13), R = 0.5, E_z= 1, F_r = 1).

2.2.3.3. Description of Breathing Zone Specifications and IAQ Simulations

Table 4 provides a summary of the ventilation specifications that were assessed in the IAQ simulations. The building characteristics, outdoor airflow rate (V_o), and zone air distribution effectiveness (E_z) were obtained from ASHRAE 62.2-2019 as detailed in the previous section [96]. The depositional loss rate (D), air infiltration rate (V_{inf}), and Portable Air Cleaner (PAC) effectiveness ($E_{f,PAC}$) were obtained from the experimental results from recent research regarding ventilation systems. Based on the experimental assumptions of Henderson et al. [101] and the experimental results of Xiang et al. [88], a constant PM2.5 deposition rate of 0.15 ACH was used in the IAQ simulations. The constant deposition rate assumption is a limitation of this study as it neglects the variable nature of the PM2.5 deposition rate. However, this simplification was justified as the selected value would represent the average characteristics of typical ventilation systems. Similarly, a singular infiltration rate assumption is a limited representation of individual building envelope conditions but provides a conservative, preliminary representation of existing residential buildings with average to low-quality building envelopes. An infiltration rate of 0.3 ACH was selected for this study based on the results of an infiltration study by Grot et al. [102]. A PAC effectiveness of 31% was obtained from a field study by Huang et al. that explored the effectiveness of PACs to reduce PM2.5 from cooking events [44]. It should be noted that the PAC effectiveness selected for use in this study is a conservative choice; other field studies regarding the application of PACs to reduce indoor PM2.5 levels have noted PAC effectiveness up to 55% [87, 88].

Several IAQ simulations were conducted to assess the impact of various building and ventilation-related factors on indoor pollutant concentration. The building and ventilation variables that were evaluated as a part of this study included the following: a) filter type, E_f; b) recirculation factor,

R; c) air distribution effectiveness, E_z; d) outdoor PM2.5 levels (city selection); and e) application of portable air cleaner (PAC). A variance-based global sensitivity analysis of the IAQ models was conducted to assess the individual impacts of various building and ventilation variables on the resultant indoor PM2.5 concentration. The analysis was executed with SALib, an open-source python library developed for sensitivity analyses [57].

Table 4. Summary of characteristics and key ventilation system variables for single-detached homes.

Single Detached Residence	
Characteristics [98, 99]	3 Bedrooms 186 m^2 (2000 ft^2) with 2.13m (7ft) ceilings
Outdoor air volumetric flow rate, V_{oz} [96]	0.39 ACH
Air Filters Tested [34, 42, 44]	MERV 6, 8, 11, 13, 16 HEPA
Recirculation flow factor, R	0, 0.2, 0.5, 0.8, 1
Zone air distribution effectiveness, E_z [95, 96]	0.7, 1.0
Flow reduction factor, F_r	0.5, 1.0
Deposition loss rate, D [43, 103]	0.15 ACH
Air infiltration rate, V_{inf} [34]	0.3 ACH
Portable Air Cleaner Effectiveness, $E_{f,PAC}$ [87]	31%

2.2.4. Financial Analysis

2.2.4.1. Mechanical Ventilation-Related Costs

Mechanical ventilation-related costs focused on the cost of purchase, installation, and scheduled maintenance of various MERV-rated air filter packages. Equations from Montgomery et al. and Sun et al. were used to evaluate the overall costs of the wildfire-resilient ventilation retrofit [104, 105]. The total annual cost of the mechanical ventilation retrofit (C) was comprised of the cost of

air filter acquisition (C_F), filter installation and disposal (C_L), and annual ventilation-related energy consumption (W_{ave}) as shown in Equation (8) below.

$$C = C_F + C_L + 8.76 W_{ave} \$_E \tag{8}$$

Where,

$$C_F = \$_F\left(\frac{31536000}{t}\right)$$

$$C_L = \$_L\left(\frac{31536000}{t}\right)$$

$$W_{ave} = \frac{Q P_{ave}}{\eta}$$

$$P_{ave} = P_{initial\ resistance} + \frac{1}{3}\left(P_{final\ resistance} - P_{initial\ resistance}\right)$$

Two filter change schedules were considered in the financial analysis: a standard 3-month filter change as recommended by air filter manufacturers (Plan 1) and a modified schedule where filters are changed every month from July – September during peak wildfire season and follow the 3-month filter change for the rest of the year (Plan 2). The annual cost of ventilation system implementation varied depending on the selected filter change schedule and on whether additional PACs were employed. Reference values used in the financial assessment of the proposed mechanical ventilation systems were obtained from both current publications regarding mechanical ventilation and directly from manufacturer and product distributor catalogues [106-113]. Table 5 summarizes the reference values used in the analysis alongside the respective sources where the values were obtained. Using the financial analysis framework detailed above, the

estimated cost of implementation was obtained for various air filter configurations within single-detached residential dwellings.

Table 5. Summary of reference values used in the cost analysis of wildfire-resilient mechanical ventilation systems.

Component Specification	Reference Values	Source(s)
Fan	Fan Efficiency: 0.7 Air flowrate: 0.39 ACH	Sachs et al. 2002 [106] ASHRAE 62.2-2019 [96]
Air Filter	Cost: $10 - $155 (dependent on MERV-rating) Dimensions: 24”x24” (0.61x0.61 m) Installation and Disposal: $2.21/filter	Various Manufacturers/Product Distributors [107-109]
Energy and Utilities	Electricity: $0.10/kWh	2016 energy rate comparison from BC Hydro [110]
Portable Air Cleaner	Initial Cost: $400 (Philips 2000i Series Air Purifier) HEPA filter replacement - $69.99/filter every 24 months A/C filter replacement - $39.99/filter every 12 months	Manufacturer/Product Distributors [111-113]

2.2.4.2. PM2.5 Exposure-Related Health Effects

Studies have noted the negative health impacts of both acute and chronic exposure to elevated levels of PM2.5 [17, 73]. Short-term exposure was found to cause the acute onset of symptoms related to the degradation of air quality [16]. Chronic exposure to elevated levels of PM2.5 has increased the risk of premature mortality due to respiratory illnesses [74].

Short-term health effects were attributed to an increased risk of various wildfire-related morbidities such as respiratory symptom days, emergency room visits, hospital admissions, and restricted activity days [72]. The 2016 national statistics from Health Canada regarding the valuation of various morbidity health endpoints were used to estimate the economic impact of short-term health effects related to PM2.5 exposure [72]. Morbidity health endpoints and their

respective valuations are included in Table 6. Although Health Canada's AQBAT model does not account for regional differences in the magnitude and duration of PM2.5 exposure in their estimate of PM2.5-related morbidities, the estimate provides insight into the scale of healthcare cost reduction as a result of improved IAQ from the wildfire-resilient mechanical ventilation retrofit.

Table 6. Economic value of health endpoints from 2016 Health Canada's AQBAT model [72].

Health Endpoint	Currency year of original study	Form	Parameter 1* (probability)	Parameter 2 (probability)	Parameter 3 (probability)
Mortality	2007	Discrete	$3,500,000 (25%)	$6,500,000 (50%)	$9,500,000 (25%)
Acute respiratory symptom days	1997	Normal	$13	$7	-
Adult chronic bronchitis cases	1996	Discrete	$175,000 (33%)	$266,000 (34%)	$465,000 (33%)
Asthma symptom days	1997	Triangular	$7	$28	$120
Cardiac emergency room visits	1996	Normal	$4400	$590	
Child acute bronchitis episodes	1996	Discrete	$150 (33%)	$310 (34%)	$460 (33%)
Elderly cardiac hospital admissions	1997	Normal	$5200	$610	-
Respiratory emergency room visits	1997	Normal	$2000	$210	-

*Note that the definition of parameters 1, 2, and 3 change depending on the data form. For valuations represented by discrete values, parameters 1, 2, and 3 represent low, medium, and high estimates, respectively. For normal distributions, parameters 1 and 2 represent the mean and standard error of the estimates, respectively. For triangular distributions, parameters 1, 2, and 3 represent minimum, most likely, and maximum values, respectively.

The long-term health effects of PM2.5 exposure are ultimately related to the overall increase in the risk of acute, premature mortality. Although prolonged exposure to slightly elevated levels of PM2.5 has been associated with similar health outcomes [114], this section focuses on risks of premature mortality related to short-term exposure to high levels of PM2.5. Such a scenario represents the conditions during the Canadian wildfire season where the PM2.5 concentration is elevated during active wildfire events. The regional rate of acute mortality related to wildfire PM2.5 exposure was obtained from the Government of Canada data blog regarding the impact of Canada's wildfires [115]. The obtained acute mortality rates were used in conjunction with the mid-range Value of Statistical Life (VSL) - $6.5M - as determined by the work of Chestnut et al. [58]. The VSL does not aim to associate a monetary value with human life. Instead, the VSL provides a valuation related to the willingness of people to pay to reduce the risk of mortality. A long-term healthcare cost estimate per region was calculated as a weighted average of the probability of premature mortality and the mid-range valuation of the VSL. The resultant value allowed for the assessment of the feasibility of wildfire-resilient ventilation retrofits within residential dwellings.

2.3.Results

2.3.1. IAQ Simulation Models

2.3.1.1. City

The city-based IAQ simulations quantified the impact of outdoor PM2.5 levels on the resultant indoor PM2.5 concentration in various regions of Canada. Figure 4 and Table 7 show the 10-day trend and peak 24-hour average indoor PM2.5 levels for single-detached residences in the selected test cities, respectively. For Vancouver and Victoria, a 2-filter system fitted with MERV13-rated air filters (model 11) was sufficient to lower the indoor peak PM2.5 concentration to 27.89 $\mu g/m^3$ and 24.03 $\mu g/m^3$, respectively, which was close to or below the recommended daily exposure limit

of 27 μg/m^3 as per CAAQS. In comparison, a 3-filter system fitted with MERV13-rate air filters (model 16) was unable to meet the recommended daily exposure limit for both sustained and transient high outdoor PM2.5 concentration, as shown in Table 7 for Prince George and Edmonton, respectively.

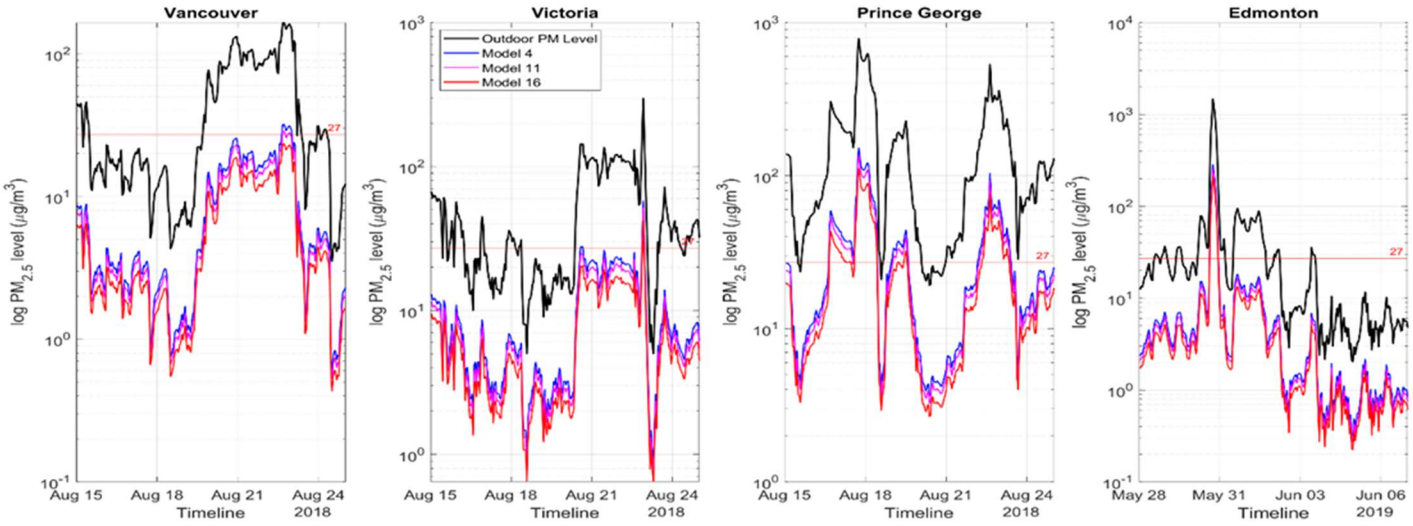

Figure 4. Indoor PM2.5 concentration comparison between test cities. Default values for simulations (E_f= 0.7 (MERV13), R = 0.5, E_z= 1, F_r= 1).

Table 7. Summary of peak 24-hour average indoor PM2.5 levels obtained for each test city.

City	Model Type	Peak 24-hour average indoor PM2.5 concentration [μg/m^3]
Vancouver	Model 4	43.38
	Model 11	27.89
	Model 16	26.39
Prince George	Model 4	131.35
	Model 11	86.86
	Model 16	82.17
Victoria	Model 4	37.62
	Model 11	24.03
	Model 16	22.73
Edmonton	Model 4	103.69
	Model 11	69.48
	Model 16	64.47

2.3.1.2. Filter Efficiency

A summary of the filter efficiency IAQ simulation results is provided in Table 8. Figure 5 shows the effect of various filter efficiencies on the resultant indoor PM2.5 level based on the Prince George outdoor PM2.5 dataset. The effect of various filter efficiencies on indoor PM2.5 concentration for Vancouver and Edmonton are included in Figures 6 and 7, respectively. It was found that the use of higher efficiency air filters resulted in a more significant decrease in the indoor PM2.5 concentration relative to the outdoor concentration. In addition, the use of multiple air filters (model 11, model 16) positively impacted reducing the indoor PM2.5 level relative to the single filter configuration (model 4).

Table 8. Peak 24-hour average indoor PM2.5 levels obtained using air filter of varying efficiencies.

City	Model Type	MERV 6 [µg/m^3]	MERV 8 [µg/m^3]	MERV 11 [µg/m^3]	MERV 13 [µg/m^3]	MERV 16 [µg/m^3]	HEPA [µg/m^3]
		Peak 24-hour Average Outdoor PM2.5 Level: 121.81 µg/m^3					
Vancouver	Model 4	109.43	84.89	65.23	43.38	25.05	22.64
	Model 11	103.59	66.85	44.54	27.89	22.12	21.89
	Model 16	102.26	64.28	42.59	26.39	21.98	21.86
%Diff. (M4 vs. M11)		5.34%	21.25%	31.72%	35.71%	11.70%	3.31%
%Diff. (M11 vs. M16)		1.28%	3.84%	4.38%	5.38%	0.63%	0.14%
		Peak 24-hour Average Outdoor PM2.5 Level: 349.87 µg/m^3					
Prince George	Model 4	322.55	251.69	194.93	131.35	78.93	71.99
	Model 11	305.75	199.87	135.50	86.86	70.51	69.83
	Model 16	301.84	192.20	129.57	82.17	70.06	69.72
%Diff. (M4 vs. M11)		5.21%	20.59%	30.49%	33.87%	10.67%	3.00%
%Diff. (M11 vs. M16)		1.28%	3.84%	4.38%	5.40%	0.64%	0.16%
		Peak 24-hour Average Outdoor PM2.5 Level: 294.06 µg/m^3					
Edmonton	Model 4	269.12	198.23	147.18	103.69	55.95	50.97
	Model 11	255.29	158.06	103.19	69.48	50.24	49.52
	Model 16	247.51	144.84	93.81	64.47	49.60	49.35
%Diff. (M4 vs. M11)		5.14%	20.26%	29.89%	32.99%	10.20%	2.86%
%Diff. (M11 vs. M16)		3.05%	8.37%	9.09%	7.22%	1.28%	0.33%

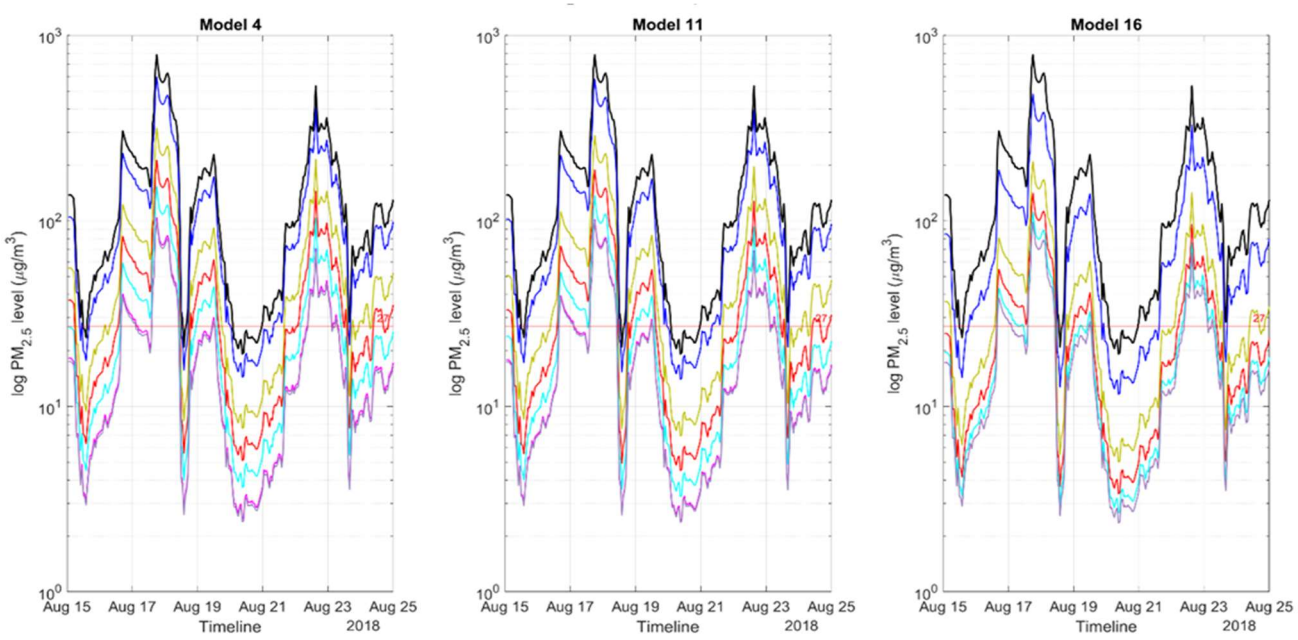

Figure 5. Indoor PM2.5 concentration comparison in Prince George with various air filter efficiencies. Default values for simulations (R = 0.5, E_z= 1, F_r= 1).

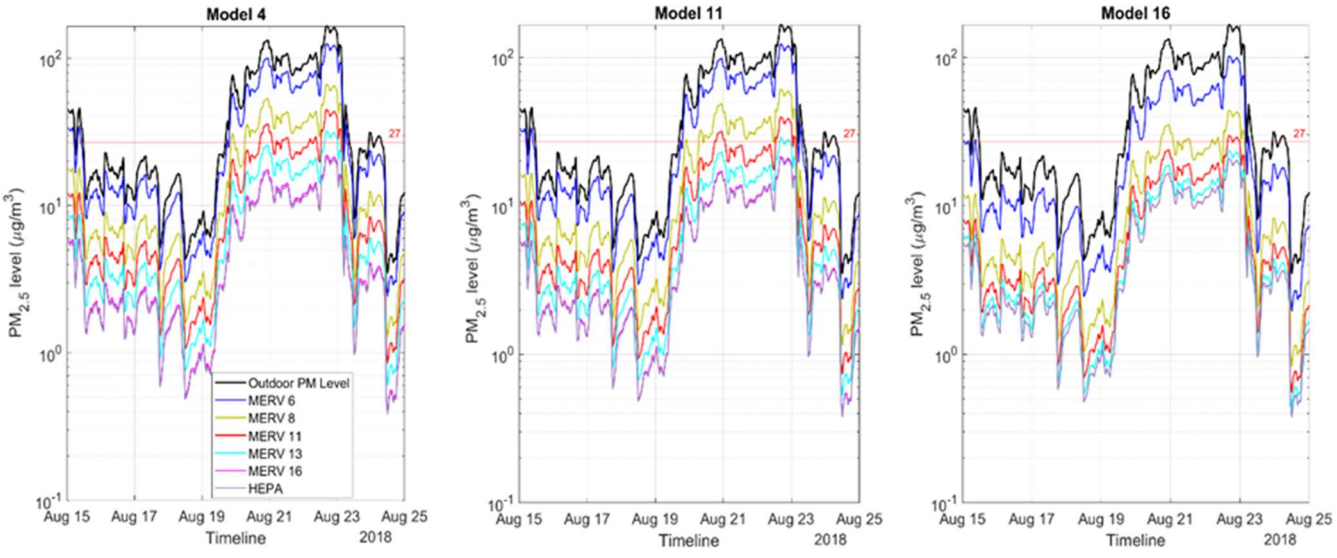

Figure 6. Indoor PM2.5 concentration comparison in Vancouver with various air filter efficiencies. Default values for simulations (R = 0.5, E_z= 1, F_r= 1).

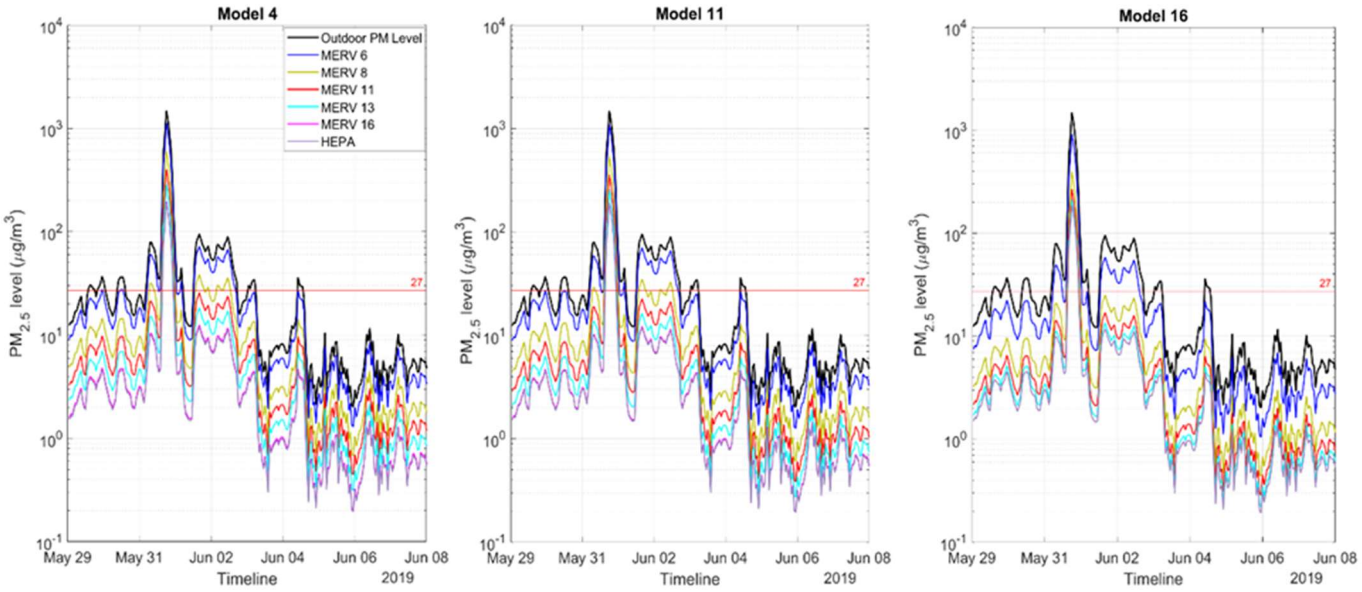

Figure 7. Indoor PM2.5 concentration comparison in Edmonton with various air filter efficiencies. Default values for simulations (R = 0.5, E_z= 1, F_r= 1).

2.3.1.3. Recirculation

The recirculation IAQ simulation results for Vancouver (Figure 8) and Prince George (Figure 9) are summarized in Table 9. These datasets correspond to two different PM2.5 exposure profiles: Prince George is representative of sustained, severe exposure, while Vancouver is representative of moderate exposure.

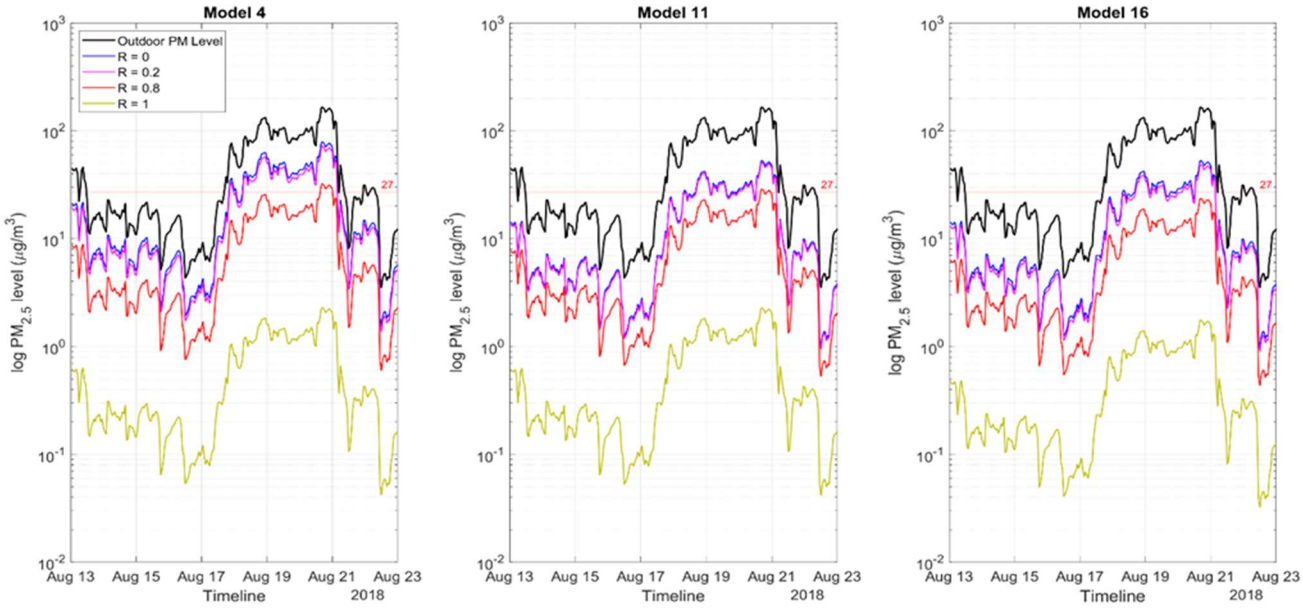

Figure 8. Indoor PM2.5 concentration comparison in Vancouver with various recirculation factors. Default values for simulations ($E_f = 0.7$, $E_z = 1$, $F_r = 1$).

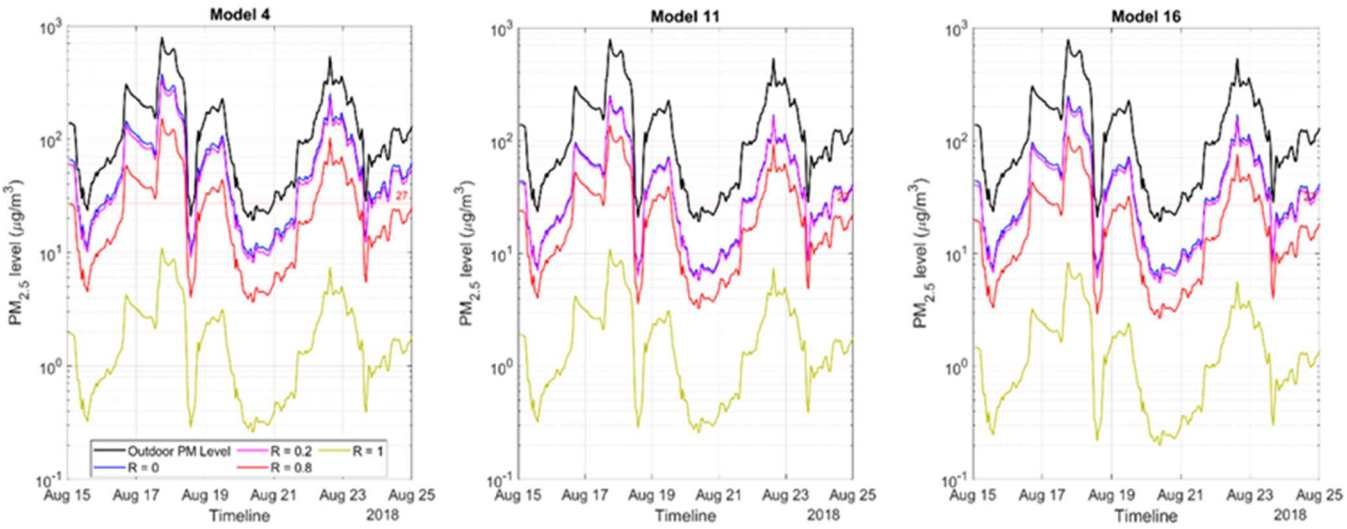

Figure 9. Indoor PM2.5 concentration comparison in Prince George with various recirculation factors. Default values for simulations ($E_f = 0.7$, E_z= 1, F_r= 1).

Table 9. Summary of results obtained from IAQ simulations applying various recirculation ratios.

City	Model Type	R = 0		R = 0.2		R = 0.8		R = 1	
		Peak 1 [μg/m³]	Peak 2 [μg/m³]	Peak 1 [μg/m³]	Peak 2 [μg/m³]	Peak 1 [μg/m³]	Peak 2 [μg/m³]	Peak 1 [μg/m³]	Peak 2 [μg/m³]
Vancouver	Model 4	41.23	57.91	37.36	52.49	16.80	23.62	1.20	1.69
	Model 11	27.60	38.78	26.45	37.17	15.02	21.11	1.20	1.68
	Model 16	27.60	38.78	25.32	35.58	12.30	17.29	0.92	1.29
Prince George	Model 4	162.25	123.40	152.56	116.03	67.99	52.04	4.87	3.73
	Model 11	111.63	85.58	107.00	82.03	60.79	46.60	4.84	3.71
	Model 16	111.63	85.58	102.42	78.52	49.78	38.17	3.73	2.86

2.3.1.4. Design Flow Reduction Factor

The design flow reduction factor applies to Variable Air Volume (VAV) mechanical ventilation systems. The results from the IAQ simulations comparing a constant flow system ($F_r = 1$) to a VAV ventilation system ($F_r = 0.5$) are summarized in Table 10 and Figures 10 and 11.

Table 10. Summary of peak 24-hour indoor PM2.5 concentration obtained with various design flow reduction factors.

City	Model Type	$F_r = 0.5$		$F_r = 1$	
		Peak 1 [µg/m^3]	Peak 2 [µg/m^3]	Peak 1 [µg/m^3]	Peak 2 [µg/m^3]
Vancouver	Model 6	14.53	46.24	11.87	43.38
	Model 13	8.47	29.73	6.92	27.89
	Model 17	8.14	28.56	6.35	26.39
Prince George	Model 6	140.01	106.49	131.35	86.97
	Model 13	92.59	70.12	86.86	57.27
	Model 17	88.94	67.35	82.17	52.61

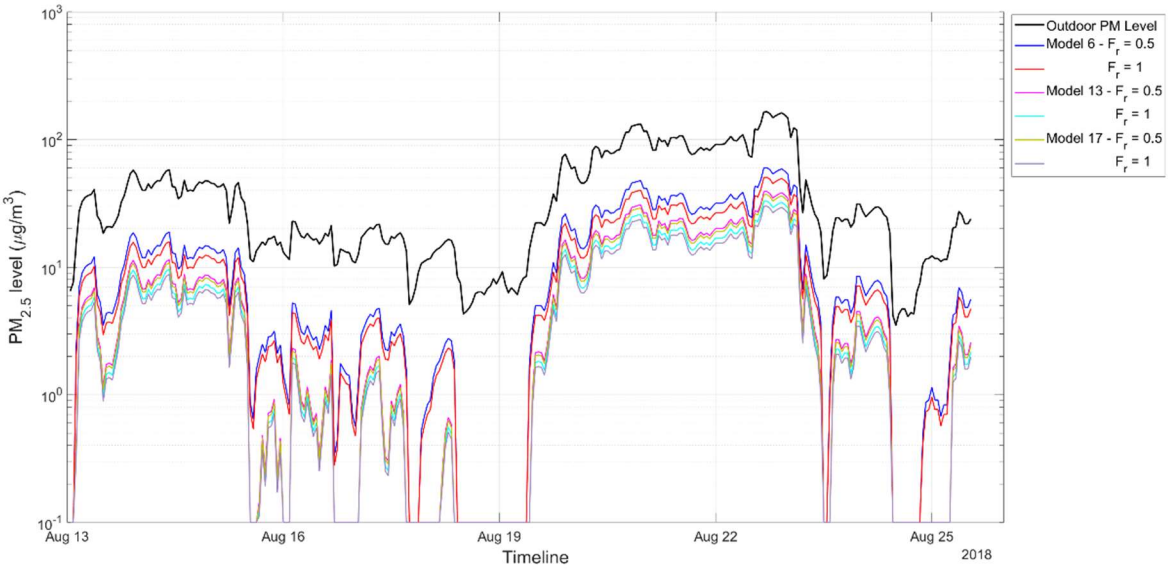

Figure 10. Indoor PM2.5 concentration comparison in Vancouver with various design flow reduction factors. Default selection for filter efficiency, zone air distribution effectiveness, and recirculation ratio ($E_f = 0.7$, $E_z = 1$, R = 0.5)

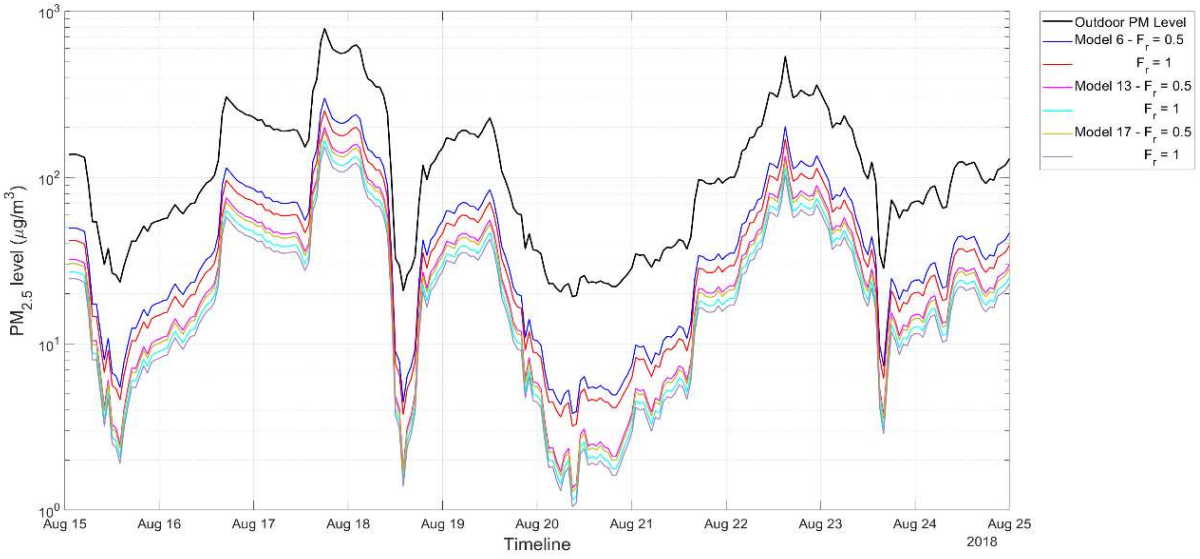

Figure 11. Indoor PM2.5 concentration comparison in Prince George with various design flow reduction factors. Default selection for filter efficiency, zone air distribution effectiveness, and recirculation ratio ($E_f = 0.7$, E_z= 1, R = 0.5)

2.3.1.5. Zone Air Distribution Effectiveness

Results from the IAQ simulations exploring the impact of the zone air distribution effectiveness on the indoor PM2.5 concentration are summarized in Table 11, with results for each test city shown in Figures 12 and 13.

Table 11. Summary of peak 24-hour indoor PM2.5 concentration with various zone air distribution effectiveness.

City	Model Type	E_z = 0.7		E_z = 1	
		Peak 1 [μg/m^3]	Peak 2 [μg/m^3]	Peak 1 [μg/m^3]	Peak 2 [μg/m^3]
Vancouver	Model 6	11.33	7.57	11.87	43.38
	Model 13	6.01	24.70	6.92	27.89
	Model 17	5.60	23.04	6.35	26.39
Prince George	Model 6	121.69	92.20	131.35	86.97
	Model 13	79.99	60.22	86.86	57.27
	Model 17	74.59	56.16	82.17	52.61

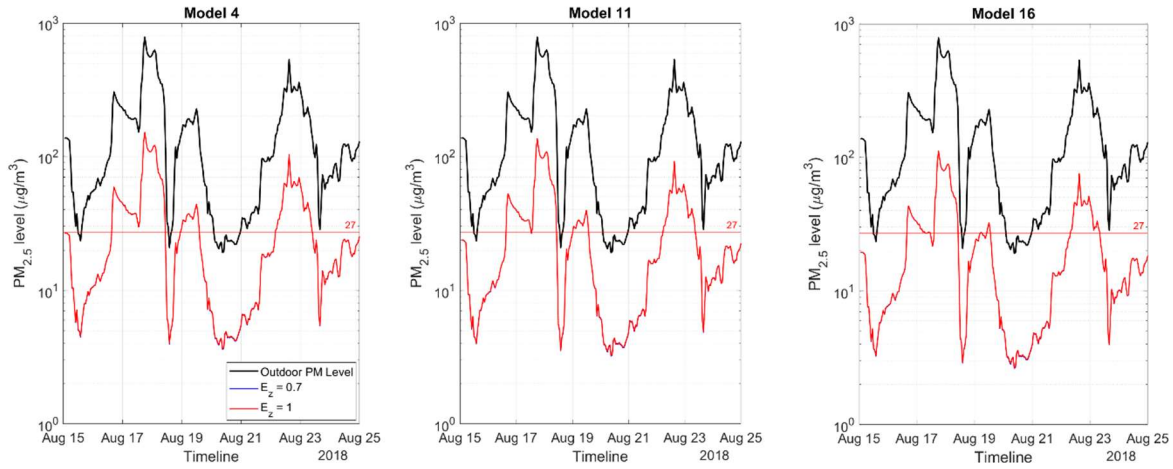

Figure 12. Indoor PM2.5 concentration comparison in Prince George with various zone air distribution effectiveness. Default selection for filter efficiency, design flow reduction factor, and recirculation ratio ($E_f = 0.7$, F_r= 1, R = 0.5)

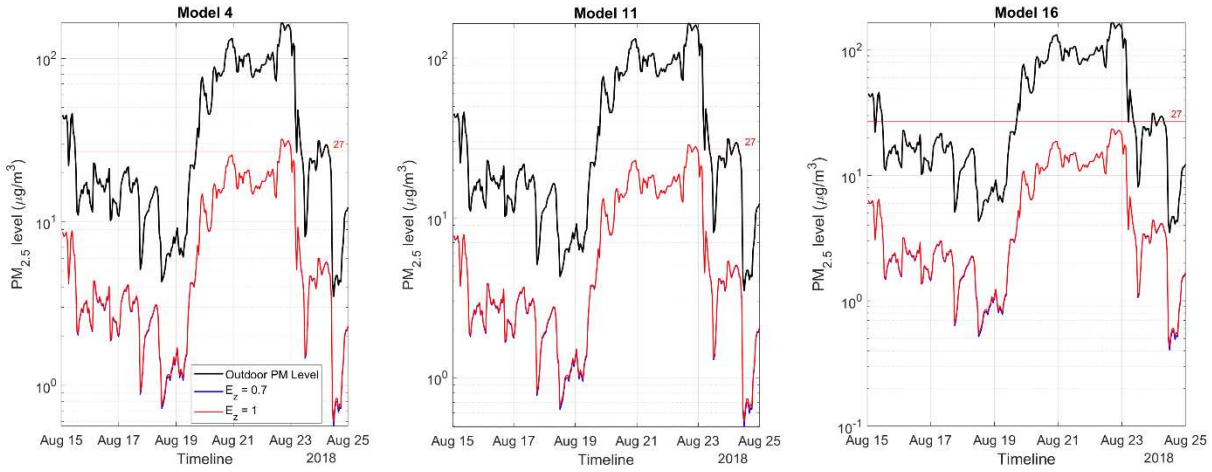

Figure 13. Indoor PM2.5 concentration comparison in Vancouver with various zone air distribution effectiveness. Default selection for filter efficiency, design flow reduction factor, and recirculation ratio ($E_f = 0.7$, F_r= 1, R = 0.5)

2.3.1.6. Portable Air Cleaner Usage

As an extension to the obtained IAQ simulation results, the impact of PAC usage on indoor PM2.5 concentration was assessed using the developed IAQ models. The compact design of PACs allows for their application directly into the indoor space without large-scale ventilation retrofits. Therefore, PAC-assisted IAQ simulation results are representative of the indoor PM2.5 level in the localized indoor space. The PAC effectiveness used within the PAC-assisted IAQ simulation

assumes that the PAC was sized correctly for the indoor space per the recommendations of a manufacturer. Results from the PAC-assisted IAQ simulations are presented in Table 12, with the original IAQ simulation results provided as a reference. Figures 14 and 15 show the impact of PAC usage on the 10-day indoor PM2.5 concentration for each test city.

Table 12. Comparison of peak 24-hour indoor PM2.5 concentration obtained both with and without portable air cleaner usage.

City	Model Type	Peak 24-hour average indoor PM2.5 concentration [µg/m^3]	
		Without PAC	With PAC
Vancouver	Model 4	43.38	29.93
	Model 11	27.89	19.24
	Model 16	26.39	18.21
Prince George	Model 4	131.35	90.63
	Model 11	86.86	59.93
	Model 16	82.17	56.70
Victoria	Model 4	37.62	25.96
	Model 11	24.03	16.58
	Model 16	22.73	15.68
Edmonton	Model 4	103.69	71.55
	Model 11	69.48	47.94
	Model 16	64.47	44.48

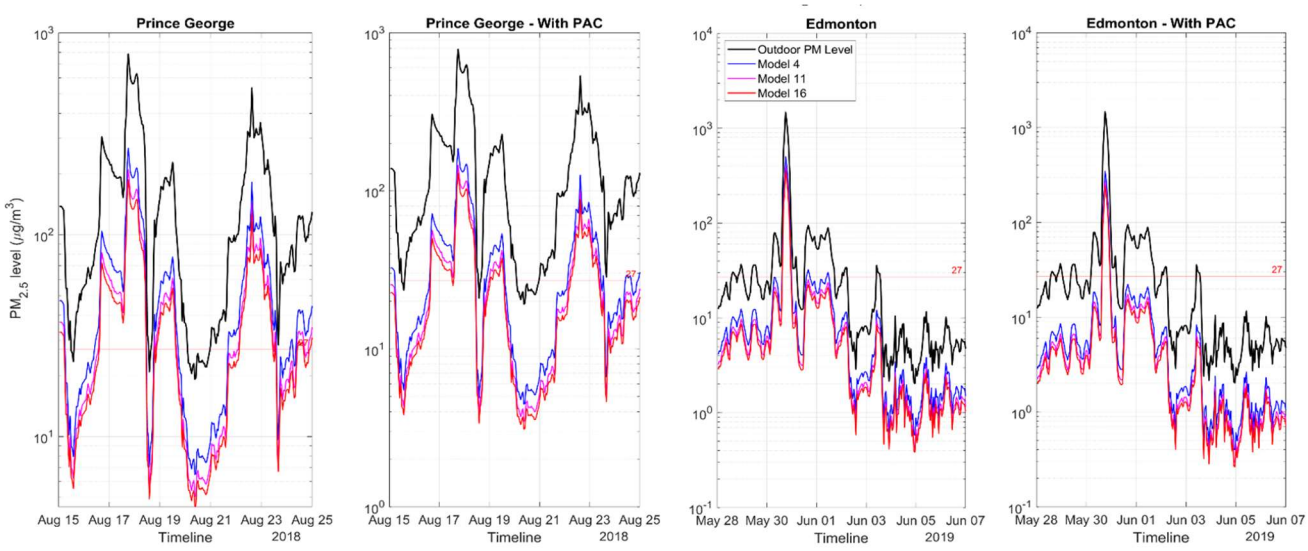

Figure 14. Indoor PM2.5 concentration comparison with the application of portable air cleaners in Prince George and Edmonton. Default selection for filter efficiency, zone air distribution effectiveness, and design flow reduction (E_f = 0.7, R = 0.5, E_z= 1, F_r= 1)

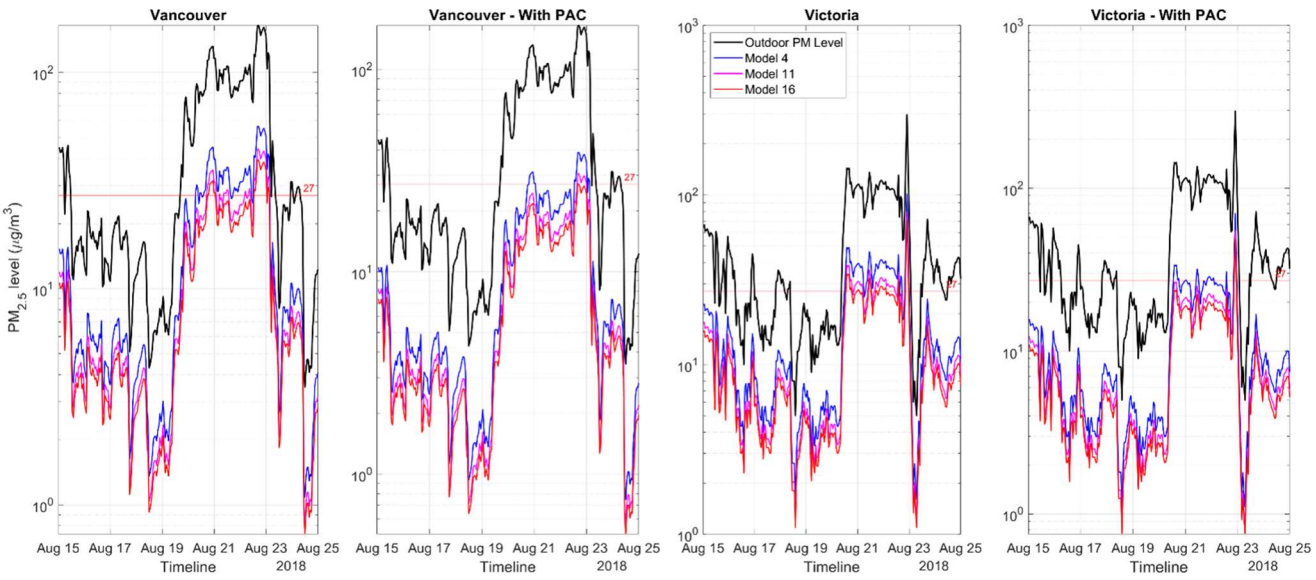

Figure 15. Indoor PM2.5 concentration comparison with the application of portable air cleaners in Vancouver and Victoria. Default selection for filter efficiency, zone air distribution effectiveness, and design flow reduction (E_f = 0.7, R = 0.5, E_z= 1, F_r= 1)

2.3.1.7. Sensitivity Analysis

A variance-based sensitivity analysis of all 17 IAQ models was conducted to assess the impact and association of the modelled input variables on the resultant indoor PM2.5 output. Results for the sensitivity analyses are shown in Table 13. The results showed three distinct results dependent upon the IAQ model type – namely, 1-filter, 2-filter, and 3-filter configurations. The total-order indices of the various input variables from models 4, 11, and 16 (representative of 1-filter, 2-filter, and 3-filter ventilation configurations, respectively) were compared to assess their relative influence in the context of single and multi-filter IAQ models. The outdoor PM2.5 concentration was the main governing input into all IAQ models – obtaining the highest total-order index for the 1-filter, 2-filter, and 3-filter mechanical ventilation configurations. In the 1-filter and 2-filter configurations, the air filter effectiveness in air filter position B obtained the second-highest total-order index at 0.373 and 0.200, respectively. This result indicates that – based on the IAQ models developed in this study – air filtration is most promising in its ability to reduce indoor PM2.5 levels

and outranks other ventilation strategies that were simulated. It was found that the total order index of the air filter in position A (9.11E-3) was significantly smaller than the total order indices of the air filter variable in positions B (0.200 and 0.149 in the 2-filter and 3-filter models, respectively) and C (0.146 and 0.126 in the 2-filter and 3-filter models, respectively).

Table 13. Results from Sensitivity Analysis of IAQ models

Model Type	Variable	Variable Range	Total-Order Index	Confidence Interval at 95% CL
Model 1	C_o	0 – 1479 [μg/m^3]	1.00E+00	6.09E-02
	D	0 – 0.15 [ACH]	7.50E-08	2.48E-08
	V_{oz}	0 – 1 [ACH]	6.70E-08	2.46E-08
	V_{inf}	0 - 0.3 [ACH]	2.68E-08	1.68E-08
	E_z	0.7 – 1	1.88E-08	1.24E-08
	F_r	0.5 - 1	1.07E-08	1.08E-08
Model 2/3	V_{oz}	0 – 1 [ACH]	6.40E-01	7.77E-02
	C_o	0 – 1479 [μg/m^3]	4.65E-01	7.05E-02
	V_{inf}	0 - 0.3 [ACH]	6.50E-02	8.18E-03
	R	0 - 1	1.01E-02	2.92E-03
	E_{fA}	0.072 - 0.997	9.76E-03	2.57E-03
	V_r	0 – 1 [ACH]	9.46E-03	2.63E-03
	F_r	0.5 - 1	1.31E-03	5.06E-04
	D	0 – 0.15 [ACH]	1.34E-07	3.59E-08
	E_z	0.7 – 1	0.00E+00	0.00E+00
Model 4/6/14/15	C_o	0 – 1479 [μg/m^3]	6.59E-01	6.38E-02
	E_{fB}	0.072 - 0.997	3.56E-01	4.56E-02
	V_{inf}	0 - 0.3 [ACH]	4.49E-02	9.58E-03
	V_{oz}	0 - 1 [ACH]	2.91E-02	6.46E-03
	V_r	0 - 1 [ACH]	2.68E-02	7.39E-03
	R	0 – 1	2.54E-02	5.62E-03
	D	0 - 0.15 [ACH]	4.98E-07	9.95E-08
	E_z	0.7 – 1	7.74E-08	4.46E-08
Model 5/7/8	C_o	0 – 1479 [μg/m^3]	5.70E-01	6.36E-02
	E_{fB}	0.072 - 0.997	2.00E-01	2.81E-02
	V_{inf}	0 - 0.3 [ACH]	1.46E-01	3.11E-02
	E_{fC}	0.072 - 0.997	1.36E-01	2.57E-02
	V_{oz}	0 - 0.89 [ACH]	1.32E-01	2.82E-02
	D	0 – 0.15 [ACH]	1.98E-05	3.62E-06
	E_z	0.7 – 1	4.03E-06	1.61E-06
	C_o	0 – 1479 [μg/m^3]	5.70E-01	6.36E-02
	E_{fB}	0.072 - 0.997	2.00E-01	2.81E-02

Model 9/10/11/13	E_{fC}	0.072 - 0.997	1.46E-01	3.11E-02
	V_{inf}	0 - 0.3 [ACH]	1.36E-01	2.57E-02
	V_{oz}	0 - 1 [ACH]	1.32E-01	2.82E-02
	R	0 – 1	4.59E-02	1.76E-02
	V_r	0 - 1 [ACH]	3.61E-02	1.10E-02
	D	0 – 0.15 [ACH]	1.98E-05	3.62E-06
	E_z	0.7 – 1	4.03E-06	1.61E-06
Model 12	C_o	0 – 1479 [μg/m^3]	4.62E-01	8.89E-02
	V_{oz}	0 - 1[ACH]	3.27E-01	5.99E-02
	V_{inf}	0 - 0.3 [ACH]	1.92E-01	3.27E-02
	E_{fC}	0.072 - 0.997	1.45E-01	4.84E-02
	E_{fB}	0.072 - 0.997	1.34E-01	3.04E-02
	F_r	0.5 - 1	5.74E-02	1.23E-02
	D	0 – 0.15 [ACH]	5.11E-07	1.28E-07
	E_z	0.7 - 1	6.69E-08	3.43E-08
Model 16/17	C_o	0 – 1479 [μg/m^3]	5.66E-01	6.35E-02
	E_{fB}	0.072 - 0.997	1.49E-01	2.21E-02
	V_{inf}	0 - 0.3 [ACH]	1.45E-01	2.91E-02
	E_{fC}	0.072 - 0.997	1.26E-01	2.25E-02
	V_{oz}	0 - 1 [ACH]	9.79E-02	1.94E-02
	V_r	0 - 1 [ACH]	6.37E-02	1.83E-02
	R	0 – 1	6.17E-02	1.45E-02
	E_{fA}	0.072 – 0.997	9.11E-03	3.16E-03
	D	0 – 0.15 [ACH]	1.08E-06	2.33E-07
	E_z	0.7 – 1	1.23E-07	7.25E-08

2.3.2. Financial Analysis

2.3.2.1. Cost of Mechanical Ventilation Retrofit Options

Cost estimates of various mechanical ventilation retrofit options were calculated based on filter package selection (air filter efficiency level and the number of filters used), maintenance schedule, ventilation-related energy consumption, and the optional integration of portable air-cleaning technologies. Table 14 summarizes the estimated ventilation retrofit costs for a variety of retrofit options. Table 15 summarizes filter specifications and estimated average power consumption for various types of pleated MERV filters. Table 16 summarizes the annual cost breakdown for filter replacements following manufacturer recommendations and a modified filter change schedule specific for wildfire-resiliency. Note that the cost estimates are in Canadian dollars ($CAD). Table 17 summarizes the total annual cost of various mechanical ventilation system upgrades. The total cost of a particular system upgrade is dependent upon the number of filters employed where model 4, model 11, and model 16 are representative of a 1-filter, 2-filter, and 3-filter configuration, respectively. Case 1 and case 2 refer to the filter maintenance and disposal schedule; case 1 represents filter changes every 3 months as per the air filter manufacturer's recommendations and case 2 represents monthly filter changes during wildfire season (July to September) while reverting to filter changes every 3 months during off-season operation. Case 2 corresponds to a conservative estimate of a wildfire-specific maintenance schedule. However, continuous monitoring of filter-induced pressure drops would provide the most accurate indication of when filter changes are required. As per ASHRAE's planning framework for wildfire ventilation, the recommendation is to replace air filters when the measured pressure drop difference across the air filter is double the original measured value [40]. Both initial and ongoing maintenance costs were accounted for in the cost estimate with the inclusion of PAC use.

Table 14. Summary of reference values used in the cost analysis of wildfire-resilient mechanical ventilation systems.

Component Specification	Reference Values	Source(s)
Fan	Fan Efficiency: 0.7 Air flowrate: 0.39 ACH	Sachs et al. 2002 [106] ASHRAE 62.2-2019 [96]
Air Filter	Cost: $10 - $155 (dependent on MERV-rating) Dimensions: 24”x24” (0.61x0.61 m) Installation and Disposal: $2.21/filter	Various Manufacturers/Product Distributors [107-109]
Energy and Utilities	Electricity: $0.10/kWh	2016 energy rate comparison from BC Hydro [110]
Portable Air Cleaner	Initial Cost: $400 (Philips 2000i Series Air Purifier) HEPA filter replacement - $69.99/filter every 24 months A/C filter replacement - $39.99/filter every 12 months	Manufacturer/Product Distributors [111-113]

Table 15. Summary of filter specifications and estimated average power consumption for various filter types.

Type	Size	Max. Initial Resistance (w.g)	Min. Final Resistance (w.g)	Max. Initial Resistance (Pa)	Min. Rated Final Resistance (Pa)	P_{ave} (ΔPa)	W_{ave} (W)
MERV 6 Pleated	24 x 24 in	0.19	1	47.27	248.84	114.45	11.29
MERV 8 Pleated	24 x 24 in	0.26	1	64.69	248.84	126.07	12.44
MERV 11 Pleated	24 x 24 in	0.20	1	49.77	248.84	116.12	11.46
MERV 13 Pleated	24 x 24 in	0.35	1	87.09	248.84	141.00	13.91
MERV 16 Pleated	24 x 24 in	0.54	1	134.37	248.84	172.53	17.02

Table 16. Total annual filter change cost breakdown for various filter types*

Case	Cost of power (C_w) $USD	Cost of filter (C_f) $USD	Cost of installation and disposal (C_I) $USD	Total cost (C) $USD / $CAD	
MERV 6 Pleated					
1: Changed every 3 month	6.93	40.56	8.96	56.45	69.43
MERV 8 Pleated					
1: Changed every 3 months	7.63	48.67	8.96	65.26	80.27
2: Changed every month from July to September, changed every 3 months for the rest of the year	7.63	73.20	13.48	94.31	116.00
MERV 11 Pleated					
1: Changed every 3 months	7.03	81.11	8.96	97.10	119.43
2: Changed every month from July to September, changed every 3 months for the rest of the year	7.03	122.00	13.48	142.51	175.28
MERV 13 Pleated					
1: Changed every 3 months	8.53	170.33	8.96	187.83	231.03
2: Changed every month from July to September, changed every 3 months for the rest of the year	8.53	256.20	13.48	278.21	342.20
MERV 16 Pleated					
1: Changed every 3 months	10.44	628.61	8.96	648.01	797.06
2: Changed every month from July to September, changed every 3 months for the rest of the year	10.44	672.50	13.48	696.42	856.60

*Note that the reference used to obtain the costs associated with the purchase and installation of the various filters was given in terms of USD. In the context of this report, the final value was presented as both USD and CAD for ease of comparison. The conversion from USD and CAD was based on the 2016 USD→CAD exchange rate.

Table 17. Total annual cost of various mechanical ventilation system upgrade configurations and filter replacement schedules.

Model No.	Case	MERV 6 Pleated		MERV 8 Pleated		MERV 11 Pleated		MERV 13 Pleated		MERV 16 Pleated	
		w/o PAC	PAC	w/o PAC	PAC	w/o PAC	PAC	w/o PAC	PAC	w/o PAC	PAC
4	1	$69	$879	$80	$890	$119	$929	$231	$1,041	$797	$1,607
	2	N/A	N/A	$116	$926	$175	$985	$342	$1,152	$856	$1,666
11	1	$138	$948	$160	$970	$238	$1,048	$462	$1,272	$1,594	$2,404
	2	N/A	N/A	$232	$1,042	$350	$1,160	$684	$1,494	$1,713	$2,523
16	1	$208	$1,018	$240	$1,050	$358	$1,168	$693	$1,503	$2,391	$3,201
	2	N/A	N/A	$348	$1,158	$525	$1,335	$1,026	$1,836	$2,569	$3,379

2.3.2.2. Cost of PM2.5-related Health Effects

The estimated costs representative of PM2.5-related health effects were calculated per region based on the cases of premature mortality based on the 2016 statistics from Health Canada [72] and the estimate of a mid-range statistical value of life from Chestnut et al. [58]. The obtained cost estimates serve as a reference point for executing a cost-benefit analysis but are limited in their representation of wildfire-resilient ventilation system's ability to decrease strain on the healthcare system and improve occupant quality of life. It should be noted that the cost estimate does not include the healthcare cost savings related to short-term PM2.5 health effects. Table 18 summarizes the regional rate of premature mortality due to PM2.5 exposure for Prince George, Vancouver, and Edmonton. Note that per test city, the total premature mortality rate was obtained as a rate of regional premature mortality due to PM2.5 exposure per 100,000 people. This was scaled to represent the rate of premature mortality exposure per regional population of each test city.

Table 18. Regional rates of premature mortality due to PM2.5 exposure from 2016 Health Canada Statistics.

Region – population	**Premature mortality due to PM2.5 exposure**	
	Rate per regional population	**Rate per 100,000**
Canada – 36,229,449	10,000	28
British Columbia – 4,689,131	1,200	26
Vancouver – 2,535,948	21.2	0.84
Prince George – 93,503	2.4	2.52
Edmonton – 1,493,305	16.2	1.08

Values from Table 18 were used as a representation of regional risk associated with wildfire exposure. These were used in conjunction with the mid-range VSL ($6.5M) to calculate an average demonization per occupant deemed acceptable to reduce their risk of premature mortality due to PM2.5 exposure from wildfire events. The calculation of this value for each test city is as follows.

Vancouver

$$\frac{\left(\frac{0.84}{100000} * \$6.5M\right)}{Population} = \frac{\$54.60}{person}$$

Prince George

$$\frac{\left(\frac{2.52}{100000} * \$6.5M\right)}{Population} = \frac{\$163.80}{person}$$

Edmonton

$$\frac{\left(\frac{1.08}{100000} * \$6.5M\right)}{Population} = \frac{\$70.20}{person}$$

The mortality risk mitigation cost estimate obtained for each city is summarized in Table 19. Note that the health effect mitigation cost estimate does attempt to put a monetary value on human life; the monetary value provided is representative of what a resident in a specific region would

willingly contribute to reducing their risk of premature mortality as a result of PM2.5 exposure above the recommended daily exposure limit. In the context of a single detached residential dwelling, the occupancy is between 2 – 4 people, therefore the total denomination that can be feasibility spent on ventilation retrofits is double or up to quadruple the calculated value for a single person.

Table 19. Estimated cost of long-term health effects based on mid-range SVL.

City	Mortality risk mitigation cost estimate ($CAD)	Cost estimate for single-detached residences (2-4 occupants)
Vancouver	$54.60/person	$109.20 – $218.40
Prince George	$163.80/person	$327.60 – $655.20
Edmonton	$70.20/person	$140.40 – $280.80

2.4. Discussion

2.4.1. City

Outdoor PM2.5 concentration varied depending on the test city's proximity to active wildfire events. Based on the test city outdoor PM2.5 datasets, the datasets were categorized into three representative scenarios. Scenario one was categorized by sustained periods of high outdoor PM2.5 concentration as was seen in the Prince George dataset, scenario two by moderate levels and durations of exposure as was seen in the Vancouver and Victoria datasets, and scenario three by transient peaks of high PM2.5 exposure as was seen in the Edmonton dataset. Comparing the IAQ simulation results for the test cities, it is recommended that a region-specific approach to wildfire-resilient mechanical ventilation needs to be implemented to accommodate unique PM2.5 exposure scenarios for geographic regions.

2.4.2. Filter Efficiency

The preliminary results from the IAQ simulations regarding filter efficiency indicate that the current minimum filter recommendation for residential indoor spaces is insufficient for indoor

ventilation with increased outdoor PM2.5 levels due to wildfires. In moderate exposure scenarios like the City of Vancouver, a single MERV16 air filter, or multiple MERV 13 filters were required to reduce the indoor 24-hour peak exposure to below the exposure limit of 27 $\mu g/m^3$, as shown in Table 8. However, in sustained or transient severe PM2.5 exposure scenarios in Prince George and Edmonton, respectively, both increasing the filter efficiency and the number of filters in the ventilation configuration were insufficient to reduce the peak 24-hour average indoor PM2.5 concentration below the recommended exposure limit. Thus, other techniques are required in addition to using a multi-filter mechanical ventilation model and upgrading the minimum filter efficiency to MERV13 to further reduce the indoor PM2.5 concentration in locations prone to severe PM2.5 exposure. A percent difference was calculated between the 1 (Model 4) and 2-filter (Model 11) and between the 2 (Model 11) and 3-filter (Model 16) configurations to assess the significance of the additional filter on indoor PM2.5 exposure. It was found that the percent difference in peak 24-hour average indoor PM2.5 was larger between the 1 and 2-filter models than between the 2 and 3-filter models regardless of filter selection, indicating a limited benefit of 3-filter ventilation configurations to achieve acceptable IAQ. The major contribution is from Model 11's additional filter (Filter C) that is added in the supply air branch before the intersection with the recirculation branch for outdoor air filtration. In addition, it was found that the impact of increasing the number of filters in the system was related to air filter efficiency. Mid MERV-rated filters (MERV 8 – MERV 13) had higher percent differences between models compared to the results in low and high MERV-rated filter configurations, suggesting that mid MERV-rated filters are best suited for multi-filter ventilation configurations.

It should be noted that the practical application of filter upgrades and retrofits is limited by the fan capacity and the airtightness of the existing ventilation system. As recommended by the ASHRAE

planning framework for wildfire ventilation, ongoing system maintenance and monitoring will help ensure the majority of the outdoor air is directed through the air filters before entering the indoor space [40]. Ongoing maintenance includes regularly changing air filters to reduce additional filter backpressure and sealing points of air leakage in the ductwork to improve system-wide airtightness.

2.4.3. Recirculation

An increased recirculation ratio (i.e. increasing the amount of recirculated air relative to outdoor air introduced into the indoor space) effectively decreased the indoor PM2.5 concentration. Notably, a recirculation nearing 1 reduced the peak 24-hour indoor PM2.5 concentration for Prince George. This result shows that increasing the recirculation ratio during the wildfire season is an effective ventilation strategy that can facilitate the use of lower-efficiency air filters while maintaining acceptable indoor PM2.5 levels. It should be noted that high recirculation ratios should be employed on an as-needed, short-term basis for times of peak PM2.5 exposure. Prolonged ventilation system operation with high recirculation may negatively affect IAQ by preventing CO_2 and other pollutants generated within the indoor space from being expelled outdoors. Thus, continuous monitoring of IAQ variables and outdoor PM2.5 concentration is required to create a wildfire-specific ventilation system operation plan that balances indoor PM2.5 concentration with other IAQ requirements.

2.4.4. Design Flow Reduction Factor

The results from section 2.3.1.4 indicate that a design flow reduction factor less than 1 – consistent with the settings in a VAV system – resulted in a higher indoor concentration of PM2.5 compared to the constant airflow case. Since design flow reduction is a limitation that is inherent to VAV ventilation systems, the simulation results emphasize the importance of implementing other ventilation strategies to offset the additional PM2.5 that VAV systems introduce into an indoor

space. Therefore, for single-detached residences situated in locations that are prone to severe PM2.5 exposure from wildfires, it is recommended that constant flow ventilation systems be selected over VAV systems.

2.4.5. Zone Air Distribution Effectiveness

It was found that the zone air distribution effectiveness variable did not have a notable contribution to the indoor PM2.5 concentration. No significant change was noted between a zone air distribution effectiveness of 0.7 and 1; the peak 24-hour average indoor PM2.5 concentration decreased by less than 1 $\mu g/m^3$ with a zone air distribution effectiveness of 0.7. A sensitivity analysis of the IAQ models showed a similar conclusion. The zone air distribution effectiveness variable consistently obtained the lowest total-order indices in comparison to other input variables at 1.51E-6, 4.03E-6, and 3.48E-6 for the 1-filter, 2-filter, and 3-filter ventilation configurations, respectively. This result indicates that the variable does not significantly influence the resultant indoor PM2.5 output. Similar to the design flow reduction factor, in practice, the zone air distribution effectiveness is a variable inherent to the existing ventilation system and would be challenging to alter or control. In addition, the implication of decreasing the zone air distribution effectiveness may negatively impact other indoor environmental quality variables that were not considered part of this study.

2.4.6. Portable Air Cleaner Usage

Overall, portable air-cleaning technology has a positive effect in further reducing indoor PM2.5 concentration. Further, the additional filtration provided by the PAC is sufficient to justify the application of less filter-intensive mechanical ventilation systems for certain PM2.5 exposure scenarios. With PAC usage, the single filter ventilation configuration (model 4) becomes a viable solution to reduce the peak indoor PM2.5 concentration to close to or below the daily exposure limit for Vancouver and Victoria, respectively, as shown in Table 12. In severe PM2.5 exposure scenarios – such as in the datasets for Prince George and Edmonton – the application of PACs serves to decrease the severity of indoor PM2.5 exposure. Based on the preliminary simulation results, a single PAC is insufficient to decrease the 24-hour indoor peak exposure below the daily

limit. Thus, it may be necessary to employ multiple PACs within indoor spaces in locations with severe exposure. Other options include combining ventilation strategies alongside the application of air cleaning technology, such as increasing the recirculation ratio or upgrading the filter efficiency.

The current mathematical model for PAC integration requires further development to account for PAC sizing, operational mode, and factors specific to the indoor space of application to provide a more accurate representation of PAC effectiveness. Though this study focused on applying PACs in residential spaces, PAC application in commercial spaces such as office buildings and lecture halls would positively impact occupants with sensitivities to smoke and other air contaminants. Additional research is required regarding the sizing and placement of PAC in commercial spaces to ensure the maximization of PAC effectiveness outside its typical residential application.

2.4.7. Sensitivity Analysis

The results from the sensitivity analysis in section 2.3.1.7 suggest that the air filter in position A may not have as significant an impact on the indoor PM2.5 concentration in comparison to air filters B and C. This result is in alignment with the trend shown in the percent difference comparison in section 2.3.1.2. Further model refinement is required to account for the effect of filter efficiency on air pressure changes and duct leakage within the ventilation system to better assess the impact of filter A on indoor PM2.5 levels. The total-order index for the infiltration rate was 0.054, 0.146, and 0.165 for the 1-filter, 2-filter, and 3-filter configurations, respectively. The magnitude of the total-order index of building infiltration rate indicates its significance and impact on the resultant indoor PM2.5 concentration. Thus, further model development is required to represent the building infiltration rate as a function of building age, building envelope quality, and the building's air pressure relative to the surrounding outdoor environment. It should be noted that

the integration of PACs into the IAQ models was not included in the sensitivity analysis due to the preliminary nature of its mathematical model. Future development of the PAC variable is required to improve model specificity that represents PAC effectiveness as a function of room size, operational mode, duration of use, and placement within the indoor space.

2.4.8. Cost-Benefit Analysis of Ventilation Strategies

A cost-benefit analysis was conducted to assess the financial feasibility of the various ventilation retrofits proposed in section 2.3.2.1. The range of reasonable financial contributions to mechanical ventilation retrofit is dependent upon region-specific PM2.5 exposure levels and occupancy. For the assessment of ventilation retrofit options in single-detached residences, typical residential occupancy (2 – 4 occupants) was assumed with the associated ranges of monetary contribution provided in Table 6 of section 3.2.2. Table 20 summarizes the ventilation retrofit options for each test city that are within or below the price range obtained for residences with typical occupancy.

Table 20. Feasible mechanical ventilation retrofits for various geographical regions in western Canada.

City	Contribution Range	Model	Ventilation Configuration Model		PAC usage (Y/N)
			3-month filter change schedule (Plan 1)	Modified filter change schedule (Plan 2)	
Vancouver	$109.20 – $218.40	1-filter	6, 8, 11	8, 11	N
		2-filter	6, 8	No suitable models.	N
		3-filter	No suitable models.	No suitable models.	N
Prince George	$327.60 – $655.20	1-filter	6, 8, 11, 13	8, 11, 13	N
		2-filter	6, 8, 11, 13	8, 11	N
		3-filter	6, 8, 11	8. 11	N
Edmonton	$140.40 – $280.80	1-filter	6, 8, 11, 13	8, 11	N
		2-filter	6, 8, 11	8	N
		3-filter	6, 8	No suitable models.	N

The results indicate that a recommendation to increase the minimum filter efficiency to a MERV11-rated air filter during the wildfire season is justified and would be deemed feasible by residents in cities prone to mid and severe PM2.5 exposure. This aligns with ASHRAE's recommendations to implement MERV11 or MERV13 air filters for ventilation systems operating during periods of poor air quality – such as during active wildfire events [71]. For Prince George and regions that experience similar severe PM2.5 exposure conditions, it is recommended and financially justified that a 3-filter configuration with MERV11 filters is considered a ventilation retrofit strategy. In addition, it was found that the use of PACs is not feasible for residential applications based on the calculated retrofit monetary contribution range of residential occupants. Since the purchasing of ventilation system air filters takes precedence over the acquisition of PAC technologies, the current price points for PAC units and accessories cannot be supported concurrently with air filter upgrades.

2.5.Conclusion

This section focused on the development of wildfire-resilient ventilation systems for application during the western Canadian wildfire season. IAQ mathematical models were developed to represent various single-zone mechanical ventilation system configurations. IAQ simulations were conducted using the IAQ models to assess the impact of various ventilation and building-related variables on the resultant indoor PM2.5 level. Results from the IAQ simulations yielded several recommendations for adequate ventilation in wildfire conditions. It is recommended that the minimum air filter efficiency requirement be increased from MERV6 to MERV 11 or MERV13 during the wildfire season and that double-filter ventilation configurations be considered for locations prone to severe outdoor PM2.5 exposure levels - such as in Prince George and surrounding areas near active wildfire events. In addition, it is recommended that near 100% recirculation be implemented as a short-term tactic during severe peaks in outdoor PM2.5 levels.

The results from both the cost-benefit analysis and model sensitivity analysis further supported the above recommendation for filter efficiency upgrades and double-filter mechanical ventilation systems. The impact of portable air cleaners as a locally applied ventilation strategy was also assessed using the developed IAQ models. Although PAC usage further decreased the indoor PM2.5 level, the cost-benefit analysis indicated that the current price point for these products deemed their application unjustifiable for wildfire-resiliency retrofits. In practice, the recommendations from this study emphasize the need to implement continuous monitoring of IAQ and ventilation variables within mechanical ventilation systems. Thus, further research is required to experimentally validate the results and recommendations from this study and assess the practicality of their application to existing residential mechanical ventilation systems.

3. Optimizing automated shading systems for enhanced energy performance in cold climate zones: strategies, savings, and comfort

3.1. Introduction

The rapid growth of urban areas worldwide has cast a spotlight on the built environment and its impact on urban sustainability [116-118]. Urban sustainability assesses the environmental, social, and economic impacts of various city infrastructure components, aiming to enhance the overall livability of urban centers while minimizing their impact on surrounding areas [116, 119]. A study by Yıldız et al. identified and ranked key environmental design elements for urban renewal [116]. Among the 32 identified design elements, those linked to building occupants, such as human comfort-focused building design and occupant-centered design considerations, ranked higher than design elements related to environmental sustainability and resource usage [116]. This result is consistent with findings from a review on Energy Efficiency Retrofitting (EER) by Maghsoudi et al. [118]. In their review, Maghsoudi et al. emphasized the significance of occupant participation and coordinated occupant behavior for the success of EER projects. In the context of built environments, sustainable buildings and building retrofits are energy efficient, comfortable for occupants, and financially viable [120]. Therefore, successfully integrating energy efficient technologies and retrofit strategies into building systems requires striking a balance between building energy performance and occupant comfort.

Maintaining adequate thermal and visual conditions within indoor spaces is critical for occupant comfort and building energy performance [121-123]. A study by Boubekri et al. found that workers in offices with natural lighting reported a higher quality of life and improved sleep quality in comparison to workers in windowless offices [121]. As a result, modern buildings tend to maximize natural lighting in indoor environments by integrating ample glazing features within the

building envelope. This design choice also reduces lighting related energy consumption by minimizing the use of artificial lighting [124, 125]. However, buildings with a high glazing area also encounter challenges regarding uncontrolled solar gain and overheating. A review by Seppanen et al. assessed the benefits of indoor temperature control on worker productivity [122]. Through a meta-analysis of existing literature, the review found that a productivity decrement of approximately 2% per degree Celsius occurred for indoor temperatures above 25°C [122]. In indoor spaces exposed to solar radiation, increased glazing area amplifies the effect of indoor solar gain [126-128]. A study by Evola et al. found that buildings with high glazing areas and solar exposure experience a degradation in indoor thermal and visual comfort due to space overheating and glare, respectively [126]. Overheating caused by excessive solar gain has also been found to increase building cooling-related energy usage during the summer season [127, 128]. For buildings located in cold climate zones, glazing-dominant buildings experience higher heat loss across the building envelope due to the limited thermal resistivity of fenestration [39, 129, 130]. This results in increased building heating-related energy usage during the heating season. For new building constructions, updated energy codes and standards ensure that a certain level of energy efficiency is met by the building [131, 132]. In addition, newer heating, cooling, and lighting equipment selections ensure an improved level of building energy performance in comparison to older constructions [133].

3.1.1 State of the Art - Automated Shading Systems

Energy efficiency and indoor comfort are essential factors in the design and retrofit of building systems. The building sector accounts for approximately 40% of global energy consumption and approximately 55% of worldwide electricity usage [134, 135]. Within the total energy consumption required for typical building operation, nearly 45% is dedicated to meeting space

heating, cooling, and lighting requirements [136]. The energy needed to fulfill the thermal and visual demands of a built environment depends on the initial design conditions, construction quality, equipment selection, and maintenance [137, 138]. Updated government policies on building energy performance and net-zero emissions goals highlight the importance of retrofit strategies applicable to existing constructions. Unlike new constructions that comply with stricter energy-related codes and standards, existing buildings often have envelope and equipment deficiencies that persist from the original construction period [139, 140]. Studies have recommended deep retrofit strategies, such as equipment upgrades and building component replacements, to improve the energy performance of existing buildings [141, 142]. However, these strategies are often costly and/or disruptive to building occupants and daily operations. Thus, minimally invasive retrofit strategies have gained traction as economical alternatives to large-scale building components and equipment upgrades [130, 143, 144]. Regarding fenestration-related retrofit strategies, recent reviews have discussed the impact of various retrofit technologies on building energy performance [38, 145, 146]. In their state-of-the-art review on retrofit technologies for fenestration applications, Shum et al. assessed the effectiveness of various technologies, including glazing coatings and films, adaptive glazing, and automated solar shading systems [145]. It was found that technologies such as automated shading systems and storm window panels were better suited for cold climate applications due to their capacity to achieve both heating and cooling-related energy savings [145].

Window shades have long served as an interior decorating feature in most commercial and residential buildings. Shading systems obstruct part or all of a window to regulate sunlight entering the indoor space and enhance privacy. However, the implementation of “complex fenestration systems” (i.e., glazing units fitted with automated window shading systems) to improve energy

efficiency remains a novel topic within building science. In cooling season-dominant climate zones, shading systems and smart windows have proven effective at reducing a building's cooling-related energy consumption [147, 148]. In heating season-dominant climate zones, there is limited research on the effectiveness and year-round applicability of automated shading systems. Studies have found that automated shading systems outperform other fenestration technologies due to their ability to address both radiative and conductive heat transfer across the glazing unit [145, 149, 150]. Radiative gain from solar exposure increases building cooling load during the summer, while conductive and convective loss across the glazing unit raises building heating load during the winter. Thus, using insulative window shade materials and automating the system with a season-differentiated control strategy is necessary to ensure both heating and cooling season energy savings are achieved [145, 151].

The functionality of automated shading systems is determined by their control strategies. Most automated shading systems currently available on the market rely on sensor or schedule-based control methods for shade operation [152, 153]. Although this approach is functional and responsive to real-time changes in room conditions, the resultant shade operation can be overly responsive to transient changes in a particular parameter. For example, an indoor lighting-based shading control strategy that uses a light sensor to determine when to shade a room tends to move the shade regardless of the duration of the shift in lighting. Frequent adjustment of shade position and configuration can become distracting to occupants, and therefore negatively impact technology acceptance and integration into various indoor spaces [154-156].

3.1.1. Study Objectives and Innovation

Though automated shading systems have been investigated for use in warm climate zones, their applications in cold climate zones remain a novel topic within building science research. This

study delves into the optimization of automated window shading systems tailored for applications in cold climate zones. A sensorless control strategy for these automated shading systems was developed, aiming to improve the year-round building energy performance during both the heating and cooling seasons. Next, the effectiveness of the energy-efficient shading strategy and the corresponding prototype shading system were evaluated. A rigorous mathematical model was developed to quantify the heating and cooling-related energy savings achieved through automated shading implementation. Finally, a field study was conducted within an office space featuring a high-glazing area using automated roller shades and the novel control strategy. Motorized roller shades were installed in southwest-facing office space with a high Window-to-Wall ratio to assess the impact of the developed control strategy on indoor thermal conditions in comparison to both shaded and unshaded static baseline operation modes. Data collected from the field study was used to assess the overall impacts of automated shading implementation on indoor thermal comfort and lighting levels. The innovation of this work lies in the development of an innovative sensorless control strategy and a comprehensive evaluation approach, bridging the gap between energy efficiency and occupant comfort throughout the year.

3.2. Methodology

3.2.1. Building Energy Modelling

To assess the energy performance of various existing control strategies, an EnergyPlus-based building energy model was developed using COMFEN (Version 5.0.33). COMFEN is a user interface for fenestration system simulations, developed by the Building Technology and Urban Systems Division of Berkeley Lab [157]. A 6.1 x 6.1 x 3 m test space was created within the virtual environment, with specifications similar to the office test space used for the field study component of this project. Key model parameters and assumptions are summarized in Table 21.

Table 21. Summary of COMFEN building energy model parameters and assumptions.

Model Parameters	Value
Wall Construction	Default climate zone-specific wall construction requirements (predefined by COMFEN)
Window Specifications	*Clear Double Glazing* Thickness: 24.13 mm U-factor: 2.689 W/m^{2}K Solar Heat Gain Coefficient (SHGC): 0.704 Visible Transmittance: 0.786
Window Dimensions (# of windows x (W x H) - orientation)	1 x (99 x 223 cm) – south 1 x (99 x 223 cm) – west 3 x (95.4 x 223 cm) – south 4 x (95.4 x 223 cm) – west
Occupancy	2 people
HVAC Equipment	Packaged Single Zone • Cooling Coil: Electric • Heating Coil: Natural Gas
Shading System Type	Interior Roller Shade • Color: white • Thickness: 0.51 mm • Solar Reflectivity: 0.65 • Thermal Emissivity: 0.7 • Thermal Conductivity: 0.865 W/mK • Shade-to-Glass Distance: 12.7 mm

Five cities were selected as test locations for the COMFEN simulations: Vancouver, Edmonton, Toronto, Quebec, and Fairbanks. All test cities were located in cool and cold climate zones as defined by ASHRAE Standard 169 [31]. Cold climate zones are heating dominant regions with a higher number of heating-degree-days (HDD) than cooling-degree days (CDD) [31]. Each test city received varying levels of annual solar intensity and exposure, as determined by the estimated PV panel output range of the geographical region where a particular city was located [158, 159]. To ensure the PV panel outputs obtained from the database were comparable to the solar exposure received by vertical glazing units, only the south-facing 90-degree vertical PV panel outputs were

considered. A summary of the climate zone characteristics and solar irradiance exposure levels is shown in Table 22.

Table 22. Summary of climate zone characteristics and solar irradiance exposure levels for selected cities.

City	**Climate** (**ASHRAE** [31] / **Köppen** [160])	**Mean daily global insolation** [158, 159]	
		Winter (MJ/m^2)	**Summer** (MJ/m^2)
Vancouver	Zone 4C / Cfb	13.4	11.6
Toronto	Zone 5A / Dfa	13.4	10.6
Quebec City	Zone 6A / Dfb	16.1	10.5
Edmonton	Zone 7 / Dfb	17.0	12.7
Fairbanks*	Zone 8 / Dfb	15.5	12.8

*Estimated based on solar exposure data for Whitehorse, Canada

A limitation of the COMFEN user interface was its restriction on the number of exterior walls with windows allowed in a simulated space. The office space used for the field study was a south-west facing, with two exterior walls with windows. Thus, the south and west exterior walls and their respective glazing units were modelled separately. The models for the south facing and west facing exterior walls are shown in Figures 16a and 16b, respectively.

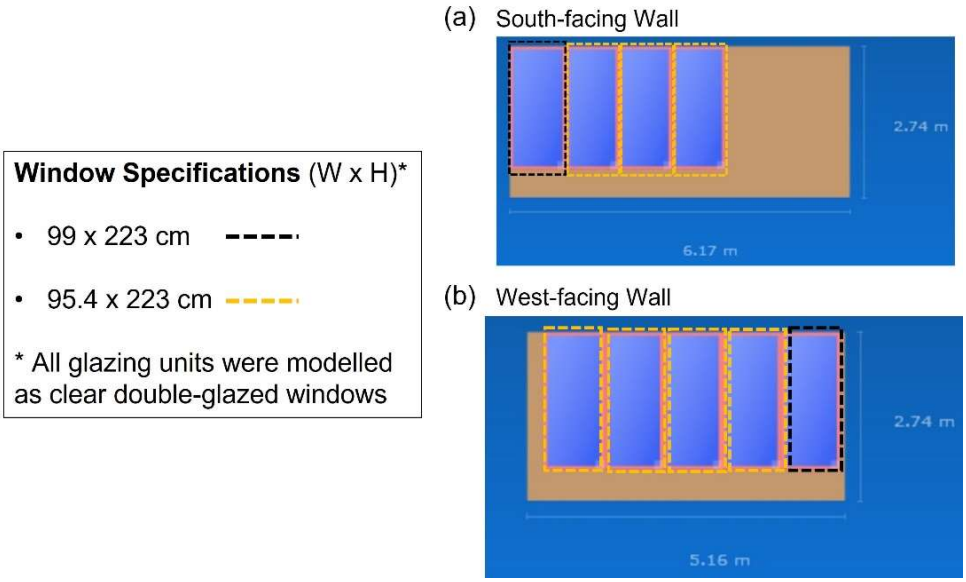

Figure 16. COMFEN model setup for exterior wall facades. (a) Specifications for south facing wall. (b) Specifications for west-facing wall.

To gain a preliminary understanding of automated shading system control strategies, five unique shading control methodologies were implemented. The heating and cooling energy performance of each control methodology was simulated through COMFEN. This process was repeated for all test cities to understand the impact of climate zone and solar exposure on the energy performance of automated shading systems. Table 23 provides a summary and description of each shading control methodology implemented within the simulations.

Table 23. Summary of automated shading system control strategies implemented in the building energy simulation.

Shading Control Strategy	**Description**
Baseline (no shade)	No shading system is implemented on the glazing unit, fully unshaded.
Control Strategy 1 (CS1)	Shade during the day if room is cooling and glazing has high solar exposure (> 150 W/m^2), fully shaded overnight.
Control Strategy 2 (CS2)	Shade during the day if room is cooling and glazing has high solar exposure (> 150 W/m^2), unshaded overnight.
Control Strategy 3 (CS3)	Shade during the day if room is cooling (> 0.50 W), shade overnight if room is heating (> 0.50 W).
Control Strategy 4 (CS4)	Shade during the day if outdoor air temperature is high and glazing has high solar exposure (>150 W/m^2).
Control Strategy 5 (CS5)	No Shading during the day, shade overnight if heating (> 0.50 W).

150 W/m^2 is above the direct solar irradiance lower limit (120 W/m^2) set by the World Meteorological Organization (WMO) to define the start and end times for calculating sunlight duration [161]. Thus, 150 W/m^2 serves as an acceptable low irradiance threshold to trigger shade operation. A default simulation threshold of 0.50 W was used for all control strategies with indoor heating/cooling status as an input variable.

3.2.2. Mathematical Model for Automated Shading Systems

A mathematical model was developed to quantify the magnitude and mechanisms of heat transfer across the glazing-shading system combination. This mathematical model was used as the foundation of a sensor-less automated shading control strategy. The goal of this control strategy was to optimize heat transfer across glazing units, allowing for the indirect tracking of estimated energy savings achieved through device implementation. Depending on the orientation and intensity of solar gain, the shade position was adjusted to its optimal configuration.

3.2.2.1. Governing Equations for Complex Fenestration Systems

The mathematical model was developed using governing equations obtained from the 2021 ASHRAE Fundamentals Handbook [34].

Eq. (9) represents radiative heat transfer across the glazing unit resulting from solar gain.

$$Q_{rad} = (IAC)\left(SHGC_{direct}(\theta)I_{direct} + SHGC_{diffuse}I_{diffuse}\right) \tag{9}$$

where I_{direct} and $I_{diffuse}$ represent the direct normal and diffuse horizontal solar irradiance, respectively. The radiative properties of the window are described by its direct and diffuse solar heat gain coefficients ($SHGC_{direct}$ and $SHGC_{diffuse}$, respectively). SHGC values for various window types are provided within the ASHRAE Fundamentals Handbook [34]. For modelling fabric roller shades, an indoor attenuation coefficient (IAC) is considered to represent the material properties of the roller shade fabric. Solar movement is a well-studied and documented topic; the solar path and its variation throughout the year are represented by changes in the solar azimuth and zenith angles [34]. Figure 17 provides a visual representation of solar angles and their interaction with the receiving surface.

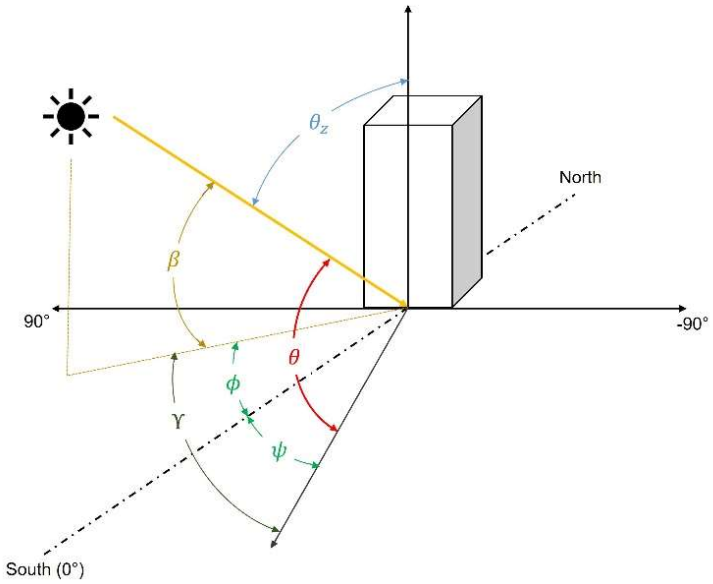

Figure 17. Graphical representation of solar angles and their interactions with the receiving surface.

The solar altitude (β) is used in conjunction with the surface-solar azimuth angle (Υ) and surface tilt angle (Σ) to obtain the incident angle (θ) as shown in Eq. (10).

$$\theta = \cos^{-1}(cos\beta cos\Upsilon \sin\Sigma + \sin\beta\cos\Sigma) \tag{10}$$

This study focused on vertical glazing surfaces ($\Sigma = 90°$), allowing Eq. (10) to be represented in a simplified form as shown in Eq. (11).

$$\theta = \cos^{-1}(cos\beta cos\Upsilon) \tag{11}$$

The surface-solar azimuth angle (Υ) is calculated using Eq. (12), where (ϕ) is the solar azimuth angle and (ψ) is the surface azimuth angle.

$$\Upsilon = \phi - \psi \tag{12}$$

The solar altitude angle (β) is complementary to the solar zenith angle (θ_z) as shown in Eq. (13).

$$\beta = 90 - \theta_z \tag{13}$$

Eq. (14) represents the conductive and convective heat transfer across the glazing unit ($Q_{cond,conv}$), resulting from the temperature gradient between indoor and outdoor conditions (ΔT). The thermal conductivity of various window types is provided within the ASHRAE Fundamentals Handbook [34]. An equivalent thermal conductivity, accounting for the roller shade material deployed over the window, was obtained through simulations in WINDOW, an EnergyPlus user interface [162]. The glazing surface area (A) is the total transparent surface area of the window that permits solar transmittance into the indoor space.

$$Q_{cond,conv} = U_{eq} A \Delta T \tag{14}$$

The total heat flux across the glazing unit (Q_{total}) is presented in Eq. (15) as a summation of the radiative (Q_{rad}) and conductive and convective ($Q_{cond,conv}$) heat transfer.

$$Q_{total} = \sum (Q_{rad} + Q_{cond,conv}) \tag{15}$$

Solar intensity varies per day, depending on weather conditions, cloud cover, and day length. Satellite-based ground level solar irradiance data were obtained from Solcast API [163] to ensure the solar intensity values used within the model are representative of local conditions pertaining to a building of interest. Data from Solcast API accounts for local weather conditions and is accurate within a 2 km radius of a point of interest. Location-specific solar azimuth and zenith

angles were obtained from the National Oceanic and Atmospheric Administration (NOAA) Solar Geometry Calculator [164].

3.2.2.2. Estimation of Energy Savings

An estimate of energy savings was determined using the mathematical model developed in section 3.2.2.1. Energy savings from automated shading system implementation are realized in reduced building heating and cooling consumption. To quantify these savings, two baseline scenarios were defined. The effectiveness of the dynamic operation mode was assessed by comparing the estimated heating and cooling-related energy usage before and after the implementation of the automated shading system.

Baseline condition 1 was a "no shading" scenario in which the baseline glazing unit was always unshaded. This condition represented buildings with fully exposed glazing units. Baseline condition 2 was a "fully shaded" scenario in which the baseline glazing unit was always entirely obstructed by the shading system. Though manual shades can be adjusted, studies on the effectiveness of manual shading systems have found that occupants rarely change the shading configuration [165, 166]. Thus, a "fully shaded" baseline condition was considered to represent glazing units equipped with manual shading systems. The "dynamic shading" test case was representative of a scenario where the shade configuration within each glazing unit varied in response to changes in solar intensity and outdoor thermal conditions, as determined by the developed control strategy. The estimated energy savings obtained through automated shading system implementation were calculated using Eq. (16).

$$Q_{savings} = Q_{total,baseline} - Q_{total,dynamic} \tag{16}$$

The relative impact of various building and weather-related variables on heating and cooling loads was determined by conducting a variance-based global sensitivity analysis. In addition to fenestration-based heat transfer, radiative, conductive, and convective heat transfer across opaque exterior wall components were also considered. The sensitivity analysis was executed using SALib, an open-source python library for sensitivity analyses and related operations [57].

The heating/cooling load offset by the building heating/cooling system was modelled as an energy balance of the various sources of heat transfer within a typical test space. The responding variable is Q_{HVAC}, the amount of additional energy required to balance out the heat flux within the test space as shown in Eq. (17).

$$Q_{HVAC} = \dot{m}_{diffuser} c_{p,air} T_{inlet} \tag{17}$$

$Q_{cond,conv,op}$ represents the conductive and convective heat transfer across the glazing surface (Eq. (18)) and $Q_{rad,op}$ represents the radiative heat transfer across opaque wall surfaces (Eq. (19)), where T_{eo} is the sol-air temperature.

$$Q_{cond,conv,op} = \frac{1}{R_{eq}} A \Delta T_{in,out} \tag{18}$$

$$Q_{rad,op} = \frac{1}{R_{eq}} A (T_{eo} - T_{in}) \tag{19}$$

The sol-air temperature, as shown in Eq. (20), is an equivalent outdoor temperature that is representative of the rate of heat transfer from both convective heat transfer with the outdoor air and the solar radiative gain on an opaque surface.

$$T_{eo} = T_{out} + \frac{\alpha I_{global}}{h_o} - \frac{\varepsilon \Delta R}{h_o}$$

(20)

Note that the term $\frac{\varepsilon \Delta R}{h_o}$ is not included in the final model as it is common to assume $\Delta R = 0$ for vertical surfaces. According to the ASHRAE handbook chapter 18, section 6.4, ΔR is defined as the difference between surrounding longwave radiation and radiation emitted by a blackbody at outdoor air temperature. When there is high solar irradiance, objects exposed to sunlight typically have a higher temperature than the outdoor air temperature. Thus, the objects longwave radiation acts as the blackbody and is equivalent to the surrounding longwave radiation; common practice to assume $\Delta R = 0$.

$Q_{cond,conv,glazi}$, as shown in Eq. (21), represents the convective heat transfer across the glazing surface. $Q_{rad,glazing}$, as shown in Eq. (22) represents the radiative gain from solar irradiance across the glazing surface.

$$Q_{cond,conv,glazing} = UA\Delta T_{in,out}$$

(21)

$$Q_{rad,glazing} = I_{dir}A\big(SHGC(\theta)\big)\big(IAC(\theta,\Omega)\big) + I_{diff}A(SHGC_{diff})(IAC_{diff})$$

(22)

For indoor temperature to remain constant over time, an equilibrium must be achieved from the various heat sources and heat sinks within the indoor space where $\sum Q = 0$, resulting in the final energy balance as shown in Eq. (23).

$$Q_{HVAC} = Q_{cond,conv,glazing} + Q_{rad,op} + Q_{cond,conv,glazing} + Q_{rad,glazing}$$

(23)

It should be noted that the energy balance described in Eq. (23) makes the following assumptions to simplify the model within the sensitivity analysis. Heat gains and losses from internal sources are not included. Heat transfer across internal walls, ceilings, and floors is also neglected such that Q_{HVAC} is isolated to the effects of heat transfer along the building envelope and exterior walls.

Table 24 defines all variables considered within the energy balance and the variable range selected for the sensitivity analysis. Variable ranges for wall reflectivity, direct indoor attenuation coefficient, glazing thermal transmittance, wall thermal resistance, direct and diffuse solar heat gain coefficient were obtained from the ASHRAE Fundamentals Handbook [34]. Climate and solar data ranges were obtained from ASHRAE climate data and solar irradiance databases, respectively [31, 163]. Table 25 summarizes all city and season-specific variables (outdoor design conditions and typical solar intensity, respectively) considered within the energy balance and the variable ranges selected for the sensitivity analysis. The winter design conditions and solar ranges were determined based on region-specific Heating DB (99.6%) and upper solar ranges during the winter months. Winter months were defined as months that exclusively contained heating degree days (HDD). The summer design conditions and solar ranges were determined based on region-specific cooling DB (1%) and upper solar ranges during the summer months. Summer months were defined as months that were cooling degree days (CDD) dominant. Using the summer and winter design temperatures as the summer maximum and winter minimum seasonal temperatures, respectively, a winter and summer outdoor temperature range was identified. For each test city, the winter temperature range would span from 10 ºC down to the city's particular winter design temperature whereas the summer temperature range would span from 10 ºC up to the city's summer design temperature.

Table 24. Summary of variable definitions and ranges used within the energy balance sensitivity analysis.

Variable	Range	Units
Air Flowrate ($\dot{m}_{diff}$)	100 – 200 (34 – 68)	ft^3/min (kg/s)
Air Specific Heat ($c_{p,air}$)	1006	J/kg°C
Indoor Air Temp (T_{in})	22	°C
Wall Reflectivity ($\frac{\alpha}{h_o}$) – light to dark surfaces	0.026 – 0.052	
GHI (I_{global})	0 - 1000	W/m^2
DNI / DHI (I_{dir}, I_{diff})	0 - 1000	W/m^2
Direct Indoor Attenuation Coefficient (IAC)	0.37 – 0.55	
Glazing Thermal Transmittance ($U_{glazing}$)	2.33 – 2.95	W/m^2K
Wall Thermal Resistance (R_{eq})	3.44 - 6.06	m^2K/W
Wall Area (A_{wall})	30	m^2
Glazing Area ($A_{glazing}$)	20 – 70% wall area	% of wall area
Direct Solar Heat Gain Coefficient ($SHGC$)	0.70 – 0.81	
Diffuse Solar Heat Gain Coefficient ($SHGC_{diff}$)	0.32 – 0.66	
cos (θ)	0 - 1	

Table 25. Summary of seasonal outdoor design conditions for various test cities [31].

City	Climate Zone	Winter Conditions		Summer Conditions		
		Design Temperature (°F/ °C)	Solar Range (months)	Design Temperature (°F/ °C)		Solar Range (months)
Ottawa	ASHRAE 6A	-11.4 / -24.1	Jan – Apr, Oct - Dec	87.5 / 30.8	84.5 / 29.2	Jun - Sept
Edmonton	ASHRAE 7	-26.2 / -32.3	Jan – Apr, Oct - Dec	82 / 27.8	79 / 26.1	Jun - Aug
Iqaluit	ASHRAE 8	-34.7 / -37.1	All year	62.8 / 17.1	57.8 / 14.3	No summer conditions

3.2.2.3. Financial Analysis

The mathematical model described in Section 3.2.2.1 was combined with the custom shading control strategy methodology to create a custom energy calculator for cold-climate optimized automated shading systems. The custom energy calculator output estimated heating and cooling-related building energy savings based on user-specified inputs such as window specifications (type, quantity, orientation), building geographical location, and heating and cooling equipment specifications (efficiency, fuel type, regional utility prices). It should be noted that a "static, no shading" baseline condition was considered in the calculator. This baseline condition assumes that the implementation site of interest does not have any type of shading system already installed with the glazing units.

A cost-benefit analysis was used to determine the financial feasibility of implementing automated shading systems in commercial buildings located in cold climate zones. A pricing range of $200 - $400 CAD per shade was used as a representative cost that included the production, installation, and maintenance of the automated shading unit [167, 168]. As shown in Eq. (24), the estimated reductions in heating and cooling load were combined with equipment efficiencies (η_{eq}) and local utility rates ($C_{utility}$) to obtain an estimate of annual monetary savings (S_{annual}) from automated shading system implementation. To promote the adoption of green retrofit strategies in buildings, many jurisdictions have implemented incentive programs that credit building utility bills based on quantifiable improvements in building energy performance. The incentive rate ($C_{incentive}$) is included in Eq. (24). It should be noted that incentive rates are often season specific, where electric savings are incentivized during the summer, while natural gas savings are incentivized during the winter [169].

$$S_{annual} = Q_{savings}\eta_{eq}C_{utility} + Q_{savings}C_{incentive}$$

(24)

A simple payback was calculated based on the price of shading system implementation and the estimated annual monetary savings. To contextualize the financial feasibility of automated shading systems, the calculated payback period was compared to the typical payback periods for various building retrofit strategies and technologies. Representative payback periods were obtained from manufacturer catalogues and local utility reports.

3.2.3. Automated Shading Prototype Field Study

A 27.23 m^2 south-west facing office space (SUB 6-24) in the Students' Union Building at the University of Alberta, located in Edmonton, Canada (53.5253° N, 113.5274° W), was selected as the field study test space, as shown in Figure 18. Due to its high window-to-wall ratio (WWR) and orientation, this office space experienced overheating issues due to excess solar gain. Key dimensions and specifications of the test space are summarized in Table 26. The field study was conducted from July 2022 – March 2023, with continuous monitoring of indoor thermal conditions. Interior motorized roller shade prototypes were installed in all glazing units within the office space. Using a custom web-based control platform, roller shade configurations were optimized and automatically adjusted through the novel dynamic shading control strategy developed for this project. The dynamic control strategy featured both a heating and cooling season optimized operation modes, Dynamic, W and Dynamic, S, respectively. Two baseline conditions were considered to assess the impact of the shading control strategy on indoor thermal conditions. Baseline 1 was a "static, no shading" operation mode where all window shades were fully retracted to expose the entire glazing area. Baseline 2 was a "static, fully shaded" operation mode where all window shades were fully deployed over the entire glazing area.

Table 26. Summary of key building specifications of the test office space.

Test Space Specification	Value
General dimensions (L x W x H)	6.4 x 4.3 x 2.7 m
Glazing properties (# of windows x (W x H) - orientation)	1 x (99 x 223 cm) – south 1 x (99 x 223 cm) – west 3 x (95.4 x 223 cm) – south 4 x (95.4 x 223 cm) – west
Glazing type [157] *Note that these values are simulated	*Clear Double Glazing** Thickness: 24.13 mm U-value: 2.689 W/m^{2}K Solar Heat Gain Coefficient (SHGC): 0.704 Visible Transmittance: 0.786
HVAC specifications	• Constant Air Volume (CAV) Air Handling Unit • Floor-Mounted Induction Unit
Indoor temperature setpoint	22 ºC

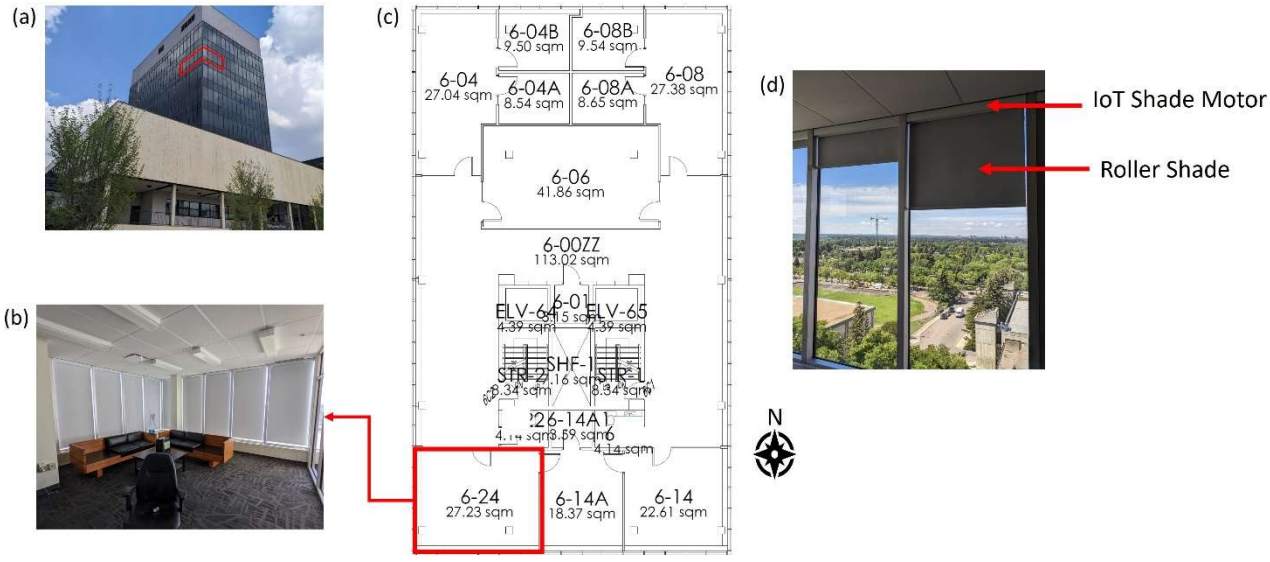

Figure 18. Test office space and floorplan of SUB 6-24 in the Students' Union Building in Edmonton, Canada. (a) Exterior view of the Students' Union Building at the University of Alberta with the test space exterior windows outlined in red. (b) Interior view of the SUB 6-24 office space with all roller shades in the fully deployed position. (c) Floorplan of the 6th floor of the Students' Union Building where the test space and associated room dimensions are outlined in red. (d) Roller shade prototype with components labelled. Note that an IoT gateway (not shown) was used to connect the shades to the control strategy.

Internet of Things (IoT) temperature and relative humidity were placed at various locations in the office test space to continuously monitor indoor thermal conditions. The sensors used in the field

study are shown in Figure 19a. Manufacturer device specifications for each sensor are summarized in Table 27. All sensors were calibrated before their use in the field study to ensure accurate measurements of thermal conditions and comparable data between sensors. Sensors were positioned away from the walls, windows, and doorways to minimize the effect of localized temperature gradients and solar exposure on the resultant measurements. Figure 19b shows the various sensor locations within the office space. Each sensor was placed at table height, approximately 1 meter above the floor level.

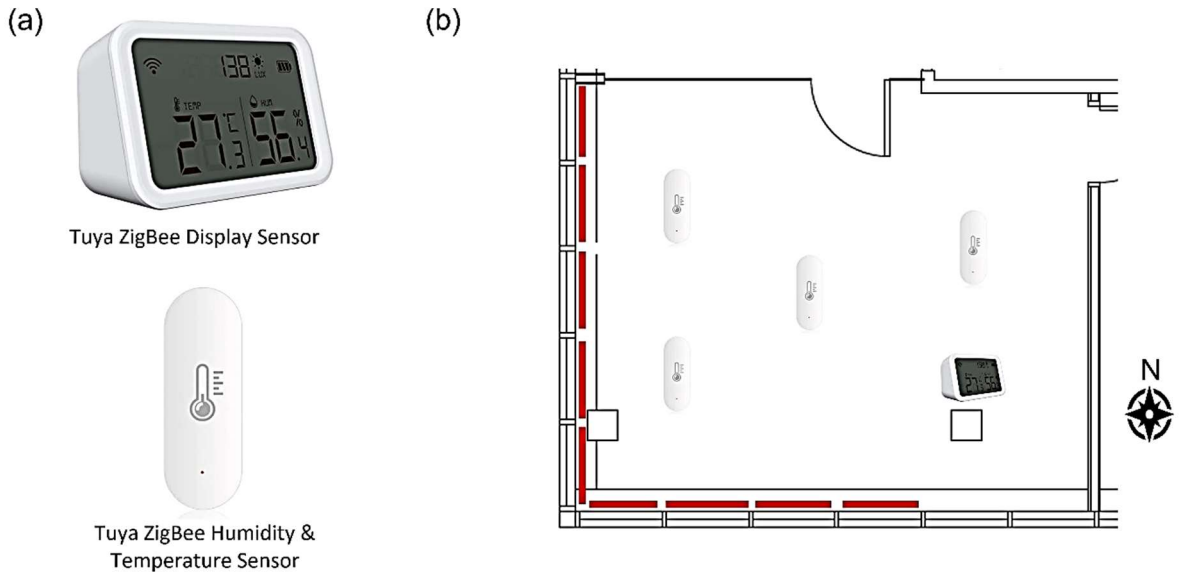

Figure 19. (a) IoT Sensors used for continuous data collection within the test space. (b) Placement of IoT sensors within the office test space. Shading prototype placement is indicated in red.

Table 27. Summary of sensor specifications.

Sensor Specifications	**Sensor Type**	
	Tuya ZigBee Humidity & Temperature Sensor	*Tuya ZigBee Display Sensor*
Protocol	Zigbee 3.0	Zigbee 3.0
Material	ABS	ABS
Temperature Detection Range	(-)20 - 60 °C (± 0.3 °C)	(-)10 - 60 °C (± 0.3 °C)
Moisture Detection Range	0 - 100% RH (±0.3%) <95%	0 - 90% RH (±0.3%)
Dimensions	69 x 24 x 19 mm	84 x 32 x 55 mm

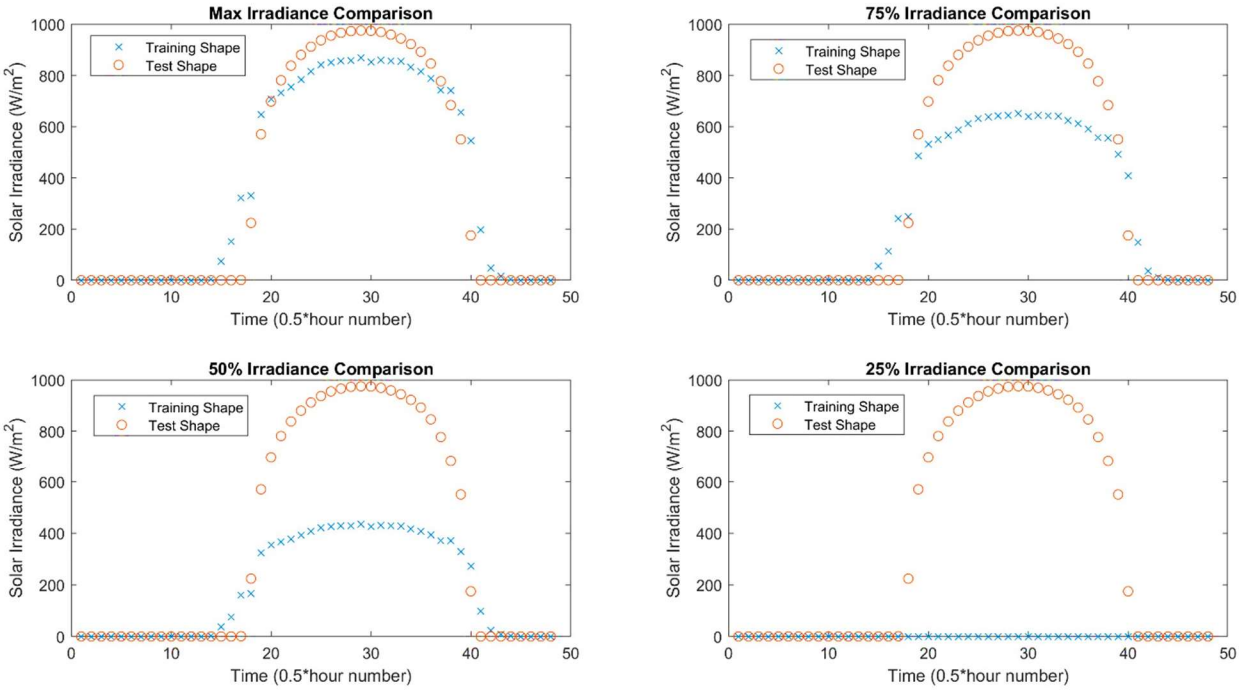

Figure 20. Visual representation of daily irradiance data categorization based on the root mean square distance between the model and test irradiance curves. Model irradiance curves (blue x's) range from 100% intensity to 25% intensity. Sample irradiance data from March 16, 2023 (red circles) is shown to visualize the irradiance categorization process.

Daily ground-level solar irradiance data were collected from Solcast API for the duration of the field study. As per Solcast API documentation, direct normal irradiance (DNI) and diffuse horizontal irradiance have a 2 km radius of accuracy for a particular location of interest [163]. Solar irradiance data is highly variable and can vary from day to day depending on weather

conditions, cloud cover, and seasonal changes in the time of sunrise/sunset. Thus, solar irradiance data for each test day was sorted and categorized according to its solar intensity characteristics. A "high solar intensity" model irradiance curve was selected and scaled down to produce four model irradiance curves with intensities ranging from 100% irradiance (representative of the "high solar intensity" irradiance curve) to 25% irradiance, as shown in Figure 20.

A root-mean-square deviation (RMSD) was calculated for each test day to quantify the level of agreement between the test day solar irradiance data and each of the four model irradiance curves, using Eq. (25). ($d_{actual,n}$) is the distance between a pair of corresponding points on the test and model irradiance curves, (d_{ideal}) is the expected distance between the pair of points, and (N) is the total number of point pairs within a dataset. Since RMSD was used to assess the closeness of fit between the test and model datasets, $d_{ide} = 0$, which is indicative of a perfect match between a pair of corresponding points.

Test days were categorized into the irradiance category that produced the smallest RMSD. In addition, the RMSD value was only accepted if it was below the maximum RMSD threshold of 150 W/m^2. This threshold allowed for additive irradiance variation between the raw data curve and model irradiance curve to be less than or equal to the low solar irradiance threshold as determined in Section 3.2.1.

$$RMSD = \sqrt{\sum_{n=1}^{N} \frac{d_{actual,n} - d_{ideal}}{N}} \tag{25}$$

Daily solar irradiance data were classified as high, moderate, moderate low, and low irradiance days based on the model irradiance curve that produced the best fit. This process ensured the impact of shade operation mode and configuration could be delineated from the effect of variable

solar irradiance on the indoor thermal conditions; test days were only comparable within a particular irradiance day category. As shown in Figure 5, the March 16, 2023 irradiance data was closest aligned to the "max irradiance" model curve. The RMSD between the test irradiance data and the "max irradiance" curve was the smallest in comparison to the other model irradiance curves. The resultant RMSD of 100.95 was also below the RMSD threshold of 150 W/m^2. As a result, March 16, 2023 was categorized as a high irradiance day.

3.3. Results and Discussion

3.3.1. Building Energy Modelling

3.3.1.1. Automated Shading Control Methodology

The energy performance of automated shading systems in cold climate zones was assessed through building energy modelling. The baseline energy consumption with unshaded windows served as the reference building energy performance to which the various automated control strategies were compared. Figures 21 – 25 show the building energy consumption breakdowns obtained for Edmonton, Vancouver, Toronto, Quebec City, and Fairbanks resulting from each automated shading control strategy for the south and west-facing walls, respectively. Table 26 summarizes the heating and cooling-related energy consumptions obtained for each control strategy in the Edmonton simulation.

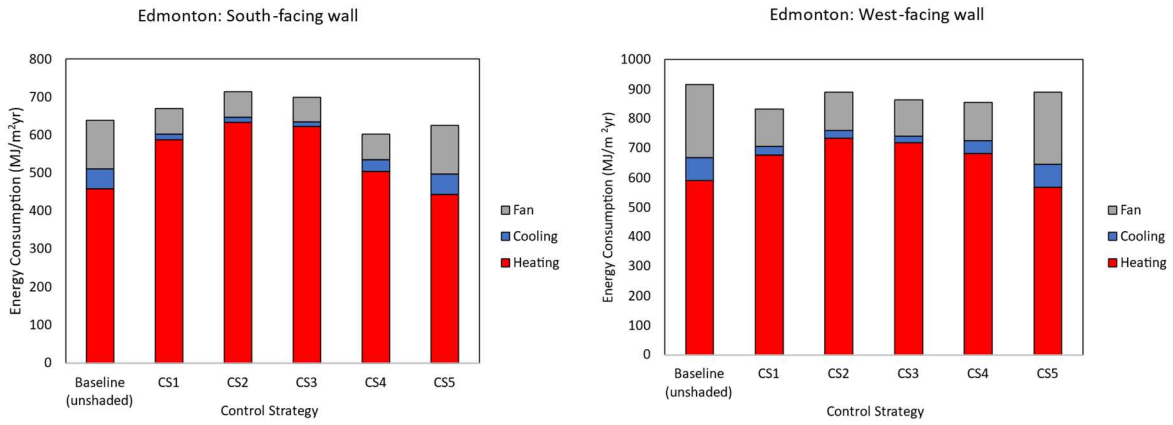

Figure 21. Building energy consumption breakdown for various automated shading control strategy simulations. Left: Results for the south-facing exterior wall. Right: Results for the west-facing exterior wall.

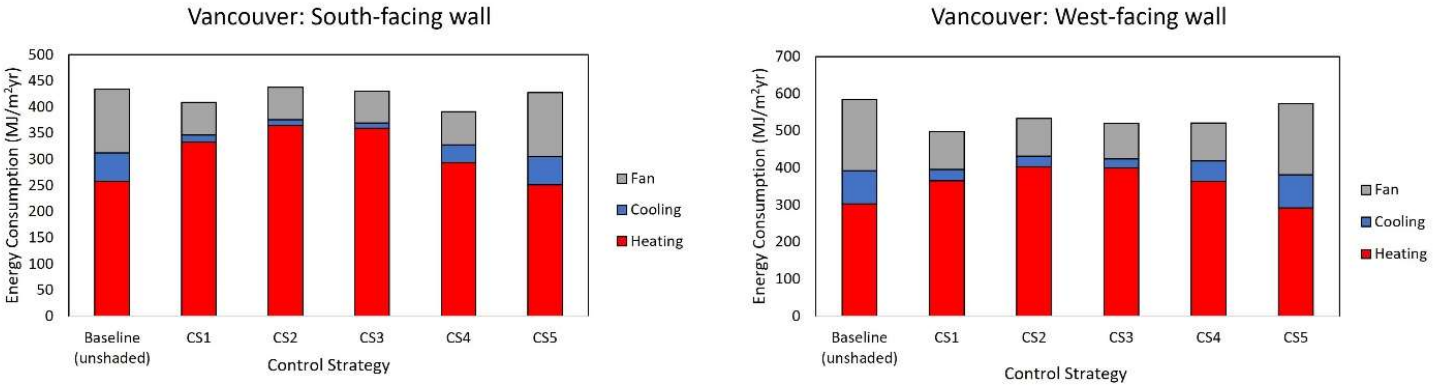

Figure 22. Building energy consumption breakdown for various automated shading control strategy simulations for Vancouver, Canada. Left: Results for the south-facing exterior wall. Right: Results for the west-facing exterior wall.

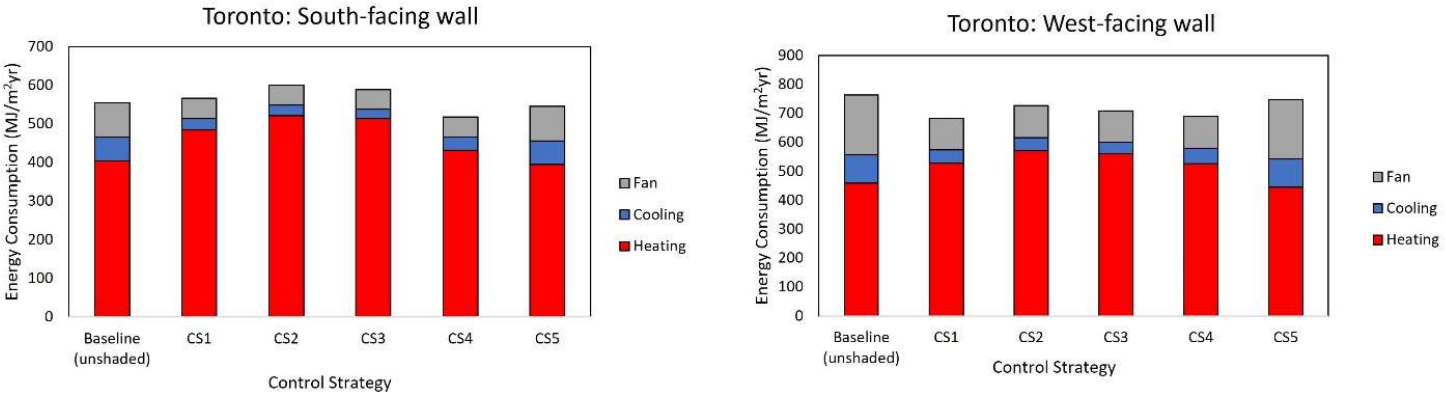

Figure 23. Building energy consumption breakdown for various automated shading control strategy simulations for Toronto, Canada. Left: Results for the south-facing exterior wall. Right: Results for the west-facing exterior wall.

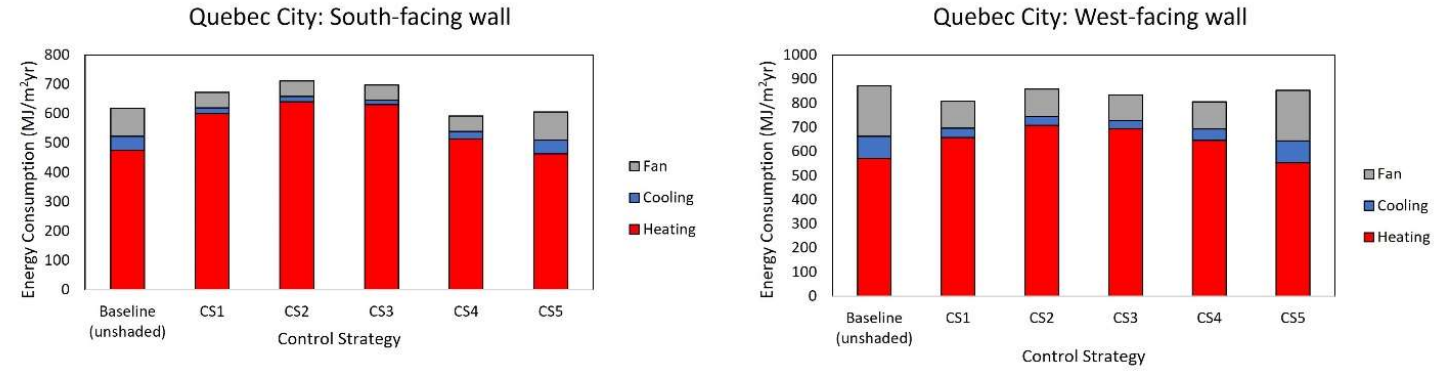

Figure 24. Building energy consumption breakdown for various automated shading control strategy simulations for Quebec City, Canada. Left: Results for the south-facing exterior wall. Right: Results for the west-facing exterior wall.

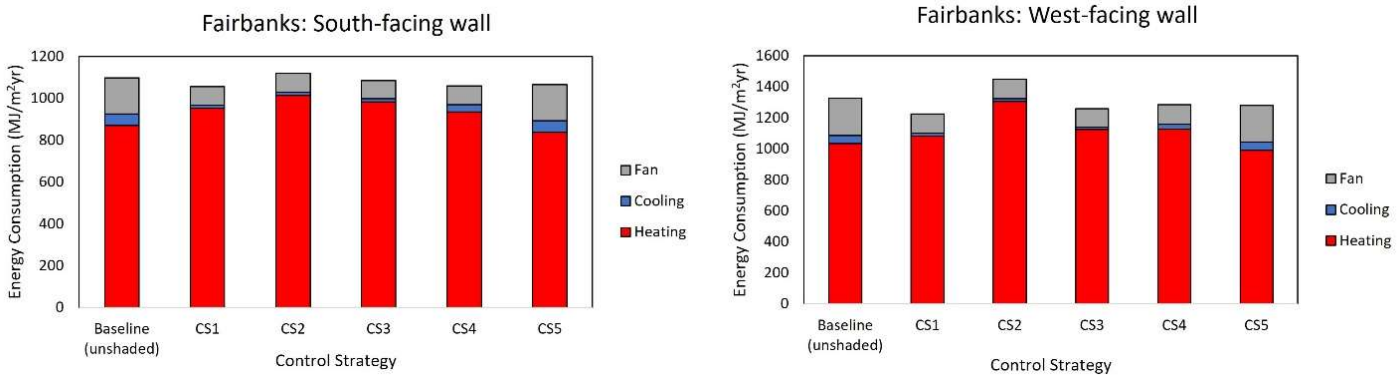

Figure 25. Building energy consumption breakdown for various automated shading control strategy simulations for Fairbanks, USA. Left: Results for the south-facing exterior wall. Right: Results for the west-facing exterior wall.

Table 28. Summary of heating and cooling-related energy consumption for Edmonton simulations of various automated shading control strategies.

Wall Orientation	Control Strategy	Heating Consumption (MJ/m^2yr)	Cooling Consumption (MJ/m^2yr)	Percent Difference (%)	
				Heating	Cooling
South Wall	Baseline (unshaded)	458.0	53.2	---	---
	CS1	587.5	14.9	28.3%	-71.9%
	CS2	633.9	13.2	38.4%	-75.1%
	CS3	622.3	12.3	35.9%	**-77.0%***
	CS4	504.3	31.3	10.1%	-41.0%
	CS5	444.4	53.3	**-3.0%***	0.3%
West Wall	Baseline (unshaded)	590.3	78.6	---	---
	CS1	677.4	28.1	14.7%	-64.2%
	CS2	734.7	25.9	24.5%	-67.1%
	CS3	718.7	22.7	21.8%	**-71.1%***
	CS4	681.8	43.6	15.5%	-44.5%
	CS5	567.5	78.6	**-3.9%***	0.1%

*Optimal heating or cooling consumption.

Figure 21 shows the simulated building energy consumptions for the city of Edmonton obtained for various automated shading system control strategies available on COMFEN. Based on the results in Table 28, the most effective control strategies for reducing cooling and heating were CS5 and CS3, respectively. For the south facing wall, CS5 and CS3 achieved a 3.0% reduction in annual heating and a 77.0% reduction in cooling energy consumption. For the west facing wall, CS5 and CS3 obtained a 3.9% reduction in annual heating and a 71.1% reduction in cooling energy consumption.

The resultant distribution of annual energy usage was dominated by heating consumption, which is consistent with the expected energy consumption distribution for cold climate zones. Most automated shading system control strategies focus on reducing cooling-related energy consumption by shading the glazing unit during the day. While this approach is effective for warmer climate zones with high cooling demand, its implementation in cold climate zones resulted in an energy penalty, as shown in Table 28 with positive percent differences in heating energy consumption for CS1, CS2, CS3, and CS4. In comparison, CS5 utilized shading during the overnight period to take advantage of the insulative properties of the roller shade material deployed over the glazing unit, resulting in a 3% reduction in heating consumption with no reduction in cooling energy consumption. A limitation of CS5 is its inability to reduce daytime heat transfer when conductive and convective heat transfer outward across the glazing surface is greater than the radiative heat gain from solar irradiance. To optimize automated shading systems for the heating season, it is necessary to implement a heating season-specific control strategy that capitalizes on radiative heat gain during the day, while minimizing conductive and convective heat loss when solar irradiance is limited (e.g., during overcast conditions, overnight, etc.).

3.3.1.2. City Selection

Based on the simulation results for Edmonton, it was found that CS5 and CS3 outperformed other control strategies in their ability to improve building heating and cooling energy performance. The impact of geographic location on automated shading energy performance was explored by comparing the heating and cooling savings obtained with CS5 and CS3 for each test city. A summary of heating and cooling energy savings for all test cities is provided in Table 29. Figure 26 shows the trends in cooling load and heating load reduction, respectively, across various cold climate zones, ranging from the warmest to coldest climate zone (ASHRAE climate zone 4C to ASHRAE climate zone 8). The Köppen climate classification for each test city has also been included.

Table 29. Summary of heating and cooling-related energy consumption for selected test cities using CS5 and CS3.

City	Orientation	Heating Load Reduction (MJ)	Percent Reduction	Cooling Load Reduction (MJ)	Percent Reduction
		CS5		CS3	
Vancouver (ASHRAE 4C / Cfb)	South	221.4	2.7%	388.3	81.1%
	West	345.5	3.6%	579.3	73.0%
Toronto (ASHRAE 5A / Dfa)	South	300.4	2.3%	324.3	59.8%
	West	426.0	2.9%	515.1	59.4%
Quebec City (ASHRAE 6A / Dfb)	South	385.5	2.5%	275.1	65.8%
	West	557.6	3.1%	509.7	63.5%
Edmonton (ASHRAE 7 / Dfb)	South	435.0	3.0%	361.8	77.0%
	West	727.1	3.9%	493.8	71.1%
Fairbanks (ASHRAE 8 / Dfb)	South	1022.3	3.7%	376.0	75.8%
	West	1370.6	4.2%	350.2	73.4%

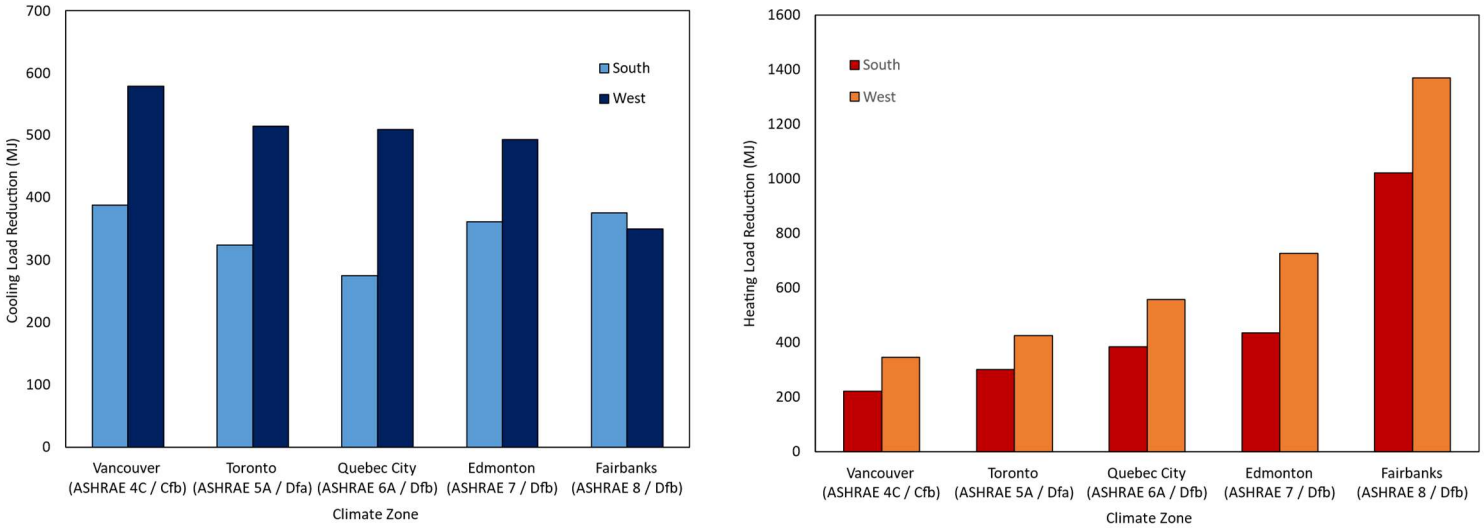

Figure 26. Simulated heating and cooling load reductions for various cold climate zone cities. Left: Simulated cooling load reduction using CS3. Right: Simulated heating load reduction using CS5.

The simulated cooling load reductions shown in Figure 26 (left) demonstrate the effectiveness of automated shading systems for summer building energy efficiency. Radiative gain from solar irradiance is responsible for much of a building's cooling load, especially for buildings with a high exterior glazing area. Thus, cities with more daylight hours and solar exposure (Vancouver, Toronto, Edmonton) saw higher heating load reductions from automated shading implementation than locations with comparatively less radiative gain. Window orientation was also a key factor that impacted the resultant energy savings realized through shading system implementation. In the northern hemisphere, south- and west-facing windows receive the highest levels of solar radiation during the day [170]. The combination of solar irradiance intensity and duration likely contributed to the higher energy savings realized for west-facing windows in most test cities.

An exception to this result was that of west-facing windows in the Fairbanks simulation. In this case, south-facing windows with automated shading achieved a greater cooling load reduction than west facing windows. This may be due to the long daylight hours in Fairbanks during the summer

season when the sun does not fully descend below the horizon. As a result, there is increased solar exposure to south-facing windows. In addition, it should be noted that although Fairbanks is the coldest climate zone location within the selected test cities, its total solar exposure for south-facing windows is comparable to that of warmer climate zones. Buildings in Fairbanks often do not have air conditioning to maintain acceptable indoor thermal conditions during the summer. However, based on the simulation results, there is merit in implementing automated shading systems in both south and west-facing windows to minimize indoor overheating and improve occupant thermal comfort.

The simulated heating load reductions shown in Figure 26 (right) emphasize the cold climate zone functionality of automated shading systems. With a heating season-aligned control strategy, automated shading unlocked additional functionality during the winter by improving the thermal properties of the glazing unit and reducing heat flux from the indoor space to the outdoor environment. The heating load reduction obtained through automated shading increased with colder climate zone locations. This was due to the severity of outdoor temperature conditions for cold climate zones which promoted heat transfer across the glazing surface. Although the overall heating load reduction was less than 5%, the heating load reduction control strategy was effective at improving building energy performance during the winter. To further improve the overall effectiveness of the shading system during the heating season, thermally resistive shading materials should be considered. This approach would increase the overall thermal resistivity of the entire fenestration system when the shade is deployed over the glazing unit.

3.3.2. Mathematical Modelling

3.3.2.1. Dynamic Control Strategy Development

Results from the building energy modelling informed the development of a custom cold climate optimized control strategy for automated shading systems. To improve ease of implementation for existing manual or motorized shades, the novel custom control strategy developed for this project was designed without the need for indoor sensor-based inputs. Instead, input data from solar and weather APIs were used to trigger various actions in response to changing weather conditions. The control logic of CS3 and CS5 were incorporated to ensure the custom control strategy was season-specific and responsive to changes in building heat flux, thermal equipment operation, and governing mechanisms of energy consumption. A flowchart outlining the control logic of the custom cold climate-optimized control strategy for automated shading systems is shown in Figure 27. Applying the governing equations for complex fenestration systems, as outlined in Section 3.2.2.1, the flowchart describes the general flow of input variables that dictate both shade operation and subsequent estimation of energy savings. Fundamental input categories represent raw input data regarding a building of interest. These are binned into their respective input variable categories for use within a particular governing equation. Solar irradiance data and solar position relative to a particular window orientation (represented by the incident angle (Eq. 10) are used in conjunction with the window type specific SHGC to model the unshaded solar heat gain that enters an office space through a particular window orientation. Depending on the shade material's radiative (represented through its indoor attenuation coefficient) and thermal properties (represented through its U-factor), a shaded solar heat gain is estimated. Solar gain that surpasses the default threshold triggers shade operation to deploy or retract the shade in response to the season-specific control strategy.

For cooling load reduction, the control strategy optimized both radiative and conductive heat flux to minimize heat gain during the day and maximize heat loss overnight. During the day, the shades were deployed when both the solar intensity (unshaded solar heat gain) and solar incident angle (default thresholds) were such that the window of interest was receiving excessive solar gain. Otherwise, the window remained unshaded to capitalize on favorable heat transfer to the outdoor space. This was achievable in cold climate zones due to the temperature gradient between the indoor and outdoor spaces often resulting in an outward direction of heat flux.

For heating load reduction, the control strategy aimed to minimize heat flux by deploying the shade over the glazing unit, unless there was sufficient radiative heat gain to offset conductive losses. This was determined through a comparison between radiative gain (unshaded solar heat gain) and estimated conductive loss. Conductive losses were estimated based on building operation schedule, indoor setpoint temperatures, and outdoor air temperature. This approach improved upon CS5, where the shades were only deployed during the overnight period. The updated control logic for the heating season allowed the thermal resistivity of the shading device to be fully applied – both during the day with minimal radiative gain, and during the overnight period.

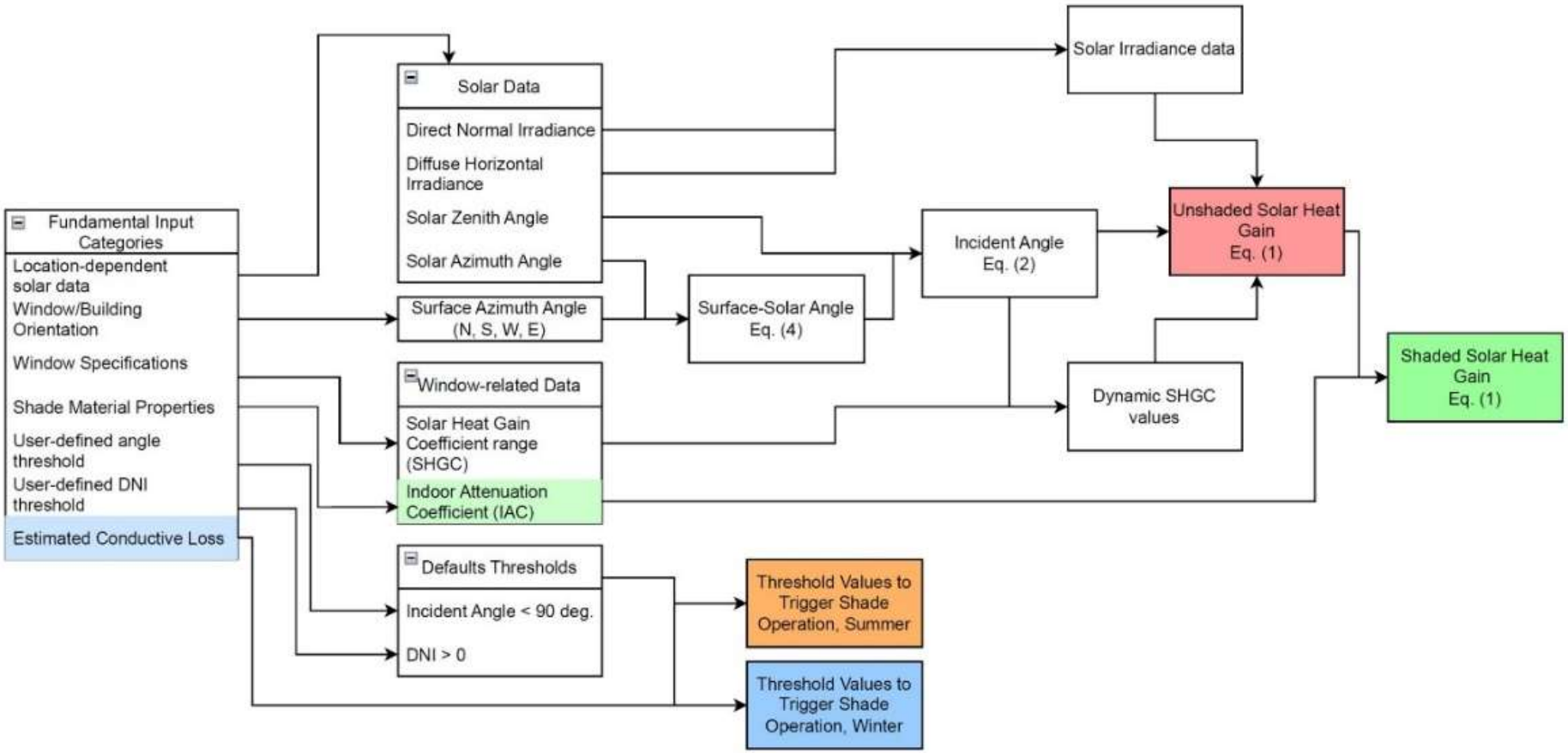

Figure 27. Flowchart depicting the logic and information flow of the developed custom control strategy for AI Shading's automated shading systems.

3.3.2.2. Sensitivity Analysis

A variance-based global sensitivity analysis was executed to understand the relationships between the various inputs of the complex fenestration system mathematical model. Table 30 provides a summary of the first-order indices obtained from the sensitivity analysis. Outdoor temperature and solar data ranges for test cities located in three distinct ASHRAE climate zones were considered in the analysis.

Table 30. Summary of results from variance-based global sensitivity analysis. The first-order indices for each analysis run are ranked from largest to smallest.

City	Rank	Winter Variable Order	1st order index	Confidence Interval at 95% CL	Summer Variable Order	1st order index	Confidence Interval at 95% CL
Ottawa (ASHRAE Zone 6A / Dfb)	1	T_{out}	0.7746	0.0759	T_{out}	0.9100	0.0731
	2	$glaze$	0.1393	0.0364	$glaze$	0.0175	0.0214
	3	U_g	0.0140	0.0127	DNI	0.0079	0.0088
	4	DNI	0.0082	0.0089	GHI	0.0059	0.0073
	5	GHI	0.0067	0.0078	IAC	0.0059	0.0075
	6	IAC	0.0063	0.0090	$theta$	0.0015	0.0042
	7	R_{eq}	0.0041	0.0047	SG_d	0.0001	0.0002
	8	$theta$	0.0014	0.0048	U_g	0.0001	0.0053
	9	SG_d	0.0001	0.0001	R_{eq}	0.0000	0.0023
	10	SG	0.0000	0.0002	SG	0.0001	0.0002
	11	$alph$	0.0000	0.0001	$alph$	0.0001	0.0005
Edmonton (ASHRAE Zone 7 / Dfb)	1	T_{out}	0.7811	0.0681	T_{out}	0.9050	0.0757
	2	$glaze$	0.1489	0.0358	DNI	0.0129	0.0106
	3	U_g	0.0129	0.0122	GHI	0.0099	0.0093
	4	R_{eq}	0.0038	0.0048	IAC	0.0098	0.0095
	5	DNI	0.0035	0.0063	$glaze$	0.0076	0.0226
	6	GHI	0.0028	0.0051	$theta$	0.0026	0.0049
	7	IAC	0.0027	0.0048	R_{eq}	0.0002	0.0022
	8	$theta$	0.0005	0.0027	SG_d	0.0001	0.0002
	9	SG_d	0.0001	0.0001	U_g	0.0001	0.0053
	10	SG	0.0000	0.0001	$alph$	0.0000	0.0002
	11	$alph$	0.0000	0.0001	SG	0.0000	0.0003
	1	T_{out}	0.7889	0.0709	$glaze$	0.2329	0.0523
	2	$glaze$	0.1387	0.0378	T_{out}	0.1620	0.0374
	3	U_g	0.0125	0.0097	DNI	0.1614	0.0404
	4	R_{eq}	0.0044	0.0063	GHI	0.1371	0.0349

Iqaluit (ASHRAE Zone 8 / ET)	5	DNI	0.0037	0.0054	IAC	0.1282	0.0352
	6	GHI	0.0035	0.0053	U_g	0.0532	0.0186
	7	IAC	0.0033	0.0068	$theta$	0.0287	0.0186
	8	$theta$	0.0007	0.0032	R_{eq}	0.0124	0.0097
	9	SG_d	0.0001	0.0001	SG_d	0.0004	0.0006
	10	SG	0.0000	0.0001	SG	0.0003	0.0009
	11	$alph$	0.0000	0.0001	$alph$	0.0001	0.0005

Results from the sensitivity analysis suggest that cold climate zone locations experience changes in glazing unit heat flux patterns between the heating and cooling seasons. During the heating season, the first-order indices representative of outdoor temperature (T_{out}), glazing to wall ratio ($glaze$), and glazing unit U-factor (U_g) ranked higher than solar irradiance (DNI, GHI) and opaque wall thermal resistivity (R_{eq}). This result indicates that conductive and convective heat flux outward across the glazing surface area has a high contribution to the overall heating load of a building. In addition, colder climate zones (such as Edmonton - ASHRAE 7, or Iqaluit - ASHRAE 8) experience more significant temperature gradients between the indoor and outdoor spaces. Thus, in these climate zones, solar irradiance-related variables are overshadowed by thermal resistivity-related variables. During the cooling season, the first-order indices representative of solar irradiance (DNI, GHI) and shade material radiative attenuation (IAC) rank higher than thermal resistivity-related variables. This result shows that radiative heat flux from solar irradiance has a significant contribution to the overall cooling load of a building. The sensitivity analysis agrees with the building energy modelling from Section 3.1.2, which found that a season-specific shading control strategy was required to adapt to changes in heat flux patterns occurring across the glazing unit.

3.3.2.3. Quantification of Energy Savings

The energy savings obtainable through automated shading implementation were assessed using the developed custom energy savings calculator. A summary of resulting equipment-based energy savings for office test spaces located in Iqaluit, Edmonton, and Ottawa is provided in Table 31. The office test space specifications defined in Table 26 served as the building data for the energy savings calculator. Solar and outdoor temperature data for each test city were obtained from the 2020 Canadian Weather Energy and Engineering Datasets (CWEEDS) and local weather stations [171, 172]. Local utility rates were employed to assess the regional payback period of automated shading systems using a simple payback calculation.

Table 31. Summary of region-specific energy savings obtained through automated shading system implementation and associated technology payback period.

City	Utility Rates [$CAD]	Energy Savings		Payback Period (yrs.)
		Heating (GJ)	Cooling (kWh)	
Ottawa (ASHRAE Zone 6A / Dfb)	Electricity [173]: $0.21/kWh Heating (Natural Gas [173]): $11.55/GJ	4.1	925.6	8.1 – 16.2
Edmonton (ASHRAE Zone 7 / Dfb)	Electricity [174]: $0.21/kWh Heating (Natural Gas [174]): $11.55/GJ	14.1	920.7	5.0 – 10.1
Iqaluit (ASHRAE Zone 8 / ET)	Electricity: not applicable Heating (Diesel Fuel [175]): $1.47/L	8.7	n/a	5.0 – 9.9

The results summarized in Table 31 highlight the varying financial feasibility of automated shading system implementation. Heating and cooling energy savings differ between regions. Consequently, regions with high solar exposure and more extreme winter design conditions, such as Edmonton, resulted in a shorter payback period for automated shading implementation. In

Iqaluit, only heating savings were assessed since cooling system installations are rare for buildings in that region. However, due to the high heating utility prices and harsh winter design conditions in the ASHRAE zone 8 test city, Iqaluit obtained the lowest payback period for automated shading implementation, ranging from approximately 5 – 10 years. It should be noted that automated shading effectiveness is highly dependent on existing building specifications and constraints. Factors such as low glazing to opaque wall ratio, high-quality glazing units, or low solar exposure to glazing will all contribute to an increased payback period for automated shading implementation. The favorable orientation (southwest facing) and high WWR conditions of the test space used in the field study resulted in more significant energy savings and a shorter technology payback period. It should be noted that in less favorable conditions, such as in the case of residential buildings with low WWR or windows oriented away from direct irradiance exposure, the energy savings and technology payback period would be negatively affected. Due to uncertainties in alignment of the API-sourced solar irradiance data to the local real time conditions of a particular test space, local measurement of solar irradiance conditions per test space is required to improve the accuracy of energy savings obtained from the developed energy savings calculator. The technology payback period is highly dependent on local utility rates. Though constant utility rates were considered in Table 29, variations in utility rates over time will also impact the technology's payback period.

3.3.2.4. Financial Analysis

Results from Table 32 show that automated shading systems have an average payback period in comparison to other retrofit strategies. Shading system implementation is similar to smart thermostat integration in that they are not deep retrofit strategies and do not directly improve the equipment efficiency within the building. However, the low "up front" financial commitment of these technologies improves their adoption by commercial and residential buildings. As stated in

Section 3.3.2.3, a limitation of payback periods for automated shading is that they can vary significantly depending on factors such as building specifications, location-specific weather conditions, and solar exposure. Thus, the shading system installation site and associated control strategy must be chosen in a way that energy savings from the technology are maximized.

Table 32. Summary of payback periods for various building retrofit strategies.

Building Retrofit Strategy	Payback Period (yrs.)
Cold Climate-Optimized Automated Shading System	5.0 – 14.8
Heating Equipment Upgrade (air-water heat pump, heat pump with photovoltaics) [176]	22.5 – 28.0
Glazing upgrade with heating and cooling equipment upgrade [177]	9.3
Smart Thermostat [178]	<1.0 – 2.5
Building Envelope Upgrades (Envelope-Cladding System) [179]	17.6 – 20.5

3.3.3. Prototype Field Study

Table 33 provides a summary of indoor thermal ranges collected during the field study. Variable ranges for the summer (July – October 2022) and winter (November 2022 – March 2023) are presented separately. The impact of various shading system operation modes was assessed through an analysis of indoor temperature fluctuations during the day and overnight.

Table 33. Summary of indoor thermal conditions within SUB 6-24, the field study test space.

Environmental Variable	Summer Range	Winter Range
Indoor Temperature (ºC)	17.1 – 32.7	14.3 – 28.5
Relative Humidity (%RH)	25.2 – 53.0	7.0 – 22.7

3.3.3.1. Cooling Season

Figure 10 summarizes the impact of shading operation mode on indoor daytime heating rates and daytime peak temperature, and overnight cooling rates. Irradiance data categorization, as described in Section 3.2.3, was used to sort test days based on their irradiance characteristics. Indoor thermal data collected on high irradiance test days were considered for further analysis to ensure the impact of shading operation mode was measurable. As shading system effectiveness is directly impacted by solar exposure intensity, ensuring similar solar conditions also improved data comparability between various shading operation modes.

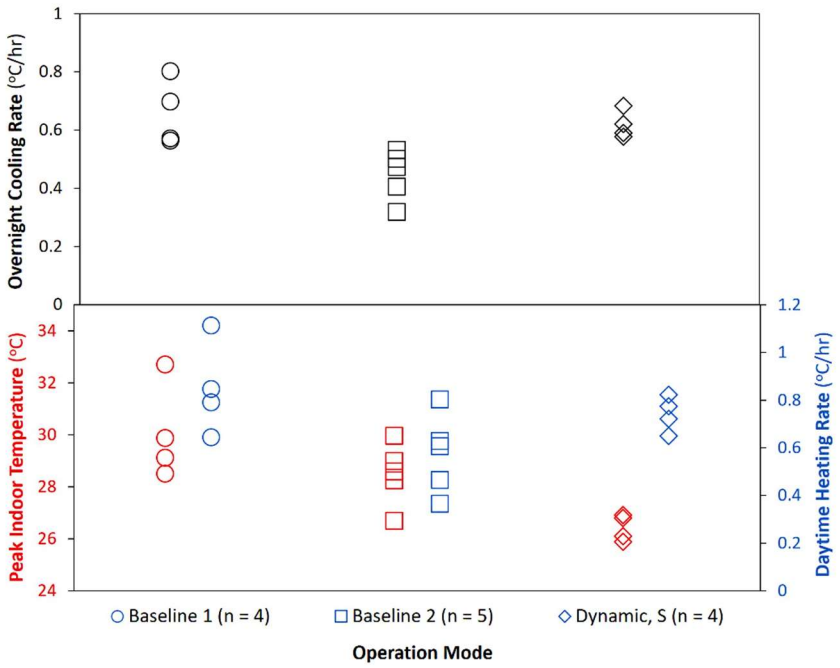

Figure 28. Individual value plots depicting summer indoor daytime heating rate, peak temperature, and overnight cooling rate distributions for various shading system operation modes. The combined effect of both south and west-facing windows in the test space was considered.

As shown in Figure 28, the average daytime heating rates for the unshaded static (baseline 1), shaded static (baseline 2), and dynamic – summer shade operations were 0.9 ºC/hr ± 0.2 ºC/hr, 0.6 ºC/hr ± 0.2 ºC/hr, and 0.7 ºC/hr ± 0.1 ºC/hr, respectively. These results support the findings from both the COMFEN-based energy simulation and mathematical modelling of the test space. Deploying the shade-over glazing unit was effective at reducing the overall heating rate of the indoor space. The heating rate measured for the dynamic shading system operation was higher than that of the shaded static operation scenario. Though, in theory, the static shaded configuration would result in the highest reduction in cooling load, it would also compromise occupant visual comfort, depriving them of indoor daylighting and an outdoor view. Thus, the utilization of dynamic shading operation allows for a balance between cooling load reduction and overall occupant comfort. The average peak indoor temperatures for baseline 1, baseline 2, and dynamic – summer shade operations were 30.0 ºC ± 1.9 ºC, 28.5 ºC ± 1.2 ºC, and 26.4 ºC ± 0.5 ºC,

respectively. The range of peak indoor temperatures for baseline 1 had the largest span, ranging from 28.5 ºC to 32.7 ºC. In comparison, baseline 2 and dynamic – summer shade operation modes had less range in indoor temperature data. This result highlights the ability of the shade material to reduce the direct impact of solar gain on indoor air temperature. The added radiative resistance of the shade material deployed over the window contributed to regulating indoor solar radiative gain, which resulted in less severe peak indoor temperatures within the test space.

The average overnight cooling rates for the unshaded static, shaded static, and dynamic – summer shade operations were 0.7 ºC/hr ± 0.1 ºC/hr, 0.4 ºC/hr ± 0.1 ºC/hr, and 0.6 ºC/hr ± 0.1 ºC/hr, respectively. These results support the utilization of window shades to improve the overall thermal resistivity of a glazing unit. The default low irradiance configuration for the summer dynamic shade operation is to have the shade fully retracted to expose the glazing unit. As a result, the overnight cooling rate for the static unshaded operation (baseline 1) and dynamic operation were similar. In addition, due to the insulative properties of the shade deployed over the glazing unit, the overnight cooling rate for the static shaded operation (baseline 2) was lower than that of baseline 1 and dynamic operation. Studies have found that occupants rarely adjust the position of manually operated window shades, especially in cases where the shade configuration does not negatively impact their ability to work within the indoor space [165, 166]. Dynamic shade operation would ensure optimal shade positioning to take advantage of favorable heat transfer as a passive method to help cool the indoor space to the setpoint temperature overnight.

3.3.3.2. Heating Season

Figure 29 summarizes the impact of shading operation mode on indoor daytime heating rates and daytime peak temperature, and overnight cooling rates. The irradiance data categorization, as described in Section 3.2.3, was used to sort test days based on their irradiance characteristics. To improve data quality for daytime testing, only high irradiance daytime heating rates and peak

temperatures were considered. This ensured that the impact of the shading operation mode on indoor thermal conditions was amplified to improve measurability. In comparison, overnight cooling rates included both moderate and high irradiance test days.

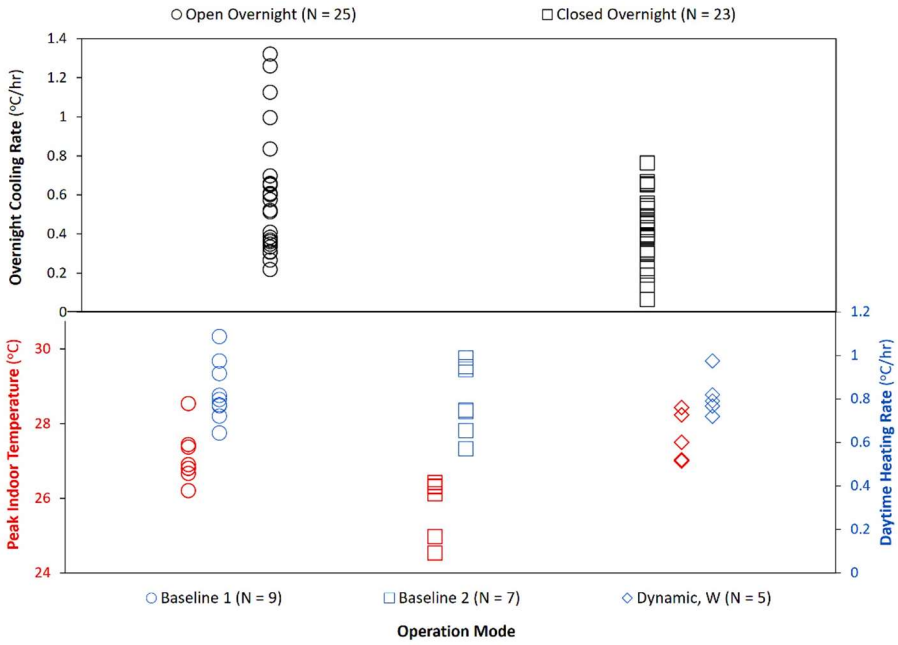

Figure 29. Individual value plots depicting winter indoor daytime heating rate, peak temperature, and overnight cooling rate distributions for various shading system operation modes. The combined effect of both south and west-facing windows in the test space was considered.

As shown in Figure 29, the average daytime heating rates for the unshaded static (baseline 1), shaded static (baseline 2), and dynamic – winter shade operations were 0.8 ºC/hr ± 0.1 ºC/hr, 0.8 ºC/hr ± 0.2 ºC/hr, and 0.8 ºC/hr ± 0.1 ºC/hr, respectively. In comparison to the summer season indoor heating rates, the winter indoor heating rates exhibited less variation between shade operation modes. The impact of various shade operation modes on the indoor heating rate was likely dampened due to the building heating system operation during the winter months. The heating system was able to compensate for changes in indoor heating load and adjust the supply air temperature in the space. The average peak indoor temperatures for the unshaded static (baseline 1), shaded static (baseline 2), and dynamic – winter shade operations were 27.1 ºC ± 0.7

ºC, 25.8 ºC ± 0.8 ºC, and 27.6 ºC ± 0.7 ºC, respectively. The differences in indoor peak temperatures were also less severe between shading operation modes.

It was found that the average overnight cooling rate for the fully open and fully closed shading configurations were 0.6 ºC/hr ± 0.3 ºC/hr and 0.4 ºC/hr ± 0.2 ºC/hr, respectively. The differences in average cooling rate between the two scenarios support the previous findings regarding the improvement of glazing unit thermal resistivity through the deployment of the window shade over the glazing surface overnight. More significant reductions in overnight cooling rate would require the use of shading materials with higher thermal resistivity.

3.4. Limitations and Future Works

Based on both the simulation and field study results, automated shading systems operating under a cold climate-optimized control strategy show promise as a green retrofit technology for existing buildings. At this point in the technology's development, there exist some limitations and weaknesses of the proposed solution. The current control strategy is limited to adjusting the shade to its maxima configuration (fully retracted or fully deployed). From the perspective of energy savings, this is the most rudimentary approach to achieving the highest energy saving from shading implementation. However, this approach does not consider the depth of solar exposure in the indoor space at various distances away from the window. The implementation of intermediate shade configurations that leave part of the window exposed would allow for improved fine adjustment capacity of indoor solar gain and natural lighting. The estimated energy savings obtained through automated shading implementation assume 100% adherence to the recommended shade configurations throughout the year. Due to the nature of adjustable shading systems, while the space is occupied, there exists the risk of occupant adjustment of shade configurations to positions that are not deemed energy-efficient. As a result, the actual reduction in building energy

consumption will vary depending on the realization rate of a particular implementation scenario. Results from Inoue et al. noted that the typical occupant rarely adjusts the position of manual shades except in instances where there is significant discomfort due to direct solar radiation or glare [180]. Thus, further development of the proposed sensorless control strategy will need to consider occupancy to determine whether the "energy saving" controls or an occupant-centered control be implemented. In addition, window specifications - such as WWR, type, and orientation, building heating and cooling equipment efficiencies, and type of shading system will impact the overall effectiveness of the proposed shading solution. Though the current study focused on control strategy integration in indoor roller shades, its implementation in exterior shading systems may yield improved building energy performance and offer opportunities to address other indoor environmental quality concerns such as noise control [181].

3.5. Conclusion

This section focused on the use of automated shading systems as a green retrofit strategy in cold climate zones to improve building heating and cooling-related energy performance. EnergyPlus-based building energy models were developed to assess the impact of various window shade control strategies on the heating and cooling load of cold climate zone test spaces. The results indicated that a season-specific control strategy was necessary for the shading system to generate both heating and cooling season energy savings. This approach also prevented the incurrence of an energy penalty during the heating season from year-round usage of a summer-optimized shading strategy. Of the simulated control strategies, CS3 and CS5 were found to be the most effective cooling and heating season control strategies, resulting in reductions in cooling and heating load by up to 81.1% and 4.2%, respectively. Based on the results from the building energy simulation, a cold climate-optimized control strategy and energy savings estimation methodology

was developed and integrated into a prototype motorized roller shading system. It was found that for various cold climate zone test cities, the simple payback period for the cold climate-optimized automated shading prototype ranged from 4.96 – 14.84 years depending on climate zone and building-related specifications. Due to its relatively short payback period, cold climate-optimized automated shading systems were found to be a suitable alternative to other green retrofit strategies such as window replacements and building thermal equipment upgrades with payback periods of up to 28 years. Finally, results from the automated shading prototype study quantified the impact of dynamic shading operations on indoor thermal conditions. It was found that the season-specific control strategies were successful in improving indoor thermal conditions compared to the static unshaded window baseline condition (baseline 1). In addition, the dynamic nature of the shading system allowed for shading to be optimized during the summer season while allowing increased natural light into the test space. The dynamic shade operation achieved an improved balance between energy efficiency and occupant visual comfort that could not be realized through manual window shade operation. The insulative properties of the shade were demonstrated within the field study where shade deployment was found to decrease the overnight cooling rate in the test space from 0.7 ºC/hr ± 0.1 ºC/hr (unshaded) to 0.4 ºC/hr ± 0.1 ºC/hr (shaded) during the summer field study and from 0.6 ºC/hr ± 0.3 ºC/hr (unshaded) to 0.4 ºC/hr ± 0.2 ºC/hr (shaded) during the winter field study.

Future works include additional research into shading materials with improved thermal properties, or the adaptation of the developed control strategy to other styles of window shades. Although the current control strategy is developed to improve building energy performance, additional work is required to better address occupant visual comfort concerns during the winter season from excessive daytime shading and discomfort glare. This work has showcased the effectiveness of

automated shading implementation to improve building energy performance. The results from this study provide the foundation for further optimization of automated shading systems for use within cold climate zone buildings.

4. Conclusion and Future Works

4.1. Conclusion

Climate change and its associated impacts on weather patterns pose a significant risk to the health and comfort of urban residents. Even in cold climate zones, such as in Canada, heatwave conditions have resulted in higher-than-average seasonal temperatures, increased direct solar irradiance due to decreased cloud formation, and the increased severity of wildfire events. These, in turn, have created challenges is IAQ and indoor thermal condition management. This emphasizes the importance of implementing retrofit technologies to support the existing HVAC systems in buildings to improve their urban resiliency to climate change. A thorough literature review has indicated that there is currently a lack of research regarding technologies that can be implemented post-construction to address IEQ challenges related to climate hazards. In addition, there is a lack of research regarding the effectiveness of existing retrofit technologies for implementation in cold climate zones. Thus, this work focused on the development of building retrofit strategies that target the climate hazards prevalent in Canadian cities.

To maintain adequate IAQ during wildfire events, a wildfire-resilient mechanical ventilation system was developed for implementation in Western Canadian cities prone to wildfire events and wildfire smoke exposure. 17 single-zone IAQ models were developed to understand the effect of outdoor PM2.5 concentration, filter efficiency, outdoor airflow rate, and various building and ventilation system-specific variables on the steady-state indoor PM2.5 concentration. A variance-based global sensitivity analysis was used to determine the relative impact of each input variable within the model on the resultant indoor PM2.5 concentration. Next, a cost-benefit analysis of various mechanical ventilation configurations, filter change schedules, and PAC usage was used to assess the financial feasibility of the ventilation system upgrade for a specific region within Western Canada. An estimate monetary contribution range towards mechanical ventilation system

upgrade was estimated based on regional exposure to wildfire-sourced PM2.5 and regional risk of premature mortality due to PM2.5 exposure. Results from the IAQ simulations yielded several recommendations to improve IAQ during wildfire events. It was found that the minimum air filter efficiency should be increased to MERV 11 or MERV 13 from the existing minimum residential standard in wildfire conditions. In addition, double-filter configurations should be considered for regions prone to severe outdoor PM2.5 exposure levels, as was seen in Prince George IAQ simulations. As a short-term relief strategy during severe peaks in outdoor PM2.5 levels, the findings from the IAQ simulations indicated that near 100% recirculation be implemented to prevent the introduction of PM2.5 into the indoor space. Results from the cost-benefit analysis and model sensitivity analysis supported the recommendations for filter upgrades and double-filter mechanical ventilation systems. Based on the IAQ simulations regarding PAC usage, the current price points for PAC deem them unjustifiable from the financial perspective for implementation in wildfire-resiliency retrofits. However, it should be noted PACs could be effective in improving occupant comfort and IAQ when considering other types of air contaminants in addition to wildfire sourced PM2.5. The recommendations from this study emphasize the importance of continuous IAQ and mechanical ventilation system monitoring and control to ensure IAQ is consistent and well maintained amid poor outdoor air quality conditions.

To maintain indoor thermal comfort during heatwave conditions, a cold climate-optimized automated shading system was developed as a strategy to decrease building cooling load during summer heatwave conditions while improving year-round building energy performance. Building energy modelling was used to assess the impact of various automated roller shade control strategies on building cooling and heating load for various cold climate zone cities. It was found that conventional automated control strategies were effective at reducing building cooling equipment

consumption, however, they increase building heating equipment load during the winter season. This effect is amplified in cold climate zone applications where the winter season is significantly harsher in comparison to warm climate zones. Based on results from the building energy modelling, a mathematical model based cold climate-optimized automated shading control strategy was developed to reduce both heating and cooling equipment related energy consumption. A mathematical model was extended to estimate shading system energy performance based on user-defined building specifications and weather-related variables. Based on the installation price points set by the shading system manufacturer, a payback period for cold climate-optimized automated shading systems was calculated with regional utility rates and the estimated shading system energy performance. It was found that the technology had a payback period range of approximately 5 – 15 years, depending on factors such as glazing type, glazing orientation, solar exposure, and local climate conditions. A field study with automated shading prototypes was used to quantify the impact of automated roller shade operation on indoor thermal conditions. Though these results cannot relate directly to the energy savings obtained through technology implementation, they serve to reinforce the results from both the building energy simulations and subsequent mathematical modelling. Using the cold climate optimized shading control strategy, the test space indoor peak temperature during the summer season was reduced to 26.4 ºC ± 0.5 ºC from 30.0 ºC ± 1.9 ºC and 28.5 ºC ± 1.2 ºC for the unshaded and shaded static operation baseline scenarios, respectively. During the winter season, optimized shading system deployment based on the modified winter control strategy reduced the overnight cooling rate from 0.6 ºC/hr ± 0.3 ºC/hr to 0.4 ºC/hr ± 0.2 ºC/hr. Findings from this study support the implementation of cold climate-optimized automated shading systems as a retrofit strategy to mitigate the effects of summer heatwaves and a viable method to improve year-round building energy performance.

In conclusion, both wildfire-resilient mechanical ventilation systems and cold climate-optimized automated shading systems are effective and feasible retrofit strategies to mitigate the hazards associated with climate change and heatwave conditions. This thesis has demonstrated the potential of these technologies to improve occupant health and comfort within the built environment. The implementation of these technologies and similar climate hazard mitigation strategies will greatly improve urban sustainability and climate change resiliency – resulting in sustainable and comfortable indoor spaces for all Canadians.

4.2. Future Works

Future works on this research topic generally emphasize the need for additional measurement and verification to assess the effectiveness of the retrofit technologies in real-world, practical applications.

Specific to wildfire-resilient ventilation systems, this work can be further extended to field study-based projects to test the actual effectiveness of the proposed mechanical ventilation system configuration upgrades. In practice, filter selection requires additional considerations to ensure the filter pressure drop does not negatively impact the heating, cooling, or general ventilation functions of then system. This is especially true in projects considering filter upgrades without upgrading the blower fan. In addition, a more comprehensive IAQ model for PACs should be considered to re-evaluate their feasibility for localized air contaminant removal. The current IAQ model fails to justify PAC usage as a feasible strategy for improving wildfire resiliency from the sole perspective of its function as an additional filter within an indoor space. Modelling PACs via their clean air delivery rate (CADR) or considering other indoor or outdoor sourced air contaminants that can be removed alongside wildfire sourced PM2.5 may help justify their feasibility as an IAQ-related retrofit strategy. Specific to cold climate-optimized automated shading systems, this work can be

extended in two aspects: (1) methodology for the measurement and verification of technology energy performance and (2) further technology development of automated shading systems. (1) In the measurement and verification of building energy savings attributed to automated shading system operations, there currently does not exist a methodology where which proxy measures of energy savings – such as indoor temperature change or indoor heating/cooling rate – can be used to quantify reductions in heating or cooling equipment energy consumption at the building level. The development of such a methodology will allow for a more representative estimation of technology energy performance from small-scale field studies. Large-scale setups should be considered for future field studies involving automated shading systems. This would allow for the comparison of heating and cooling equipment energy consumption before and after technology implementation and serve as a direct measure of the automated shading system's impact on building energy performance. (2) The continuous development of cold climate-optimized automated shading systems requires combining the functionality of the shading system with other green retrofit strategies to form a holistic retrofit package to improve IEQ and energy efficiency in buildings. The retrofit package could include shading system integration with HVAC controls, lighting, and natural ventilation to further reduce heating and cooling equipment consumption while maintaining indoor thermal comfort, IAQ and occupant visual comfort. For automated shading system implementation in the coldest climate zones (ASHRAE 7 – ASHRAE 8), it would be beneficial to adapt and implement the existing cold climate optimized automated shading control strategy to exterior shading systems or more insulative styles of interior window shades. This would further improve the relevance of the window shading systems in heating dominant regions and, in turn, increase the heating-related energy savings obtained through technology implementation.

References

[1] G. Luber and N. Prudent, "Climate change and human health," (in eng), *Trans Am Clin Climatol Assoc,* vol. 120, pp. 113-7, 2009.

[2] IPCC, "Climate Change 2022: Impacts, Adaptations and Vulnerability," 2022.

[3] N. Mimura, "Sea-level rise caused by climate change and its implications for society," (in eng), *Proc Jpn Acad Ser B Phys Biol Sci,* vol. 89, no. 7, pp. 281-301, 2013, doi: 10.2183/pjab.89.281.

[4] B. Clarke, F. Otto, R. Stuart-Smith, and L. Harrington, "Extreme weather impacts of climate change: an attribution perspective," *Environmental Research Climate,* 2022, doi: 10.1088/2752-5295/ac6e7d.

[5] C. Matz *et al.*, "Effects of Age, Season, Gender and Urban-Rural Status on Time-Activity: Canadian Human Activity Pattern Survey 2 (CHAPS 2)," *International Journal of Environmental Research and Public Health,* vol. 11, no. 2, pp. 2108-2124, 2014, doi: 10.3390/ijerph110202108.

[6] L. B. Ford, "Climate change and health in Canada," (in eng), *Mcgill J Med,* vol. 12, no. 1, pp. 78-84, Jan 2009.

[7] A. Yusa *et al.*, "Climate Change, Drought and Human Health in Canada," (in eng), *Int J Environ Res Public Health,* vol. 12, no. 7, pp. 8359-412, Jul 17 2015, doi: 10.3390/ijerph120708359.

[8] "Canada's Changing Climate Report," Government of Canada, Ottawa, ON., 2019.

[9] A. A. Khan, "Heat related illnesses. Review of an ongoing challenge," (in eng), *Saudi Med J,* vol. 40, no. 12, pp. 1195-1201, Dec 2019, doi: 10.15537/smj.2019.12.24727.

[10] K. G. Arbuthnott and S. Hajat, "The health effects of hotter summers and heat waves in the population of the United Kingdom: a review of the evidence," *Environmental Health,* vol. 16, no. 1, p. 119, 2017/12/05 2017, doi: 10.1186/s12940-017-0322-5.

[11] J. Liu *et al.*, "Is there an association between hot weather and poor mental health outcomes? A systematic review and meta-analysis," *Environment International,* vol. 153, p. 106533, 2021/08/01/ 2021, doi: https://doi.org/10.1016/j.envint.2021.106533.

[12] X. Wang, D. K. Thompson, G. A. Marshall, C. Tymstra, R. Carr, and M. D. Flannigan, "Increasing frequency of extreme fire weather in Canada with climate change," *Climatic Change,* vol. 130, no. 4, pp. 573-586, 2015, doi: 10.1007/s10584-015-1375-5.

[13] W. Haider, D. Knowler, R. Trenholm, J. Moore, P. Bradshaw, and K. Lertzman, "Climate change, increasing forest fire incidence, and the value of visibility: evidence from British Columbia, Canada," *Canadian Journal of Forest Research,* vol. 49, no. 10, pp. 1242-1255, 2019/10/01 2019, doi: 10.1139/cjfr-2018-0309.

[14] J. Wang and K. Strong, "British Columbia's forest fires, 2018," Statistics Canada, 2019.

[15] W. J. Fisk and W. R. Chan, "Health benefits and costs of filtration interventions that reduce indoor exposure to PM 2.5 during wildfires," *Indoor Air,* vol. 27, no. 1, pp. 191-204, 2017, doi: 10.1111/ina.12285.

[16] A. Karanasiou *et al.*, "Short-term health effects from outdoor exposure to biomass burning emissions: A review," *Science of The Total Environment,* vol. 781, p. 146739, 2021/08/10/ 2021, doi: https://doi.org/10.1016/j.scitotenv.2021.146739.

[17] R. Xu *et al.*, "Wildfires, Global Climate Change, and Human Health," *New England Journal of Medicine,* vol. 383, no. 22, pp. 2173-2181, 2020, doi: 10.1056/nejmsr2028985.

[18] K. O'Dell *et al.*, "Outside in: the relationship between indoor and outdoor particulate air quality during wildfire smoke events in western US cities," *Environmental Research: Health,* vol. 1, no. 1, p. 015003, 2023, doi: 10.1088/2752-5309/ac7d69.

[19] Y. Liang, D. Sengupta, M. J. Campmier, D. M. Lunderberg, J. S. Apte, and A. H. Goldstein, "Wildfire smoke impacts on indoor air quality assessed using crowdsourced data in California," *Proceedings of the National Academy of Sciences,* vol. 118, no. 36, p. e2106478118, 2021/09/07 2021, doi: 10.1073/pnas.2106478118.

[20] S. M. D'Evelyn *et al.*, "Wildfire, Smoke Exposure, Human Health, and Environmental Justice Need to be Integrated into Forest Restoration and Management," (in eng), *Curr Environ Health Rep,* vol. 9, no. 3, pp. 366-385, Sep 2022, doi: 10.1007/s40572-022-00355-7.

[21] M. Burke, A. Driscoll, S. Heft-Neal, J. Xue, J. Burney, and M. Wara, "The changing risk and burden of wildfire in the United States," *Proceedings of the National Academy of Sciences,* vol. 118, no. 2, p. e2011048118, 2021/01/12 2021, doi: 10.1073/pnas.2011048118.

[22] S. Wu *et al.*, "Local mechanisms for global daytime, nighttime, and compound heatwaves," *npj Climate and Atmospheric Science,* vol. 6, no. 1, p. 36, 2023/05/15 2023, doi: 10.1038/s41612-023-00365-8.

[23] E. Infusino, T. Caloiero, F. Fusto, G. Calderaro, A. Brutto, and G. Tagarelli, "Characterization of the 2017 Summer Heat Waves and Their Effects on the Population of an Area of Southern Italy," (in eng), *Int J Environ Res Public Health,* vol. 18, no. 3, Jan 22 2021, doi: 10.3390/ijerph18030970.

[24] J. Nawaro, L. Gianquintieri, A. Pagliosa, A. Silvaroli, G. M. Sechi, and E. G. Caiani, "Heat Waves and Cardiovascular Events in Milan, Italy: A Geospatial Case-Crossover Approach Using Data from Emergency Medical Services," *Medical Sciences Forum*, vol. 19, no. 1*,* doi: 10.3390/msf2023019005.

[25] R. H. White *et al.*, "The unprecedented Pacific Northwest heatwave of June 2021," *Nature Communications,* vol. 14, no. 1, p. 727, 2023/02/09 2023, doi: 10.1038/s41467-023-36289-3.

[26] A. Gasparrini and B. Armstrong, "The Impact of Heat Waves on Mortality," *Epidemiology,* vol. 22, no. 1, 2011. [Online]. Available: https://journals.lww.com/epidem/Fulltext/2011/01000/The_Impact_of_Heat_Waves_on_Mortality.11.aspx.

[27] Z. Wu, H. Lin, J. Li, Z. Jiang, and T. Ma, "Heat wave frequency variability over North America: Two distinct leading modes," *Journal of Geophysical Research: Atmospheres,* vol. 117, no. D2, pp. n/a-n/a, 2012, doi: 10.1029/2011jd016908.

[28] D. H. García, "Analysis of Urban Heat Island and Heat Waves Using Sentinel-3 Images: a Study of Andalusian Cities in Spain," (in eng), *Earth Syst Environ,* vol. 6, no. 1, pp. 199-219, 2022, doi: 10.1007/s41748-021-00268-9.

[29] M. Santamouris, "Cooling the cities – A review of reflective and green roof mitigation technologies to fight heat island and improve comfort in urban environments," *Solar Energy,* vol. 103, pp. 682-703, 2014/05/01/ 2014, doi: https://doi.org/10.1016/j.solener.2012.07.003.

[30] "Reducing Urban Heat Island Effect," United States Environmental Protection Agency, 2023.

[31] *ANSI/ASHRAE Standard 169, Climate Data for Building Design Standards*, ASHRAE, 2021.
[32] S. B. Henderson, K. E. McLean, M. J. Lee, and T. Kosatsky, "Analysis of community deaths during the catastrophic 2021 heat dome: Early evidence to inform the public health response during subsequent events in greater Vancouver, Canada," (in eng), *Environ Epidemiol,* vol. 6, no. 1, p. e189, Feb 2022, doi: 10.1097/ee9.0000000000000189.
[33] A. Alberini, W. Gans, and M. Alhassan, "Individual and public-program adaptation: coping with heat waves in five cities in Canada," (in eng), *Int J Environ Res Public Health,* vol. 8, no. 12, pp. 4679-701, Dec 2011, doi: 10.3390/ijerph8124679.
[34] "2021 ASHRAE handbook, Fundamentals," ASHRAE, 2021, ch. 15.
[35] R. S. Jose and J. L. Perez-Camanyo, "Modelling infiltration rate impacts on indoor air quality," *International Journal of Thermofluids,* vol. 17, p. 100284, 2023/02/01/ 2023, doi: https://doi.org/10.1016/j.ijft.2023.100284.
[36] L. C. Ng, W. S. Dols, and S. J. Emmerich, "Evaluating Potential Benefits of Air Barriers in Commercial Buildings using NIST Infiltration Correlations in EnergyPlus," (in eng), *Build Environ,* vol. 196, Jun 2021, doi: 10.1016/j.buildenv.2021.107783.
[37] R. Hart, S. Selkowitz, and C. Curcija, "Thermal performance and potential annual energy impact of retrofit thin-glass triple-pane glazing in US residential buildings," *Building Simulation,* vol. 12, no. 1, pp. 79-86, 2019/02/01 2019, doi: 10.1007/s12273-018-0491-3.
[38] B. P. Jelle, A. Hynd, A. Gustavsen, D. Arasteh, H. Goudey, and R. Hart, "Fenestration of today and tomorrow: A state-of-the-art review and future research opportunities," *Solar Energy Materials and Solar Cells,* vol. 96, pp. 1-28, 2012/01/01/ 2012, doi: https://doi.org/10.1016/j.solmat.2011.08.010.
[39] M. Detsi, A. Manolitsis, I. Atsonios, I. Mandilaras, and M. Founti, "Energy Savings in an Office Building with High WWR Using Glazing Systems Combining Thermochromic and Electrochromic Layers," *Energies,* vol. 13, no. 11, 2020, doi: 10.3390/en13113020.
[40] ASHRAE, "Planning Framework for Protecting Commercial Building Occupants from Smoke During Wildfire Events."
[41] P. Azimi, D. Zhao, and B. Stephens, "Estimates of HVAC filtration efficiency for fine and ultrafine particles of outdoor origin," *Atmospheric Environment,* vol. 98, pp. 337-346, 2014/12/01/ 2014, doi: https://doi.org/10.1016/j.atmosenv.2014.09.007.
[42] T. Fazli, Y. Zeng, and B. Stephens, "Fine and ultrafine particle removal efficiency of new residential HVAC filters," (in eng), *Indoor Air,* vol. 29, no. 4, pp. 656-669, Jul 2019, doi: 10.1111/ina.12566.
[43] Y. Zhang, X. He, Z. Zhu, W.-N. Wang, and S.-C. Chen, "Simultaneous removal of VOCs and PM2.5 by metal-organic framework coated electret filter media," *Journal of Membrane Science,* vol. 618, p. 118629, 2021/01/15/ 2021, doi: https://doi.org/10.1016/j.memsci.2020.118629.
[44] C.-H. Huang *et al.*, "Impacts of using auto-mode portable air cleaner on indoor PM2.5 levels: An intervention study," *Building and Environment,* vol. 188, p. 107444, 2021/01/15/ 2021, doi: https://doi.org/10.1016/j.buildenv.2020.107444.
[45] S. Batterman, "Review and Extension of CO(2)-Based Methods to Determine Ventilation Rates with Application to School Classrooms," *Int J Environ Res Public Health,* vol. 14, no. 2, Feb 4 2017, doi: 10.3390/ijerph14020145.

[46] T. Ben-David, S. Wang, A. Rackes, and M. S. Waring, "Measuring the efficacy of HVAC particle filtration over a range of ventilation rates in an office building," *Building and Environment,* vol. 144, pp. 648-656, 2018, doi: 10.1016/j.buildenv.2018.08.018.

[47] E. Moretti, E. Belloni, and E. Lascaro, "The Influence of Solar Control Films on Energy and Daylighting Performance by Means of Experimental Data and Preliminary Unsteady Simulations," *Energy Procedia,* vol. 78, pp. 340-345, 2015/11/01/ 2015, doi: https://doi.org/10.1016/j.egypro.2015.11.660.

[48] A. Sedaghat *et al.*, "Effects of Window Films in Thermo-Solar Properties of Office Buildings in Hot-Arid Climates," (in English), *Frontiers in Energy Research,* Original Research vol. 9, 2021-May-20 2021, doi: 10.3389/fenrg.2021.665978.

[49] Y. Zhao, A. W. Dunn, and D. Shi, "Effective reduction of building heat loss without insulation materials via the photothermal effect of a chlorophyll thin film coated "Green Window"," *MRS Communications,* vol. 9, no. 2, pp. 675-681, 2019, doi: 10.1557/mrc.2019.52.

[50] F. Hu *et al.*, "Transparent and Flexible Thermal Insulation Window Material," *Cell Reports Physical Science,* vol. 1, no. 8, p. 100140, 2020/08/26/ 2020, doi: https://doi.org/10.1016/j.xcrp.2020.100140.

[51] Z. Zeng, J. Chen, and G. Augenbroe, "Movable window insulation as an instantiation of the adaptive building envelope: An investigation of its cost-effectiveness in the U.S," *Energy and Buildings,* vol. 247, p. 111138, 2021/09/15/ 2021, doi: https://doi.org/10.1016/j.enbuild.2021.111138.

[52] A. E. Ben-Nakhi, "Minimizing thermal bridging through window systems in buildings of hot regions," *Applied Thermal Engineering,* vol. 22, no. 9, pp. 989-998, 2002/06/01/ 2002, doi: https://doi.org/10.1016/S1359-4311(01)00121-1.

[53] K. A. Tabet Aoul, R. Hagi, R. Abdelghani, M. Syam, and B. Akhozheya, "Building Envelope Thermal Defects in Existing and Under-Construction Housing in the UAE; Infrared Thermography Diagnosis and Qualitative Impacts Analysis," *Sustainability,* vol. 13, no. 4, 2021, doi: 10.3390/su13042230.

[54] S. Gutiérrez, J. Álvarez, R. Velázquez, and A. Lay-Ekuakille, "Use of automated blinds in smart buildings for energy savings: A mexican case," in *2017 IEEE 37th Central America and Panama Convention (CONCAPAN XXXVII)*, 15-17 Nov. 2017 2017, pp. 1-5, doi: 10.1109/CONCAPAN.2017.8278509.

[55] C. T. Do and Y.-C. Chan, "Evaluation of the effectiveness of a multi-sectional facade with Venetian blinds and roller shades with automated shading control strategies," *Solar Energy,* vol. 212, pp. 241-257, 2020, doi: 10.1016/j.solener.2020.11.003.

[56] C. Oleskowicz-Popiel and M. Sobczak, "Effect of the roller blinds on heat losses through a double-glazing window during heating season in Central Europe," *Energy and Buildings,* vol. 73, pp. 48-58, 2014, doi: 10.1016/j.enbuild.2013.12.032.

[57] J. Herman and W. Usher, "SALib: An open-source Python library for Sensitivity Analysis," *The Journal of Open Source Software,* vol. 2, no. 9, p. 97, 2017, doi: 10.21105/joss.00097.

[58] L. G. Chestnut and P. De Civita, "Economic Valuation of Mortality Risk Reduction: Review and Recommendations for Policy and Regulatory Analysis," Government of Canada, 2009.

[59] C. Aponte, W. J. De Groot, and B. M. Wotton, "Forest fires and climate change: causes, consequences and management options," *International Journal of Wildland Fire,* vol. 25, no. 8, p. i, 2016, doi: 10.1071/wfv25n8_fo.

[60] N. P. Gillett, "Detecting the effect of climate change on Canadian forest fires," *Geophysical Research Letters,* vol. 31, no. 18, 2004, doi: 10.1029/2004gl020876.
[61] Y. Liu, J. Stanturf, and S. Goodrick, "Trends in global wildfire potential in a changing climate," *Forest Ecology and Management,* vol. 259, no. 4, pp. 685-697, 2010, doi: 10.1016/j.foreco.2009.09.002.
[62] J. Castagna *et al.*, "Multiscale assessment of the impact on air quality of an intense wildfire season in southern Italy," *Science of The Total Environment,* vol. 761, p. 143271, 2021/03/20/ 2021, doi: https://doi.org/10.1016/j.scitotenv.2020.143271.
[63] X. Zong, X. Tian, and Y. Yin, "Impacts of Climate Change on Wildfires in Central Asia," *Forests,* vol. 11, no. 8, 2020, doi: 10.3390/f11080802.
[64] C. D. Butler, "Climate Change, Health and Existential Risks to Civilization: A Comprehensive Review (1989–2013)," (in eng), *International journal of environmental research and public health,* vol. 15, no. 10, p. 2266, 2018, doi: 10.3390/ijerph15102266.
[65] S. Fawzy, A. I. Osman, J. Doran, and D. W. Rooney, "Strategies for mitigation of climate change: a review," *Environmental Chemistry Letters,* vol. 18, no. 6, pp. 2069-2094, 2020/11/01 2020, doi: 10.1007/s10311-020-01059-w.
[66] P. Goglio *et al.*, "Advances and challenges of life cycle assessment (LCA) of greenhouse gas removal technologies to fight climate changes," *Journal of Cleaner Production,* vol. 244, p. 118896, 2020/01/20/ 2020, doi: https://doi.org/10.1016/j.jclepro.2019.118896.
[67] A. I. Osman, M. Hefny, M. I. A. Abdel Maksoud, A. M. Elgarahy, and D. W. Rooney, "Recent advances in carbon capture storage and utilisation technologies: a review," *Environmental Chemistry Letters,* vol. 19, no. 2, pp. 797-849, 2021/04/01 2021, doi: 10.1007/s10311-020-01133-3.
[68] G. Forzieri, A. Cescatti, F. B. E Silva, and L. Feyen, "Increasing risk over time of weather-related hazards to the European population: a data-driven prognostic study," *The Lancet Planetary Health,* vol. 1, no. 5, pp. e200-e208, 2017, doi: 10.1016/s2542-5196(17)30082-7.
[69] Y. Jabareen, "Planning the resilient city: Concepts and strategies for coping with climate change and environmental risk," *Cities,* vol. 31, pp. 220-229, 2013/04/01/ 2013, doi: https://doi.org/10.1016/j.cities.2012.05.004.
[70] N. E. Klepeis *et al.*, "The National Human Activity Pattern Survey (NHAPS): a resource for assessing exposure to environmental pollutants," *Journal of Exposure Science & Environmental Epidemiology,* vol. 11, no. 3, pp. 231-252, 2001/07/01 2001, doi: 10.1038/sj.jea.7500165.
[71] G. R. Tom Javins, Emily Gibb Snyder, Gregory Nilsson, Steven J. Emmerich, "Protecting Building Occupants From Smoke During Wildfire and Prescribed Burn Events," *ASHRAE Journal,* IEO Applications, 2021.
[72] "Estimates of premature deaths and nonfatal outcomes," in "Health Impacts of Air Pollution in Canada," Public Health Agency of Canada, 2021.
[73] G. Davison *et al.*, "Creating Clean Air Spaces During Wildland Fire Smoke Episodes: Web Summit Summary," (in eng), *Front Public Health,* vol. 9, pp. 508971-508971, 2021, doi: 10.3389/fpubh.2021.508971.
[74] N. R. Martins and G. Carrilho da Graça, "A simulation study of decreased life expectancy from exposure to ambient particulate air pollution (PM2.5) in naturally ventilated workspaces," *Journal of Building Engineering,* vol. 30, p. 101268, 2020/07/01/ 2020, doi: https://doi.org/10.1016/j.jobe.2020.101268.

[75] L. A. Richardson, P. A. Champ, and J. B. Loomis, "The hidden cost of wildfires: Economic valuation of health effects of wildfire smoke exposure in Southern California," *Journal of Forest Economics,* vol. 18, no. 1, pp. 14-35, 2012, doi: 10.1016/j.jfe.2011.05.002.
[76] L. Pimpin *et al.*, "Estimating the costs of air pollution to the National Health Service and social care: An assessment and forecast up to 2035," *PLOS Medicine,* vol. 15, no. 7, p. e1002602, 2018, doi: 10.1371/journal.pmed.1002602.
[77] A. Alberini and A. Krupnick, "Cost-of-Illness and Willingness-to-Pay Estimates of the Benefits of Improved Air Quality: Evidence from Taiwan," *Land Economics,* vol. 76, no. 1, p. 37, 2000, doi: 10.2307/3147256.
[78] *Canadian Ambient Air Quality Standards* CCME, 2020.
[79] "Fine Particulate Matter - PM2.5 dataset," Alberta Environment and Parks and Airshed, 2019.
[80] "BC Air Data Archive," British Columbia Ministry of Environment, 2018.
[81] M. Zaatari, A. Novoselac, and J. Siegel, "The relationship between filter pressure drop, indoor air quality, and energy consumption in rooftop HVAC units," *Building and Environment,* vol. 73, pp. 151-161, 2014/03/01/ 2014, doi: https://doi.org/10.1016/j.buildenv.2013.12.010.
[82] F. Wang, D. Meng, X. Li, and J. Tan, "Indoor-outdoor relationships of PM2.5 in four residential dwellings in winter in the Yangtze River Delta, China," *Environmental Pollution,* vol. 215, pp. 280-289, 2016/08/01/ 2016, doi: https://doi.org/10.1016/j.envpol.2016.05.023.
[83] T. N. Quang, C. He, L. Morawska, and L. D. Knibbs, "Influence of ventilation and filtration on indoor particle concentrations in urban office buildings," *Atmospheric Environment,* vol. 79, pp. 41-52, 2013/11/01/ 2013, doi: https://doi.org/10.1016/j.atmosenv.2013.06.009.
[84] Q. Cao, F. Li, T. Zhang, and S. Wang, "A ventilator that responds to outdoor conditions for ventilation and air filtration," *Energy and Buildings,* vol. 229, p. 110498, 2020/12/15/ 2020, doi: https://doi.org/10.1016/j.enbuild.2020.110498.
[85] B. Stephens, A. Novoselac, and J. Siegel, "The Effects of Filtration on Pressure Drop and Energy Consumption in Residential HVAC Systems (RP-1299)," *HVAC&R Research,* vol. 16, no. 3, pp. 273-294, 2010, doi: 10.1080/10789669.2010.10390905.
[86] J. F. Montgomery, S. Storey, and K. Bartlett, "Comparison of the indoor air quality in an office operating with natural or mechanical ventilation using short-term intensive pollutant monitoring," *Indoor and Built Environment,* vol. 24, no. 6, pp. 777-787, 2015/10/01 2014, doi: 10.1177/1420326X14530999.
[87] D. A. Stauffer, D. A. Autenrieth, J. F. Hart, and S. Capoccia, "Control of wildfire-sourced PM2.5 in an office setting using a commercially available portable air cleaner," *Journal of Occupational and Environmental Hygiene,* vol. 17, no. 4, pp. 109-120, 2020, doi: 10.1080/15459624.2020.1722314.
[88] J. Xiang *et al.*, "Field measurements of PM2.5 infiltration factor and portable air cleaner effectiveness during wildfire episodes in US residences," *Science of The Total Environment,* vol. 773, p. 145642, 2021, doi: 10.1016/j.scitotenv.2021.145642.
[89] P. Barn, T. Larson, M. Noullett, S. Kennedy, R. Copes, and M. Brauer, "Infiltration of forest fire and residential wood smoke: an evaluation of air cleaner effectiveness," *Journal of Exposure Science & Environmental Epidemiology,* vol. 18, no. 5, pp. 503-511, 2008, doi: 10.1038/sj.jes.7500640.

[90] "Evaluation of In-Room Particulate Matter Air Filtration Devices," United States Environmental Protection Agency, 2008.
[91] "Guide to Air Cleaners in the House," United States Environmental Protection Agency, 2018.
[92] G. Drago *et al.*, "Relationship between domestic smoking and metals and rare earth elements concentration in indoor PM2.5," *Environmental Research,* vol. 165, pp. 71-80, 2018/08/01/ 2018, doi: https://doi.org/10.1016/j.envres.2018.03.026.
[93] "Wildfire Smoke FAQs," California Department of Public Health, 2019.
[94] F. Reisen, J. C. Powell, M. Dennekamp, F. H. Johnston, and A. J. Wheeler, "Is remaining indoors an effective way of reducing exposure to fine particulate matter during biomass burning events?," *Journal of the Air & Waste Management Association,* vol. 69, no. 5, pp. 611-622, 2019, doi: 10.1080/10962247.2019.1567623.
[95] *ANSI/ASHRAE Standard 62.1-2019. Ventilation for Acceptable Indoor Air Quality*, ANSI/ASHRAE, Atlanta, GA, 2019.
[96] *ANSI/ASHRAE Standard 62.2-2019, Ventilation and Acceptable Indoor Air Quality in Residential Buildings*, ANSI/ASHRAE, 2019.
[97] "City of Prince George Wildland/Urban Interface Wildfire Management Strategy," City of Prince George, 2005.
[98] *British Columbia Building Code*, N. R. C. o. Canada, 2018.
[99] *National Building Code - 2019 Alberta Edition*, N. R. C. o. Canada, 2019.
[100] "Living area and assessment value per square foot of residential properties by property type and period of construction, provinces of Nova Scotia, Ontario and British Columbia," Statistics Canada, 2019.
[101] D. E. Henderson, J. B. Milford, and S. L. Miller, "Prescribed Burns and Wildfires in Colorado: Impacts of Mitigation Measures on Indoor Air Particulate Matter," *Journal of the Air & Waste Management Association,* vol. 55, no. 10, pp. 1516-1526, 2005, doi: 10.1080/10473289.2005.10464746.
[102] R. A. Grot and A. K. Persily, "Measured Air Infiltration and Ventilation Rates in Eight Large Office Buildings," H. R. Trechsel and P. L. Lagus Eds. West Conshohocken, PA: ASTM International, 1986, pp. 151-183.
[103] W. Xie, Y. Fan, X. Zhang, G. Tian, and P. Si, "A mathematical model for predicting indoor PM2.5 concentration under different ventilation methods in residential buildings," *Building Services Engineering Research and Technology,* vol. 41, no. 6, pp. 694-708, 2020/11/01 2020, doi: 10.1177/0143624420905102.
[104] C. Sun and D. Woodman, "Delivering Sustainability Promise to HVAC Air Filtration--Part I: Classification of Energy Efficiency for Air Filters," *ASHRAE Transactions,* Article vol. 115, no. 2, pp. 581-585, 2009. [Online]. Available: https://login.ezproxy.library.ualberta.ca/login?url=https://search.ebscohost.com/login.aspx?direct=true&db=a9h&AN=47597857&site=ehost-live&scope=site.
[105] J. F. Montgomery, S. I. Green, S. N. Rogak, and K. Bartlett, "Predicting the energy use and operation cost of HVAC air filters," *Energy and Buildings,* vol. 47, pp. 643-650, 2012/04/01/ 2012, doi: https://doi.org/10.1016/j.enbuild.2012.01.001.
[106] H. M. Sachs, T. Kubo, S. Smith, and K. Scott, "Residential HVAC fans and motors are bigger than refrigerators," *ACEEE Summer Studies on Energy Efficiency in Buildings* vol. 1, pp. 261-272, 2002.

[107] "BestAir Furnace Filters." https://bestairproducts.com/bestair-furnace-filters/ (accessed Sept. 2, 2021).
[108] "Duststop Air Filters Inc." Duststopfilters.com (accessed Sept. 2, 2021).
[109] "Filtrate Air Filters." Filtrate.com (accessed Sept. 2, 2021).
[110] "BC Hydro - Have you ever wondered how our rates compare?" https://www.bchydro.com/news/conservation/2016/how-our-rates-compare.html (accessed Sept. 2, 2021).
[111] K. P. N.V. "Nano Protect Filter FY1410/30." https://www.philips.ca/c-p/FY1410_30/nano-protect-filter (accessed Sept. 5, 2021).
[112] K. P. N.V. "Series 1000 Nano Protect Filter." https://www.philips.ca/c-p/FY1413_30/series-1000-nano-protect-filter (accessed Sept. 5, 2021).
[113] K. P. N.V. "Philips 1000i Series Air Purifier." https://www.philips.ca/c-p/AC1214_40/series-1000i-air-purifier (accessed Sept. 20, 2021).
[114] Y.-F. Xing, Y.-H. Xu, M.-H. Shi, and Y.-X. Lian, "The impact of PM2.5 on the human respiratory system," (in eng), *J Thorac Dis,* vol. 8, no. 1, pp. E69-E74, 2016, doi: 10.3978/j.issn.2072-1439.2016.01.19.
[115] G. o. Canada, "Canada: Land of wildfires?," vol. 2021, ed, 2020.
[116] S. Yıldız, S. Kıvrak, A. B. Gültekin, and G. Arslan, "Built environment design - social sustainability relation in urban renewal," *Sustainable Cities and Society,* vol. 60, p. 102173, 2020/09/01/ 2020, doi: https://doi.org/10.1016/j.scs.2020.102173.
[117] X. Fang, X. Shi, and W. Gao, "Measuring urban sustainability from the quality of the built environment and pressure on the natural environment in China: A case study of the Shandong Peninsula region," *Journal of Cleaner Production,* vol. 289, p. 125145, 2021/03/20/ 2021, doi: https://doi.org/10.1016/j.jclepro.2020.125145.
[118] E. Maghsoudi Nia, Q. K. Qian, and H. J. Visscher, "Analysis of Occupant Behaviours in Energy Efficiency Retrofitting Projects," *Land,* vol. 11, no. 11, p. 1944, 2022, doi: 10.3390/land11111944.
[119] E. Sofeska, "Understanding the Livability in a City Through Smart Solutions and Urban Planning Toward Developing Sustainable Livable Future of the City of Skopje," *Procedia Environmental Sciences,* vol. 37, pp. 442-453, 2017/01/01/ 2017, doi: https://doi.org/10.1016/j.proenv.2017.03.014.
[120] A. Schuurmans, S. Dyrbøl, and F. Guay, "Buildings in Urban Regeneration," IntechOpen, 2019.
[121] M. Boubekri, I. N. Cheung, K. J. Reid, C.-H. Wang, and P. C. Zee, "Impact of Windows and Daylight Exposure on Overall Health and Sleep Quality of Office Workers: A Case-Control Pilot Study," *Journal of Clinical Sleep Medicine,* vol. 10, no. 06, pp. 603-611, 2014, doi: 10.5664/jcsm.3780.
[122] O. Seppanen, W. Fisk, and D. Faulkner, "Control of Temperature for Health and Productivity in Offices," *ASHRAE Transactions,* vol. 111, 06/01 2004.
[123] A. M. Bueno, A. A. de Paula Xavier, and E. E. Broday, "Evaluating the Connection between Thermal Comfort and Productivity in Buildings: A Systematic Literature Review," *Buildings*, vol. 11, no. 6, doi: 10.3390/buildings11060244.
[124] F. Kheiri, "Optimization of building fenestration and shading for climate-based daylight performance using the coupled genetic algorithm and simulated annealing optimization methods," *Indoor and Built Environment,* vol. 30, no. 2, pp. 195-214, 2021/02/01 2019, doi: 10.1177/1420326X19888008.

[125] F. Hammad and B. Abu-Hijleh, "The energy savings potential of using dynamic external louvers in an office building," *Energy and Buildings,* vol. 42, no. 10, pp. 1888-1895, 2010/10/01/ 2010, doi: https://doi.org/10.1016/j.enbuild.2010.05.024.
[126] G. Evola, F. Gullo, and L. Marletta, "The role of shading devices to improve thermal and visual comfort in existing glazed buildings," *Energy Procedia,* vol. 134, pp. 346-355, 2017/10/01/ 2017, doi: https://doi.org/10.1016/j.egypro.2017.09.543.
[127] R. Wang, S. Lu, W. Feng, and B. Xu, "Tradeoff between heating energy demand in winter and indoor overheating risk in summer constrained by building standards," *Building Simulation,* vol. 14, no. 4, pp. 987-1003, 2021/08/01 2021, doi: 10.1007/s12273-020-0719-x.
[128] F. Nicoletti, C. Carpino, M. A. Cucumo, and N. Arcuri, "The Control of Venetian Blinds: A Solution for Reduction of Energy Consumption Preserving Visual Comfort," *Energies,* vol. 13, no. 7, 2020, doi: 10.3390/en13071731.
[129] K. Banionis, J. Kumžienė, A. Burlingis, J. Ramanauskas, and V. Paukštys, "The Changes in Thermal Transmittance of Window Insulating Glass Units Depending on Outdoor Temperatures in Cold Climate Countries," *Energies*, vol. 14, no. 6*,* doi: 10.3390/en14061694.
[130] Q. He, S. T. Ng, M. U. Hossain, and M. Skitmore, "Energy-Efficient Window Retrofit for High-Rise Residential Buildings in Different Climatic Zones of China," *Sustainability*, vol. 11, no. 22*,* doi: 10.3390/su11226473.
[131] *Canada's National Energy Code*, G. o. Canada, 2015.
[132] S. Cox, "Building Energy Codes: Policy Overview and Good Practices," Office of Scientific and Technical Information (OSTI), 2016. [Online]. Available: https://dx.doi.org/10.2172/1238537
[133] N. Asim *et al.*, "Sustainability of Heating, Ventilation and Air-Conditioning (HVAC) Systems in Buildings—An Overview," *International Journal of Environmental Research and Public Health,* vol. 19, no. 2, p. 1016, 2022, doi: 10.3390/ijerph19021016.
[134] "Chapter 5: Increasing Efficiency of Building Systems and Technologies," in "Quadrennial Technology Review: An Assessment of Energy Technologies and Research Opportunities," US Department of Energy, 2015.
[135] M. Santamouris and K. Vasilakopoulou, "Present and future energy consumption of buildings: Challenges and opportunities towards decarbonisation," *e-Prime - Advances in Electrical Engineering, Electronics and Energy,* vol. 1, p. 100002, 2021/01/01/ 2021, doi: https://doi.org/10.1016/j.prime.2021.100002.
[136] D. Ürge-Vorsatz, L. F. Cabeza, S. Serrano, C. Barreneche, and K. Petrichenko, "Heating and cooling energy trends and drivers in buildings," *Renewable and Sustainable Energy Reviews,* vol. 41, pp. 85-98, 2015/01/01/ 2015, doi: https://doi.org/10.1016/j.rser.2014.08.039.
[137] F. S. Hafez *et al.*, "Energy Efficiency in Sustainable Buildings: A Systematic Review with Taxonomy, Challenges, Motivations, Methodological Aspects, Recommendations, and Pathways for Future Research," *Energy Strategy Reviews,* vol. 45, p. 101013, 2023/01/01/ 2023, doi: https://doi.org/10.1016/j.esr.2022.101013.
[138] M. Alwetaishi, "Energy performancein residential buildings: Evaluationof the potential of buildingdesignand environmental parameter," *Ain Shams Engineering Journal,* vol. 13, no. 4, p. 101708, 2022/06/01/ 2022, doi: https://doi.org/10.1016/j.asej.2022.101708.

[139] H. Liao, R. Ren, and L. Li, "Existing Building Renovation: A Review of Barriers to Economic and Environmental Benefits," (in eng), *Int J Environ Res Public Health,* vol. 20, no. 5, Feb 24 2023, doi: 10.3390/ijerph20054058.
[140] H. Huang, H. Wang, Y.-J. Hu, C. Li, and X. Wang, "The development trends of existing building energy conservation and emission reduction—A comprehensive review," *Energy Reports,* vol. 8, pp. 13170-13188, 2022/11/01/ 2022, doi: https://doi.org/10.1016/j.egyr.2022.10.023.
[141] M. Saffari and P. Beagon, "Home energy retrofit: Reviewing its depth, scale of delivery, and sustainability," *Energy and Buildings,* vol. 269, p. 112253, 2022/08/15/ 2022, doi: https://doi.org/10.1016/j.enbuild.2022.112253.
[142] S. K. Sharma *et al.*, "Retrofitting Existing Buildings to Improve Energy Performance," *Sustainability*, vol. 14, no. 2*,* doi: 10.3390/su14020666.
[143] R. Fitton, W. Swan, T. Hughes, and M. Benjaber, "The thermal performance of window coverings in a whole house test facility with single-glazed sash windows," *Energy Efficiency,* vol. 10, no. 6, pp. 1419-1431, 2017/12/01 2017, doi: 10.1007/s12053-017-9529-0.
[144] B. Bueno, J. M. Cejudo-López, A. Katsifaraki, and H. R. Wilson, "A systematic workflow for retrofitting office façades with large window-to-wall ratios based on automatic control and building simulations," *Building and Environment,* vol. 132, pp. 104-113, 2018, doi: 10.1016/j.buildenv.2018.01.031.
[145] C. Shum and L. Zhong, "A review of smart solar shading systems and their applications: Opportunities in cold climate zones," *Journal of Building Engineering,* vol. 64, p. 105583, 2023/04/01/ 2023, doi: https://doi.org/10.1016/j.jobe.2022.105583.
[146] F. Feng, N. Kunwar, K. Cetin, and Z. O'Neill, "A critical review of fenestration/window system design methods for high performance buildings," *Energy and Buildings,* vol. 248, p. 111184, 2021/10/01/ 2021, doi: https://doi.org/10.1016/j.enbuild.2021.111184.
[147] M. Oh, S. Tae, and S. Hwang, "Analysis of Heating and Cooling Loads of Electrochromic Glazing in High-Rise Residential Buildings in South Korea," *Sustainability,* vol. 10, no. 4, 2018, doi: 10.3390/su10041121.
[148] Y. Wu, J. H. Kämpf, and J.-L. Scartezzini, "Automated 'Eye-sight' Venetian blinds based on an embedded photometric device with real-time daylighting computing," *Applied Energy,* vol. 252, p. 113317, 2019/10/15/ 2019, doi: https://doi.org/10.1016/j.apenergy.2019.113317.
[149] R. Singh, I. J. Lazarus, and V. V. N. Kishore, "Effect of internal woven roller shade and glazing on the energy and daylighting performances of an office building in the cold climate of Shillong," *Applied Energy,* pp. 317-333, 2015, doi: DOI:101016/japenergy201509009.
[150] K. A. Cort, J. A. McIntosh, G. P. Sullivan, T. A. Ashley, C. E. Metzger, and N. Fernandez, "Testing the Performance and Dynamic Control of Energy-Efficient Cellular Shades in the PNNL Lab Homes," Office of Scientific and Technical Information (OSTI), 2018. [Online]. Available: https://dx.doi.org/10.2172/1477792
[151] S. Grynning, B. Time, and B. Matusiak, "Solar shading control strategies in cold climates – Heating, cooling demand and daylight availability in office spaces," *Solar Energy,* vol. 107, pp. 182-194, 2014/09/01/ 2014, doi: https://doi.org/10.1016/j.solener.2014.06.007.

[152] G. R. Newsham and C. Arsenault, "A camera as a sensor for lighting and shading control," *Lighting Research & Technology,* vol. 41, no. 2, pp. 143-163, 2009/06/01 2009, doi: 10.1177/1477153508099889.
[153] S. Jain and V. Garg, "A review of open loop control strategies for shades, blinds and integrated lighting by use of real-time daylight prediction methods," *Building and Environment,* vol. 135, pp. 352-364, 2018/05/01/ 2018, doi: https://doi.org/10.1016/j.buildenv.2018.03.018.
[154] L. Karlsen, P. Heiselberg, and I. Bryn, "Occupant satisfaction with two blind control strategies: Slats closed and slats in cut-off position," *Solar Energy,* vol. 115, pp. 166-179, 2015/05/01/ 2015, doi: https://doi.org/10.1016/j.solener.2015.02.031.
[155] B. W. Meerbeek, C. de Bakker, Y. A. W. de Kort, E. J. van Loenen, and T. Bergman, "Automated blinds with light feedback to increase occupant satisfaction and energy saving," *Building and Environment,* vol. 103, pp. 70-85, 2016/07/01/ 2016, doi: https://doi.org/10.1016/j.buildenv.2016.04.002.
[156] A. Luna-Navarro, G. Lori, D. Callewaert, and M. Overend, "Semi-automated vs manually controlled dynamic facades: assessment through a field study on multi-domain occupant satisfaction," *Energy and Buildings,* vol. 286, p. 112912, 2023/05/01/ 2023, doi: https://doi.org/10.1016/j.enbuild.2023.112912.
[157] S. Selkowitz, R. Mitchell, M. Mcclintock, D. Mcquillen, A. McNiel, and M. Yazdanian, "COMFEN 3.0 - Evolution of an Early Design Tool for Commericial Facades and Fenestration Systems," Lawrence Berkeley National Laboratory, 2011.
[158] D. W. McKenney *et al.*, "Spatial insolation models for photovoltaic energy in Canada," *Solar Energy,* vol. 82, no. 11, pp. 1049-1061, 2008/11/01/ 2008, doi: https://doi.org/10.1016/j.solener.2008.04.008.
[159] S. Pelland *et al.*, "THE DEVELOPMENT OF PHOTOVOLTAIC RESOURCE MAPS FOR CANADA," 01/01 2006.
[160] M. Amani *et al.*, "Canadian Wetland Inventory using Google Earth Engine: The First Map and Preliminary Results," *Remote Sensing,* vol. 11, p. 842, 04/08 2019, doi: 10.3390/rs11070842.
[161] WorldMeteorologicalOrganization, *Guide to Instruments and Methods of Observation. Volume I - Measurements of Meteorological Variables.* Geneva, Switzerland, 2021, pp. 308–323.
[162] R. Hart, H. Goudey, and D. C. Curcija, "Experimental validation and model development for thermal transmittances of porous window screens and horizontal louvred blind systems," *Journal of Building Performance Simulation,* vol. 11, no. 2, pp. 190-204, 2018/03/04 2018, doi: 10.1080/19401493.2017.1323010.
[163] N. Engerer. *Global Solar Irradiance Data via API*, The Australian National University Data Commons, doi: 10.25911/5c073e713e5dd.
[164] C. Cornwall, A. Horiuchi, and C. Lehman. "Solar Geometry Calculator." https://gml.noaa.gov/grad/antuv/SolarCalc.jsp (accessed.
[165] J. Yao, D. H. C. Chow, R.-Y. Zheng, and C.-W. Yan, "Occupants' impact on indoor thermal comfort: a co-simulation study on stochastic control of solar shades," *Journal of Building Performance Simulation,* vol. 9, no. 3, pp. 272-287, 2016/05/03 2016, doi: 10.1080/19401493.2015.1046492.

[166] J. Yao and R. Zheng, "Stochastic Characteristics of Manual Solar Shades and their Influence on Building Energy Performance," *Sustainability,* vol. 9, no. 6, 2017, doi: 10.3390/su9061070.
[167] "AI Shading." https://aishading.com/solution (accessed March 15, 2023).
[168] "Budget Blinds." https://budgetblinds.com/en-ca/blog/how-much-do-motorized-window-shades-cost/ (accessed March 15, 2023).
[169] "The Consolidated Edison Commercial and Industrial (C&I) Energy Efficiency Program Manual 2023," Con Edison Commercial and Industrial Energy Efficiency Program, 2023.
[170] J. M. Djoković *et al.*, "Selection of the Optimal Window Type and Orientation for the Two Cities in Serbia and One in Slovakia," *Energies,* vol. 15, no. 1, 2022, doi: 10.3390/en15010323.
[171] *Canadian Weather Energy and Engineering Datasets (CWEEDS)*.
[172] *Historical Weather Data, Canada*.
[173] "Ontario Natural Gas Rates." Ontario Energy Board. (accessed.
[174] "Government of Alberta, Natural Gas Price." Government of Alberta. (accessed.
[175] *Nunavut Pretroleum Products Division, Retail Price List*.
[176] K. Stokowiec, S. Wciślik, and D. Kotrys-Działak, "Innovative Modernization of Building Heating Systems: The Economy and Ecology of a Hybrid District-Heating Substation," *Inventions,* vol. 8, no. 1, p. 43, 2023. [Online]. Available: https://www.mdpi.com/2411-5134/8/1/43.
[177] K. Bataineh and A. Al Rabee, "A cost effective approach to design of energy efficient residential buildings," *Frontiers of Architectural Research,* vol. 11, no. 2, pp. 297-307, 2022/04/01/ 2022, doi: https://doi.org/10.1016/j.foar.2021.10.004.
[178] F. Seri, M. Arnesano, M. M. Keane, and G. M. Revel, "Temperature Sensing Optimization for Home Thermostat Retrofit," (in eng), *Sensors (Basel),* vol. 21, no. 11, May 26 2021, doi: 10.3390/s21113685.
[179] C. Zhang, M. Hu, B. Laclau, T. Garnesson, X. Yang, and A. Tukker, "Energy-carbon-investment payback analysis of prefabricated envelope-cladding system for building energy renovation: Cases in Spain, the Netherlands, and Sweden," *Renewable and Sustainable Energy Reviews,* vol. 145, p. 111077, 2021/07/01/ 2021, doi: https://doi.org/10.1016/j.rser.2021.111077.
[180] T. Inoue, T. Kawase, T. Ibamoto, S. Takakusa, and Y. Matsuo, "The development of an optimal control system for window shading devices based on investigations in office buildings," *ASHRAE transactions,* vol. 94, pp. 1034-1049, 1988.
[181] N. Zuccherini Martello, P. Fausti, A. Santoni, and S. Secchi, "The Use of Sound Absorbing Shading Systems for the Attenuation of Noise on Building Façades. An Experimental Investigation," *Buildings,* vol. 5, no. 4, pp. 1346-1360, 2015. [Online]. Available: https://www.mdpi.com/2075-5309/5/4/1346.